Geochemical and Petrographic Characterization of the Transition Boundary between the MG2 package to MG3 package at Dwarsrivier Chrome Mine, Bushveld Complex, South Africa

By

Adam Ramushu

A thesis submitted in fulfillment of the requirement for the degree of

Magister Scientiae

In

Applied Geology

Department of Earth Sciences, Faculty of Natural Science, University of the Western Cape.

Supervisor: Prof. Charles Okujeni

Co-Supervisors: Dr. Abdi Mohamoud Siad and Dr Russel Bailie

Keywords

Bushveld Complex

Geochemical characterisation

Transition boundary

MG2 package

MG3 package

Chromitites

Feldspathic pyroxenites

Anorthosites

Chromitite pyroxenites

Cluster analysis

Discriminant analysis

Factor analysis

Abstract

This study area is situated within the Eastern Bushveld complex at Dwarsrivier chrome mine, which is approximately 30 km from Steelpoort and 60km from Lydenburg in the Mpumalanga province. The primary aim of the project is to identify the petrological and geochemical characteristics that can be used to distinguish the various rock types of feldspathic pyroxenites, chromitites, anorthosites and chromitite pyroxenites and determine whether the various rock types are from the MG2 package and MG3 package were formed from a single or multiple magma pulses. The geochemical and mineralogical variation studies were carried out using cores from borehole DWR74 and DWR172 located on the farm Dwarsrivier 372 KT. Using the combination of various multivariate statistical techniques (factor, cluster and discriminant analysis) multi element diagrams and trace element ratios, the outcome of the study demonstrated that each of the four rock types can be sub-divided into two groups. The MG3 feldspathic pyroxenites consist of high content of chromitite and plagioclase which can be associated with Cr_2O_3, Fe_2O_3, Al_2O_3, NiO and TiO_2, while MG2 feldspathic pyroxenites demonstrate high content of orthopyroxene and clinopyroxene which are associated with K_2O, MgO, CaO, P_2O_5, MnO and Na_2O. Nickel oxide and MnO can be used to distinguish the MG3 feldspathic pyroxenites from the MG2 feldspathic pyroxenites. The MG3 chromitites illustrates lower clinopyroxene content with the absence of orthopyroxene; these are associated with Cr_2O_3, Fe_2O_3, NiO, MnO and TiO_2. Higher clinopyroxene content and absence of plagioclase characterise the MG2 chromitites and are associated with elements such as CaO, MgO, P_2O_5, Na_2O and Al_2O_3. The MG3 chromitites and MG2 chromitites can be differentiated by CaO and NiO. The anorthosites below the MG3 package demonstrate enrichment of chromitite and orthopyroxene with traces of clinopyroxene, while the anorthosites above the MG2 package consist of high content of clinopyroxene and depleted orthopyroxene and chromitites. The high content of SiO_2, Na_2O and P_2O_5 can be associated with anorthosite above the MG2 package, while those below the MG3 package are associated with Fe_2O_3 and CaO. The anorthosites above the MG2 package can be distinguished from the anorthosites below the MG3 package by using NiO and K_2O. The upper chromitite pyroxenites show the high content of plagioclase, clinopyroxene and depletion in chromitite content. They can be associated with MgO, CaO, K_2O, P_2O_5 and MnO while the lower chromitite pyroxenites consist of high content chromitite, which can be associated with Cr_2O_3, Al_2O_3, Fe_2O_3 and TiO_2. Magnesium oxide and potassium oxide can be used to differentiate the lower chromitite pyroxenites from the upper chromitite pyroxenites. The classification of feldspathic pyroxenites, chromitites, anorthosites and chromitite pyroxenites within the Dwarsrivier chrome mine transition boundary does not correspond to the geochemical classification. Majority of the samples classified as either from the MG3 package or MG2 package according their location and occurrence, through

petrographic study do not correspond to the geochemical classification and only a few were correctly classified. There is slight change from the MG2 package to MG3 package in the ratios; Ba/Sr, Co/V, TiO_2 and V and Mg number. This indicates that the Dwarsrivier chrome mine transition boundary from the MG2 package to MG3 package was formed from a single magma pulse. The MG3 chromitites are the most suitable package for future exploitation, due to the high content of Cr_2O_3 content and Cr: Fe ratio. Although both MG2 and MG3 chromitites can be used to make refractory products, but due to the low Cr_2O_3 and high Al_2O_3 and MgO within the MG2 chromitites, the MG3 chromitites would be the most suitable product.

Abbreviations

PGM	Platinum Group Metals
MG2	Middle Group chromitite seam 2
MG3	Middle Group chromitite seam 3
UCZ	Upper Critical Zone
Mg#	Magnesium number
LZ	Lower Zone
CZ	Critical Zone
RLS	Rustenburg Layered Suite
LG	Lower Group
MG	Middle Group chromitite seam
MG4	Middle Group chromitite seam 4
ARM	Africa Rainbow Mineral
LHD	Load Haul Dump
XRF	X Ray Fluorescence
Cpx	Clinopyroxene
Opx	Orthopyroxene
Chr	Chromitite
Plag	Plagioclase
SPSS	Statistical Package for Social Sciences
Wt. %	Weight percentage

Declaration

I, hereby declare that the *Geochemical and Petrographic Characterisation of the Transition Boundary between the MG2 package to MG3 package at Dwarsrivier Chrome Mine, Bushveld Complex, South Africa*, has not been submitted before for any degree or examination in any other university. It is my own work in design and execution and that all the materials cited have been acknowledged.

Adam Ramushu

August 2018

Signed ……

Acknowledgement

I would like to thank God Almighty for giving me the strength and perseverance from the beginning of this project, all the way to the end.

I would to thank Dwarsrivier Chrome mine management and technical staff for giving me the opportunity to use their mine as my study area, singling out Chris Letsoele (Geologist), Silas Hlapolosa (Technical Manger) and Moses (Assistant geologist) for their support and advices when I was collecting my data.

I would like to thank my supervisor, Prof C. Okujeni for his guidance, time and patience throughout this research project, to Dr. Russel Bailie and Dr Abdi Siad for their constructive criticism and advice in improving my work. I further extend my gratitude to my friends (Senzangakhona Ndumo, Hukundi Madende and Moses Magoba). I am also grateful to the technical and administration staff at the Department of Applied Geology for providing technical assistance that allowed the successful completion of this work.

Dedication

To my parents Mafori Charles and Mahlatse Rosinah Ramushu and my siblings Kalewa Jack and Mokganyetji Eva Ramushu

Table of content

List of figures

List of plates

List of Tables

1 . Introduction

South Africa is the world leading producer of chromium. This is mined from the chromitite layers that are characteristic of the Critical zone of the Bushveld Complex as well as massive chromitite bodies in the Lower Zone and Syn Bushveld Uitkomst satellite mafic-ultramafic intrusion.

The Bushveld complex contains 14 major chromitite horizons (21 in all); Fourie 1959; Cousins and Feringa, 1964; Scoon and Teigler 1994; Schuurman et al, 1998; Mondal and Mathez, 2007; Maier and Barnes, 2008) together with numerous less developed seams that occur intermittently and have not been named. The stratigraphy of the Bushveld complex is made up of four zones, which have distinctive mineralogical, geochemical and petrological characteristics and distinctive style of mineralisation and are bounded by significant unconformities or major petrological changes (Kruger, 1990, 1992, 1994).

The Middle Group is situated at the transitions zone from an ultramafic to more mafic rock which marks the transition from the Lower Critical Zone to the Upper Critical Zone. This boundary is identified by the first appearance of cumulus plagioclase and it's in the Eastern limb. Despite the lithological change of the host rocks of the chromitites layers, there is no significant change in the mineral and whole rock geochemistry (Cameron, 1977; Scoon and Teigler, 1994). Chromite composition changes from the top of the Critical zone in the Eastern Bushveld (Cameron, 1977).

The Lower Critical Zone chromite in the chromitites layers show increasing Cr/Fe ratio and Mg# from the bottom to the top while in the Upper Critical Zone there is no systematic change. The chromitite layers of the Lower critical zone are on of high quality in chromite resource, but very low platinum group elements (Scoon and Teigler, 1994).

The aim of this investigation is to characterise the lithologies within the MG2 and MG3 package based on their geochemical and petrographic characteristics. This will help to get a better understanding on the processes which led to the formation of the chromitites and also enable mining personnel to determine the best package for exploitation.

1.1 Previous work

The chromitite layers within the MG2/MG3 zone transition are characterised by the highest PGE contents relative to the LG1 and MG4 chromitites layers (Lee and Parry, 1988; Scoon and Teigler, 1994; Nardlett et al, 2009).

Van der Walt (1941) noted that the chromite within the silicates is richer in FeO and poorer in MgO as compared to the chromitite bands. He concluded that this was because the chromite in the silicate bands crystalized simultaneously with a relative abundance of pyroxenes.

Wayer and Brown (1968) suggested that the Rustenburg Layered Suite was formed as a result of gravity controlled crystal settling. Many authours have given diverse explanations to the compositional changes in minerals, which they suggest relates to gravity settling, contamination, magma mixing and fractional crystallization. They further suggested that the magmas were emplaced at various stages during the crystallization of the Rustenburg Layered suite and the successive intrusions of the magma resulted in the mixing of the resident magma with the primitive magma.

Irvine (1975) proposed that the large layered ultramafic intrusions such as the Bushveld complex and Mushox were formed as a result of contamination of the parental basic magma by the granitic melt which is derived from the sialic roof rocks. The basic magma composition would have been modified to an extend that it would evolve from olivine to clinopyroxene crystallization. The compositional differences could arise from the magma contamination.

Irvine et al (1983) suggested that the mixing of the Mg-basaltic primitive magma with the evolved U-type (ultramafic) and A-type (anorthositic) magma resulted in the formation of the chromitite layers. The crystallization sequence for the U-type magma is olivine, orthopyroxene and plagioclase, while for the A-type of magma is plagioclase, olivine, clinopyroxene and orthopyroxene.

Hatton (1988) proposed that the formation of the LZ and CZ was as a result of the three parental magmas, B1, B2 and B3. The B1 magma is compositionally similar to that of the U-type of magma of Irvine et al, (1983) and the formation of the LZ was as a result of the parental liquid. While the B2 and B3 liquids formed the CZ and are similar to the A-type of magma. The B1 is considered to be boninitic, while B2/B3 is suggested to be of tholeiitic origin. Hatton and

Von Gruenewaldt (1985), Schuurman (1991), Maier and Eales (1997) proposed that the precipitation of the large volumes of chromitites were as a result of the mixing between the B1 and the B2/B3 magma, where it's supposed that the B1 is less dense than the B2 and B3.

Eales et al (1990) and Teigler et al (1992) suggested that the cyclic layering in the critical zone were as a result of the mixing from two magmas, which are of similar composition. They however pointed out that the cumulate rocks of the CZ compositional variation don't support the presences of two magmas that are of different composition.

Teigler and Eales (1993) divided the chromitite layers into the critical zone of the northwestern sector of the RLS in the western limb into types based on their host rock. The first type of chromitites are associated with ultramafic cumulates; while the second types of chromitites consist of abundant plagioclase cumulates.

Diog (2000) suggested that the compositional variation of the LG and MG chromitites seams is due the compositional contrast between the replenishing magma and the resident magma. The LG and MG chromitite layers and the host cumulate rocks don't support the existence of two different magmas within the critical zone. The chemical variation and cyclic layering is ascribed to the mixing of the resident magma with the primitive magma, which is similar in composition.

Kottke-Levin (2011) did a geochemical study on the middle chromitite of Helena Mine in the Bushveld complex. A general progressive geochemical evolution of the MG chromitite layers can be derived from the chromitite composition which show decreasing whole-rock Mg#. At the transition boundary between the lower critical zone and the upper critical zone, there was no change in the mineral and whole rock geochemistry, which was observed. This concluded that the MG sequence is derived from a continuous progressive evolving melt.

Godel et al (2011) combined the textural studies with the ablation analysis of minerals to illustrate that the LZ and LCZ crystallised from magma composition of that of the B1 and calculated the percentage of the trapped liquid component to be consistent with the petrographic observations.

Jolayeni (2012) studied the textures and major element geochemistry of the silicate rocks that overlie and underlie the MG4. He suggested that there was no major compositional variation of major elements. The similarities between the rocks above and below the MG4 chromitites illustrated that they originated from a single magma or two magmas that are of similar composition. The MG4 pyroxenites are mainly composed of orthopyroxene rather than the clinopyroxene throughout the sequence.

1.2 Aims and Objectives

The aim of the project is to identify the petrological and geochemical characteristics that can be used distinguish the various rock types of feldspathic pyroxenites, chromitites, anorthosites and chromitite pyroxenites. And determine whether or not the various rock types from the MG2 package and MG3 package were formed by single or multiple magma pulses.

The specific objectives of the project are as follows:

- Do a comparative study to validate the field rock identification using petrological or geochemical and multivariate classification.
- Develop a simplified stratigraphy column that will help in the easy identification and distinguish the various feldspathic pyroxenites, chromitites, anorthosites and chromitite pyroxenites in terms of their geochemistry and petrography
- Determine whether transition boundary from the MG3 package to MG2 package was as a result of a single magma pulse or multiple magma pulses based on the compositional variations in the rock suites.
- Determine the most suitable package between the MG2 package and MG3 package for suitable exploitation based on the refractory chromite properties and Cr:Fe ratio .

1.3 Project Area

1.3.1 Location

Assmang Dwarsrivier Chrome Mine is situated on the farm Dwarsrivier 372KT, approximately 30 kilometers from Steelpoort and 60 kilometers from Lydenburg, in Mpumalanga province , South Africa (ARM annual report, 2005). It is geographical located at longitude 30°05'00"E and latitude 24°59'00"S within the Eastern Bushveld Complex South Africa within the Tweenfontein section as illustrated in figure 1.1 below.

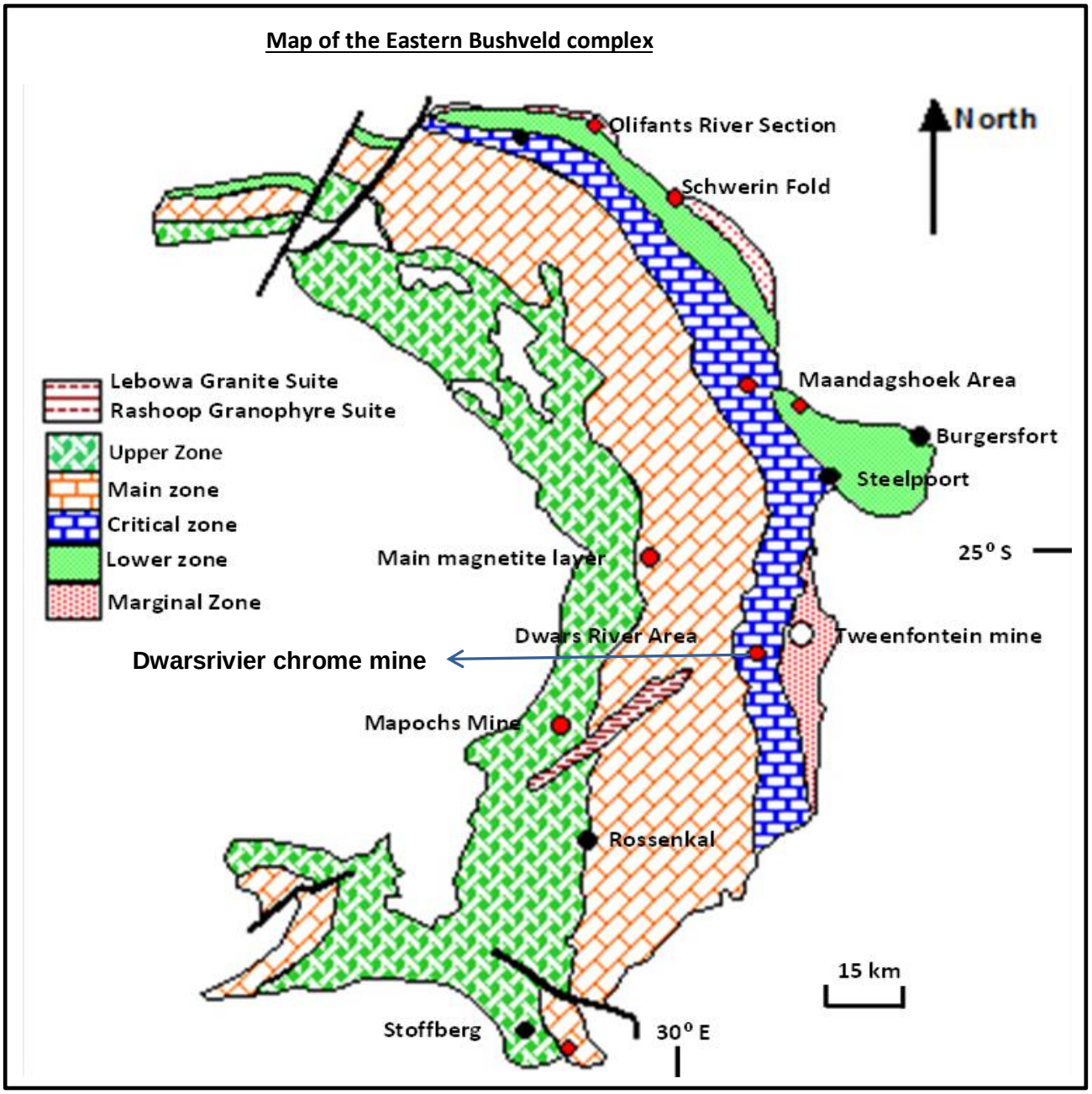

Figure 1.1:Map of the Eastern Bushveld complex with the location of Dwarsrivier chrome mine (Kinnaird J.A, 2005)

1.3.2 Climate

The province of Mpumalanga is known as a summer rainfall area. The area is further divided into two halves by the escarpment, namely the high lying grassland savannah of the Highveld escarpment and the subtropical lowveld plains.

The Highveld receives of cold, frosty winters and moderate summers while the lowveld plains receive of subtropical climates and mild winters. The temperature ranges from -4°C to 38°C with and an annual rainfall of approximately 600mm which is influenced by the topography of the area.

The rainfall which is received between December and February makes about 48% of the annual rainfall of the area, while spring rainfall makes about 28%. January is considered is the warmest month and July being the coldest.

2 2. Geology

2.1 Geology of the Bushveld Complex

The Bushveld Complex intruded into the sediments of the Transvaal Supergroup approximately 2.06 billion years ago. The intrusion is the world's largest mafic intrusion of its kind with an areal extent of 66 000km^2 (Eales and Cawthorn, 1996).The maximum vertical thickness of the layered rocks approaches 8km and is regarded as a unique occurrence, representing special development of genetically related rocks, both intrusive and extrusive (Cawthorn et al,2006).

The BIC consist of the basal mafic to ultramafic rocks known as the Rustenberg Layered Suite and the upper part consisting of the Rooiberg felsites and Rashoop granophyres suite which are found between the Bushveld granite and Rustenburg Layered Suite (SACS, 1980).

The BIC contains some of the richest ore deposits on earth. The reserves of the platinum group metals (PGM); platinum, palladium, osmium, iridium, rhenium and ruthenium are the world largest and there are vast quantities of iron, tin, chromium, titanium and vanadium (Barker et al, 2004).

The emplacement of the BIC involved numerous igneous activities (SACS, 1980); the felsic phase, the norite phase and the granite phase. Harmer (2000) suggested that the Bushveld cycle of formation had occurred within few million of years The Rustenburg Layered Suite consists of five limbs which are the Eastern Limb, Western Limb, the far Western Limb, Northern Limb and South Eastern Bethal Limb which is obscured by the younger sediments of the Transvaal Supergroup (Cawthorn et al,2006).

The Northern Limb to a certain extend is covered by the younger rocks, while the Eastern Limb stretches from Chuniespoort all the way to Stoffberg; a distance of 200km.The south eastern or Bethal Limb which was mapped using gravity geophysical method sounding (Kinnaird et al., 2004). The Western Limb similar to the Eastern Limb, extends for a distance of about 200km along an arc shape from near Thabazimbi to north of Pretoria. It outcrops poorly compared to the Eastern Limb.

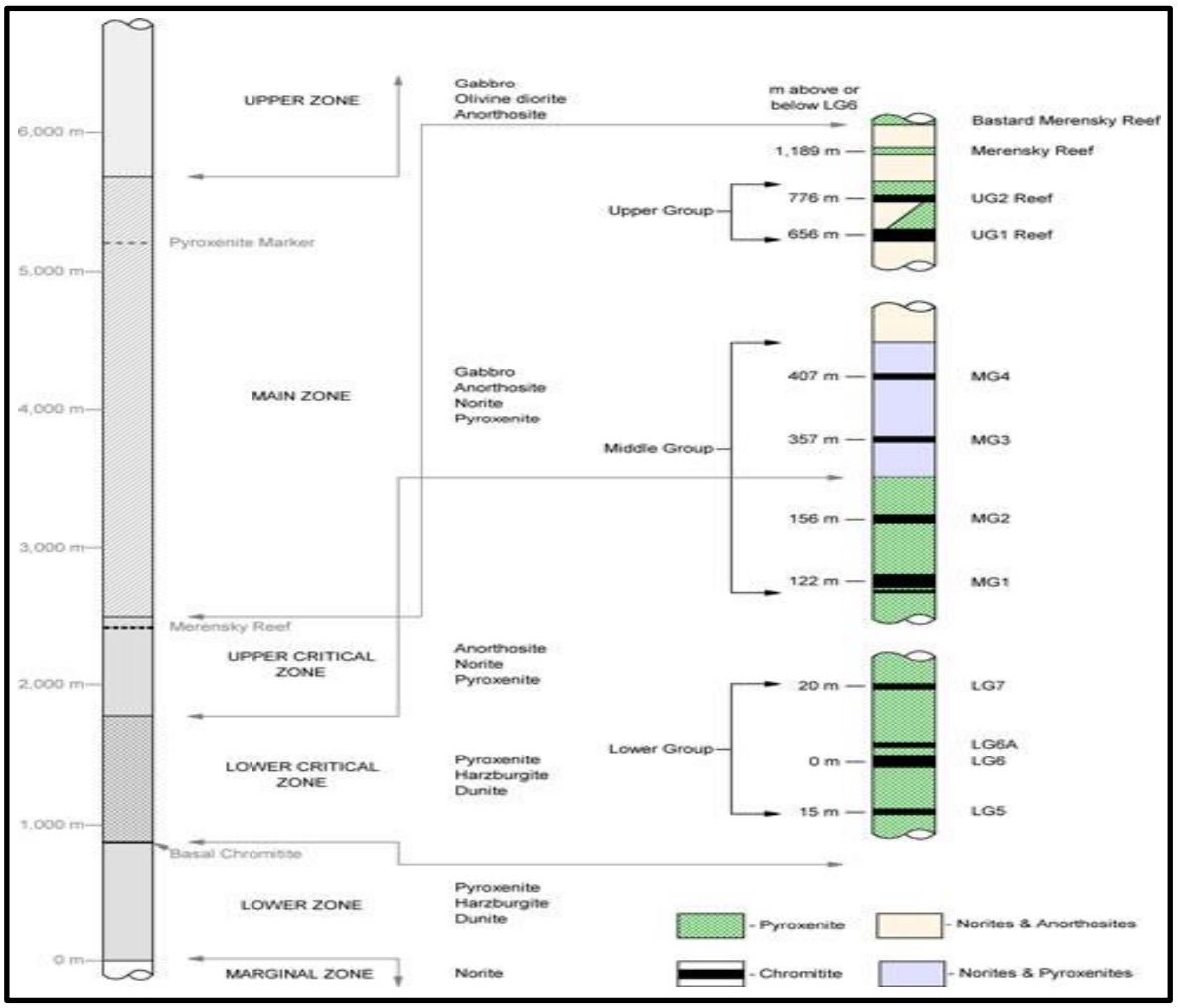

Figure 2.1: General stratigraphy of the Bushveld complex (Lomberg et al., 2004).

2.1.1 Stratigraphy of the Bushveld Complex

The stratigraphy of the Bushveld complex can be explained in terms of the Rashoop Granophyre Suite which overlies the RLS, Lebowa Granite Suite and the Rustenburg Layered Suite which is the largest and oldest mafic layered complex as illustrated by figure 2.2.

2.1.1.1 Rooiberg Group Volcanics

The Rooiberg Group occurs overlies the Rustenburg layered suite and it can also be subdivided based on lithology and chemistry. The four formations in the order in which they are superimposed from the oldest to the youngest; Dullstroom, Kwaggasnek, Schrikkloof and Damwal (Cawthorn et al., 2006). The Dullstroom Formation is the lowermost unit of the Rooiberg Group and overlies the sedimentary rocks of the Pretoria Group and near Stoffberg occurs both below and above the Rustenburg Layered Suite.

The Dullstroom Formation consists of basalt and basaltic andesite near the base and suddenly changes to more felsic upward, with various pyroclastic and aranaecous layers (Schweitzer et al., 1995).

2.1.1.2 Rashoop Granophyre Suite

The Rashoop granophyric rocks of the Bushveld complex occur between the Rustenburg Layered Suite and the Rooiberg volcanic rocks. The most predominating granophyres rocks are the Stavoran granophyres, these are shallow intrusive facies which lie in-between the rhyolites in the Rooiberg Group (Walraven 1987).

2.1.1.3 Rustenburg Layered Suite

The Rustenburg Layered Suite is regarded as a shallow intrusion which occurs below the Rooiberg felsites and Rashoop granophyres within the Transvaal Supergroup.

The rocks that are found within the Rustenburg Layered Suite ranges from the ultrabasic pyroxenites to the anorthosite in the lower parts and the norite, gabbro and magnetite gabbro in the upper part.

The basic rocks within the Bushveld complex are widely developed in eastern and central parts of the Rustenburg Suite. The Rustenburg Layered Suite is divided into five major zones namely the Marginal Zone, Lower Zone, Critical Zone, Main Zone and Upper Zone (Fig 2.1). These zones occur in the Northern, Eastern and Western limbs of the Bushveld complex (SACS, 1980; Eales and Cawthorn 1996).

2.1.1.4 Marginal zone

The Marginal zone is not always present throughout the Bushveld complex as it may have been eroded away. However the Marginal Zone thickness up hundred meters along the Bushveld Complex basal contact. This does not host any mineralization of economic importance. The Marginal Zone comprises mainly of medium grained norites and pyroxenites (Kolobeng norite and Ratasegae norite) with varying proportions of accessory clinopyroxenes, quartz, biotite and hornblende (SACS, 1980). The presences of the other accessory minerals indicate that there was contamination from the underlying sediments of the Transvaal super group (Walraven F, 1981).

2.1.1.5 Lower zone

The Lower Zone is poorly exposed and not extensive in many parts of the Bushveld complex intrusion. Good exposure occurs within the eastern limb along the Olifants River trough and with a thickness of 800m. In the eastern limb's, the lower zone is dominated by the presences of orthopyroxene rich rocks. The Lower Zone can be sub-divided into three zones, namely - the lower pyroxenites that contain an average of 98% orthopyroxene with minor plagioclase and clinopyroxene and the interlayered olivine rich and orthopyroxene rich cumulates which are harzburgites and dunites. Overlying the above is the upper pyroxenite, is similar to the lower pyroxenite in terms of composition but the variation in the size of the grains, and distinguishes the layering of the various rock units.

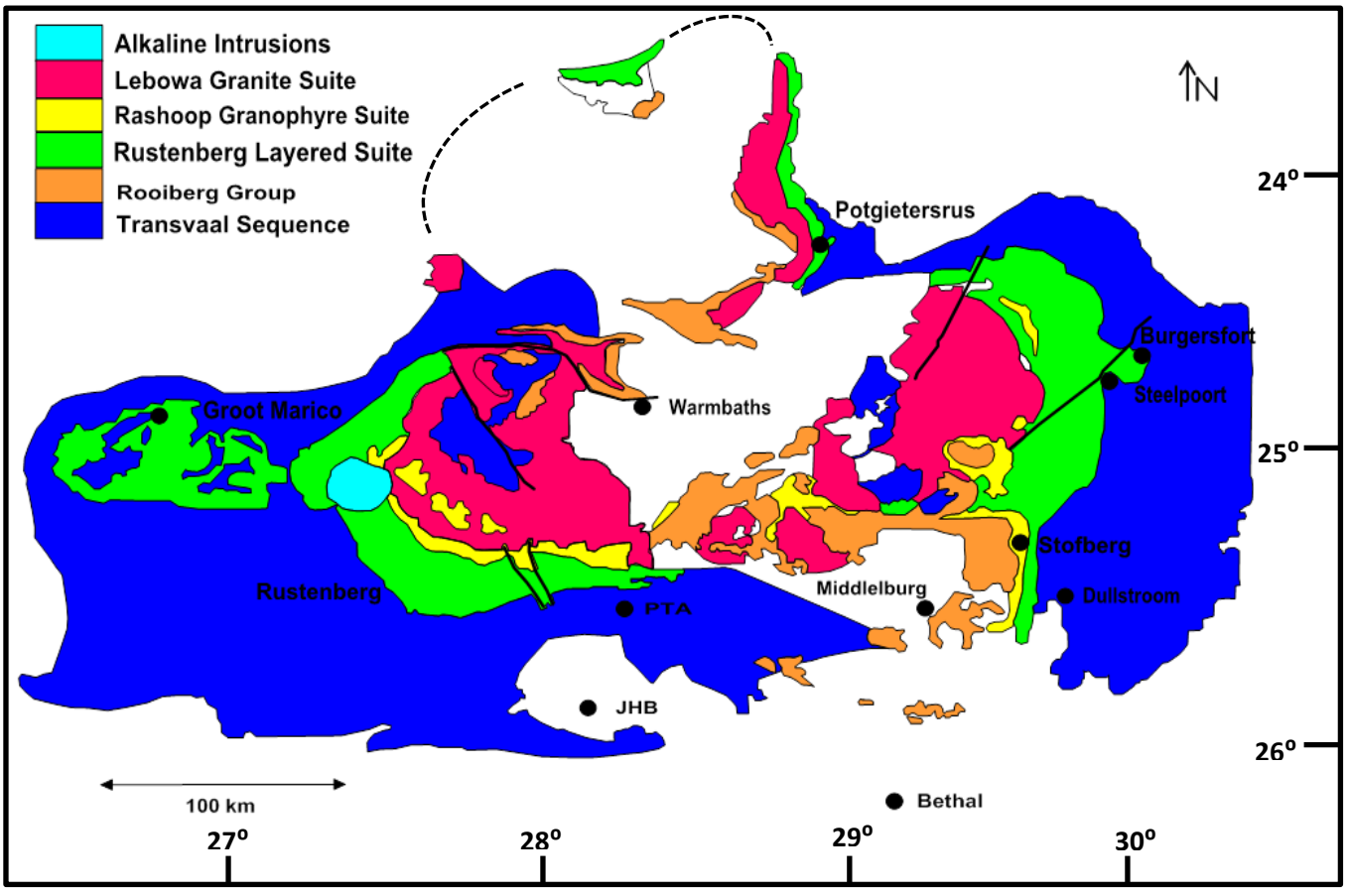

Figure 2.2: Geology of the Bushveld complex, illustrating the five limbs (Kinnaird J.A,2005)

2.1.1.6 Critical zone

The Critical Zone in the Bushveld Complex hosts the platinum and the chromitite deposits in its layers. The Critical Zone is about 1500m thick and can be further subdivided into the Lower Critical Zone and the Upper Critical Zone based on their mineral compositional variation. The sub division is marked by to the presence of the cumulus plagioclase, which forms an anorthosite layers between the MG2 and MG3.

The Lower Critical Zone is mainly composed of the ultramafic rocks such as dunites, pyroxenite and harzburgite while the Upper Critical Zone consists of pyroxenite, norites and anorthosite. Both the Upper and Lower Critical Zones contain numerous layers of chromitite layers (Cawthorn; et al., 2006).

Within the Eastern, Western, Northern and far Western limbs of the Bushveld Complex, the chromitite layers sub-divided into the Lower Group, Middle Group and Upper group (Hatton and Van Gruenewaldt, 1987; Schurmann et al, 1998).

The Lower Group (LG) consists of seven chromitite layers which are hosted within the feldspathic pyroxenite. The thickest and economically mineable layer is the LG6 (also known as the Steelpoort seam). The Middle Group (MG) which is found between the Lower and Upper Critical Zone, usually consist of four chromitite layers hosted within the feldspathic pyroxenite. This is not always the case as in the Eastern limb where only three chromitite layers are visible (MG1 to MG3). The Upper Group (UG1-UG3) and Middle Group (MG1-MG4) chromitite layers are hosted within a series of norite and anorthosite.

2.1.1.7 Main zone

The Main Zone is more than 3000m in thickness and considered to be the thickest zone of the Rustenburg Layered Suite. The Main Zone can be further subdivided into upper and lower zone. The Main Zone extends from the top contact at the Giant mottled anorthosite to the cumulus magnetite. It consists of gabbronorites with minor amounts of anorthosite, while the occurrence of pyroxenite bands in this zone is quiet rare. There is no olivine and chromitite present in the zone, but there is a presence of cumulus magnetite at the top of the zone.

2.1.1.8 Upper zone

The most striking feature about the upper zone is the presence of some 25 magnetite layers in the Eastern limb (Molyneaux, 1974).The Upper Zone has been divided into four subzones by Molyneaux (1970) and Von Gruenewaldt (1973).

The basal subzone A is marked the first appearance of magnetite, subzone B refers to the olivine-free lithologies above the main magnetite layer, the base of subzone C and is marked by the reappearance of cumulus olivine and subzone D by the appearance of cumulus apatite. The magnetite layers consist of sharp bases, but gradational tops.

2.1.1.9 Lebowa Granite Suite

The Bushveld granite suite is also known as the Lebowa Granite Suite, which mainly consists of the Nebo Granite.

This granite lies beneath the mafic rocks of the Rooiberg Group. The two rock suites are separated by a granophyric rock except in the Eastern limb of the Bushveld Complex where a dyke cuts the Rustenburg Layered Suite.

The Nebo granite consists of mainly of the potassium feldspar, quartz, plagioclase and some other mafic minerals. In some parts of the Potgietersrus it has been established that the granite is not the same but rather has shown an enrichment of the barium and rubidium (SACS, 1980).

There has also been a decrease in the content of the hornblende from the bottom to the top of this Granite suite and the hornblende being replaced by biotite in the uppermost of this suite (Walraven F, 1981).

The Lebowa Granite Suite consist of seven facies with variety of finer grained intruding the porphylitic types, namely the paramount one being the Nebo granite, aplitic lease granite, coarse grained red Bobberjaarkop granite, coarse grained porpylitic Venera granites, porphylitic Balmoral leucogranite, porphylitic biotite rich Makutso granite and the fine to medium grained Klipkloof granite.

2.2 Geology of the Eastern Bushveld complex

Chromite deposits on the six farms in the eastern Bushveld Complex, where mapped in detail from 1952 -1955. The detailed field mapping was followed by diamond drilling on two of these farms. This work indicated that between Chuniespoort and farm Thorncliffe, the critical zone is divisible along strike into three sectors (Fig 2.3). The western sector extends from south of Chuniespoort to the Olifants River, the central sector, extends from the Olifants River in the south to Steelpoort River and the southern sector from Steelpoort to the Farm Thorncliffe (Cameroon, 1963).

2.2.1 Western sector

The Western sector extends from south of Chuniespoort to the Olifants River. The Western sector is poorly exposed and no adequate section of the critical zone in it can be given. It is only clear that the sequence of the rock units in the Western sector differs from those of the Central sector (Cameron, 1963).

2.2.2 Central sector

From the Olifants River to Steelpoort, the critical zone within the central sector is well exposed. On Farms Jagdlust, Winterveld and Umkoanes Stad, south of the Winterveld, the critical zone is exposed continuously from its base to the Merensky reef.

The Critical Zone, within the central sector can be sub-divided into two major series of rocks, namely;- the lower pyroxenite series, which consist predominately of pyroxenite and norites, and the upper anorthosites series consisting of anorthosites and norites.

The thickest chromitite layer in the Lower Group is the LG6 layer, also known as the Steelpoort seam (Schurmann et al.,1998). The continuity of the Steelpoort seam throughout the central sector is interrupted by the presences of faults and diabase dykes. The leader seam (Steelpoort seam) is continuous from Steelpoort to east of the Olifants River, on Farm Zeekoegat. The anorthosite series are composed of a thick anorthosite and nortic anorthosites. Some sections of the anorthosite series are interrupted by four pyroxenites that are accompanied by chromitites in certain sections.

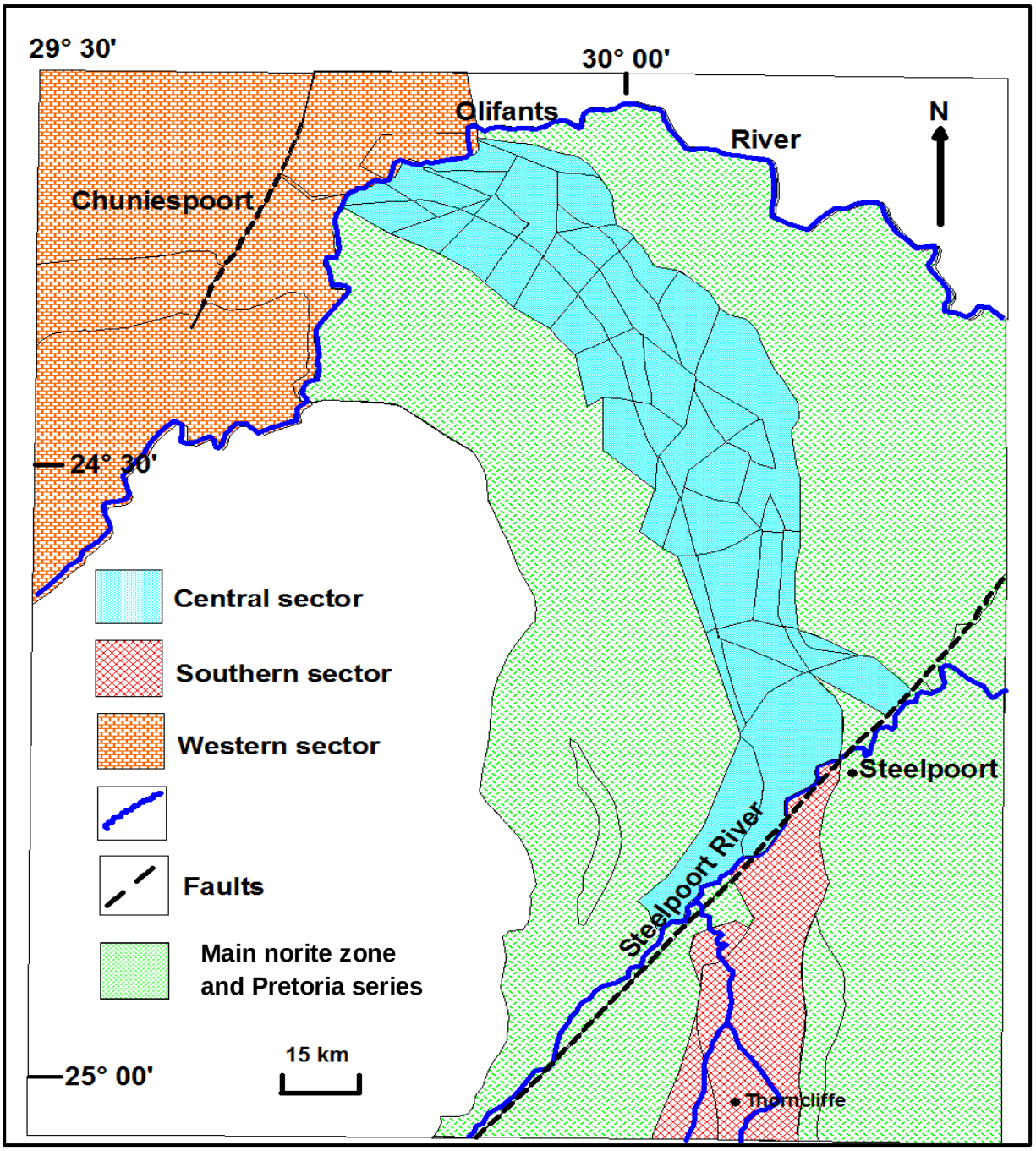

Figure 2.3: Map of the Eastern Bushveld complex, showing the Southern, Central and Western sector (from Viljoen and Schurmann, 1998).

2.2.3 Southern sector

In the northern part of the southern sector, the critical zone is made up of the upper anorthosite series and a lower pyroxenite series. The anorthosite series within the southern sector shows similar characteristics as to those of the central sector, but consist of anorthosite units that are separated by pyroxenite units with or without chromitites.

The pyroxenite series are composed of a succession of feldspathic pyroxenites, which towards the top they are disrupted by a zone of the interlayering of chromitites, anorthosites and pyroxenites (Cameron, 1963).

2.3 Geology of Dwarsrivier Chrome mine

Dwarsrivier Chrome Mine is located in the Tweenfontein section of the Eastern Bushveld Complex. The chromitite deposits within the Eastern Bushveld Complex are stratiform type of deposits, and occur as horizontal to sub-horizontal. These type of deposits contain high content of iron (40% - 46%) and a Fe/Cr ratio of <2. The stratiform deposits account for 90% of the economically exploitable chromitite resources in the world (Schurmann et al, 1998).

There are various layers of chromitites within the Eastern limb of the Bushveld Complex and they occur within the lower and upper critical zone in three different groups namely the Lower Group, Middle Group and the Upper Group. The Lower Group (LG) has seven chromitite layers, which are hosted within feldspathic pyroxenite units. These layers are named the LG1-LG7 (Boorman et al., 2003) The LG6 layer (also known as the Steelpoort seam) is the thickest chromitite which is currently being mined at Dwarsrivier Chrome mine.

The Middle Group has four chromitite layer named the MG1-MG4 which are hosted in either feldspathic pyroxenite or norite. Plate 2.1 shows the MG2 and MG3 chromitites layers, anorthosites, cumulus feldspathic pyroxenites and feldspathic pyroxenites at the portal entrance to Assmang Dwarsrivier chrome mine. The LG6 chromite layer at Dwarsrivier Chrome Mine is dips at 9^0 to 10^0 towards the west with approximately north-south strike and an average thickness of 1.86m meters (figure 2.4). The chromitite consist of pyroxene oikcrysts, which makes LG6 appear spotted.

Due to the gentle dip of the LG6 layer mining at Dwarsrivier Chrome Mine is conducted at an apparent dip instead of true dip. This is done for two reasons, firstly in order to enable the load haul dump (LHD) and other mining machinery easily access into the working areas. Secondly, mining on apparent dip makes it easy to control underground water because with the apparent the rate of water accumulation in the section is slower. So water gets pumped quicker than it accumulates.

The orebody at Dwarsrivier Chrome mine is associated with geological features: such as joints, dykes, faults, potholes as well as reef rolls. There are two types of joints found at Dwarsrivier mine, which are low angle joints or shallow dipping joints and vertical joints, which are classified according to their dip angle. The joints trend north to south, north east to south west, east to

west and northwest to south east direction. The low angle joints dip from 0^0 to 70^0 and while the vertical joints dips from 70^0 to 90^0. The most common faults that occur at the mine are normal faults and these results in a moderate displacement of the reef which ranges from 0.5m to 3m.

Plate 2.1: A photograph showing the different lithological units at the portal entrance to Assmang Dwarsrivier chrome mine (Letsoele, 2013).

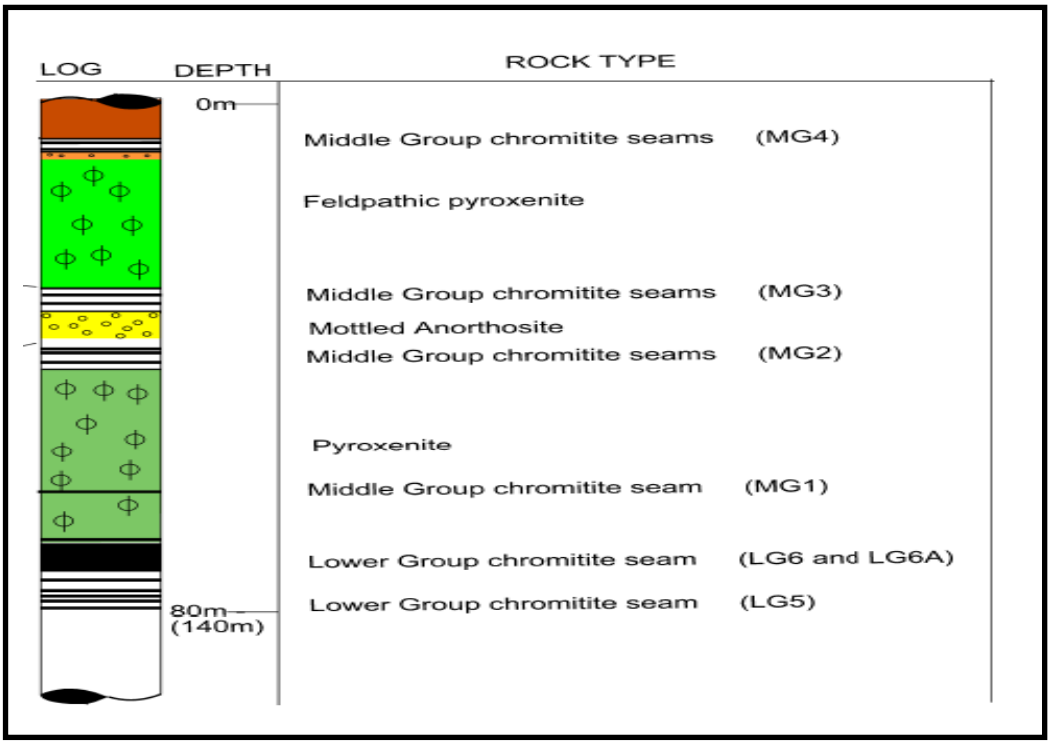

Figure 2.4: South stratigraphy of Assmang Dwarsrivier chrome mine (Christopher Letsoele,2010)

3 Methodology

3.1 Field methods and Sampling

Two surface boreholes were logged in detail at the transition boundary (between the MG2 and MG3 package) in order to identify the different lithologies, the contacts between the various rock lithologies and the structural features such as fault, joints and intrusions.

Quarter core samples of about 10 cm to 15 cm where taken from two surface boreholes. Borehole DWR74 was drilled on the far eastern side and DWR 172 which was drilled on the far western side of the mining property of Dwarsrivier 372KT farm. The sampling was done within the MG2 and MG3 package at regular intervals. Dwarsrivier chrome mine sampling procedure was used to ensure that no contamination took place during the sampling process.

Sixty-nine samples collected 34 samples from borehole DWR 74 and 35 samples from borehole DWR 172. There were used for petrography and geochemical analysis.

3.1.1 Laboratory Studies

3.1.1.1 Petrography

Petrographic studies were carried out at the University of the Western Cape's microscope lab. Petrography was used to determine the mineralogical composition of the feldspathic pyroxenites, chromitites, anorthosites and chromitite pyroxenites which occur in the MG3 package and MG2 package. This involves identification of the major rock forming minerals, accessory minerals, and evaluation the description of the texture of the rocks, grain size distribution as well alteration.

3.1.2 Geochemical sample preparations

The rock samples were washed with distilled water and dried. A portion of the quarter core was cut and put in the electric jaw crusher, to reduce the size of the sample and then placed the crushed sample in the milling machine to pulverise the sample to fine homogenous powder at University of the Western Cape Geology laboratory.

After every sample was milled, the milling pot was washed, dried and wiped with acetone to ensure that there is no contamination of the next samples to be milled. All 68 samples where milled and place in sealable bags and taken the University of Stellenbosch, Environmental laboratory for XRF (X-Ray Fluorescence) analysis using pressed pallets.

The pressed pellets where prepared at the University of Stellenbosch, Environmental laboratory. The pressed pellets are prepared by pressing loose powder filled in a ring using a set of dices and press machine.

Ease of pelletization depends on the sample characteristics and grain size and this can be improved by sufficient pulverization. Mixing the powder sample with a forming agent is another solution if pelletisation is difficult. Manual press and automatic press machine are available and both have either 300KN or 500 KN maximum loads (Gakuto Takahashi, 2015).

The complete geochemical data for boreholes DWR74 and DWR172 was produced through XRF analysis from pressed pellets. The major and trace elements results are found in appendix A (DWR74 borehole) and B (DWR172 borehole). The XRF analysis for major elements or oxides was carried out on SiO_2, Al_2O_3, Fe_2O_3, MnO, MgO, CaO, Na_2O, K_2O, TiO_2, P_2O_5 , while for trace elements, the XRF analysis was carried out on pressed pellet which includes Ba, Ce, Co, Cr, Cu, Nb, Ni, Pb, Rb, Sr, Th, U, V, Y, Zn and Zr. Au Pd Pt.

For the LOI (loss on ignition), 0.5g of each milled sample was dried in an oven for 30 minutes to remove the moisture. The LOI was done at 1000ºC for a period of 40 minutes. The LOI included the total of volatiles content of the rock (including the water combined to the lattice of silicate minerals) and the gain on ignition related to the oxidation of the rock (mostly due to Fe).The calibration method for major and trace element analysis was by XRF, Rh Tube 3kWatt.

Data evaluation/ analysis

Petrographic studies where carried out on the one quarter core samples of feldspathic pyroxenites, chromitites, anorthosites and chromitite pyroxenites from the two surface boreholes, to determine their mineral composition, texture, alteration and grain size distribution. This was done in order to identify and classify the rock types and also to identify the petrographic characteristics which maybe as a result of certain geological processes.

In order to determine the geochemical and petrographic characteristics which distinguish the different rock types within the MG2 and MG3 package, the analytical data of the DWR 74 and DWR172 where processed using IBM SPSS 21, Geochemical Data Toolkit and Downhole Explorer.

Firstly the geochemical classification was performed using the cluster and discriminant analysis (IBM SPSS 21) applied on the oxides analytical data of the rocks, to identify the groupings that

correspond to the various rock types. The results of rock type's classification are illustrated by tables 5.13, 5.17, 5.21 and 5.25.

The cluster analysis coupled with discriminant analysis and field identification coupled with discriminant analysis are the two methods that were compared to see which one is the most reliable in terms of classification. The classification results of these two methods can be seen in table 5.50. Factor analysis was also used, in that it grouped elements into associations that may reveal a single process or geochemical characteristics that are regulated by the observed relationships.

Multivariate statistical methods such as factor analysis, cluster analysis and discriminant analysis were used for the rock classification. The cluster analysis was used to separate the geochemical samples into groups on the basis of similarities in their measured attributes. The discriminant analysis was used to characterise and classify new observation into a number of pre-defined groups, while the factor analysis was used to reduce the number of variables into smaller number of new combinations and to highlight the close similarities of variables with corresponding combination that could reflect the operation of a single process or geochemical characteristic.
Based on the multivariate statistical methods such as factor, cluster and discriminant analysis used to characterise the different types of chromitite, chromitite pyroxenite, feldspathic pyroxenite and anorthosite, in terms of trace elements. The results were used to construct spider diagrams that illustrated the difference in concentration of the trace elements within the samples of the different types of chromitite, chromitite pyroxenite, feldspathic pyroxenite and anorthosites.

The purpose for factor analysis is to reduce the number of variables into smaller number of new combinations and to highlight the close similarities of variables with corresponding combination that could reflect the operation of a single process or geochemical characteristic (Rose et al., 1979). It is a useful tool for investigating variable relationships for complex concepts. It permits the investigation of concepts, which are difficult to measure directly, by collapsing large number of variables into fewer interpretable underlying factors. The number of factors is selected based on the Kaiser criterion (Kasier, 1958) for which only the factors with eigenvalues greater than 1 are retained (Cloutier et al., 2008) and the varimax rotation is utilized to maximize the variance of the factor.

In geological studies, factor analysis has been mainly applied for analysis of whole rock samples and to identify geochemical trends of environmental or economic interest (Artiolli et al.,

2008; Dawson and Sinclair, 1974; Hubert, 1986; Moh'd and Powell, 2010; Patinha, 2002; Reimann et al; 2002; Winderbaum et al.; 2012).

Factor analysis was used in the characterisation of sulphide mineralisation and grouping these hydrothermal vein Pb-Zn-Cu-Ag deposits in Portugal. The study of minor elements in the sulphides and characterise the deposits into different geochemical categories, illustrating the difference between the individual deposits and group of deposits. This experiment provided evidence that proves that indeed factor analysis can be used as a powerful tool for the study of minor and trace elements that are present in minerals and the characterisation and categorization of districts in which they occur (Marques de Sa et al, 2014).

A group of forty two coal samples, which included coal blends, prepared for coking and lump coal. The samples were characterised based on the 16 coal properties. The separation of the 42 samples where performed by principal component analysis and hierarchical clustering. Results of the statistical evaluation indicated that, the blends suitable for coking can be distinguished from lump coal. The use of the multivariate statistical methods has shown that they it's an appropriate tool for separation of a single coal from coal seam and coal blends prepared for coking (Zdeněk Klika et al, 2014).

The hierarchical cluster analysis is an effective graphical statistical method of data classification into hierarchical clusters. There are different clustering techniques, but hierarchical clustering is one of the most widely applied in earth science (Davies, 1986). It can separate geochemical samples into groups on the basis of similarities in their measured attributes (Rose et al., 1979).
In clustering, the objects are grouped such that a similar object falls into the same class. In hierarchical clustering, the larger similarity observations are first grouped and then successively the next most similar observations. The steps are repeated until all the observations have been classified. The levels of similarity were observations are used to develop a dendrogram. Cluster analysis using ward method, as the linkage method, to calculate the Euclidean distance between the variable averages is used. Ward method is more successful to form cluster that are more or less homogenous and distinct from the cluster, compared to the other methods such as weighted pair-group and furthest neighbor.
It was used to analysis the geochemical data from five boreholes in the Jinwozi goldfields in North Western China, to investigate the mineralisation similarities of the samples in the boreholes.
The geochemical data from Jinwozi goldfield used factor analysis for determining element association and delineation of anomalies. The first factor is positively loaded with Ag, Au, As

and Hg which is the major mineralization, while the second factor (minor mineralization) is positively loaded with Cu and Zn. Multivariate analysis is of great importance in interpreting the complexity of multi-dimensional geochemical data set.

Multivariate techniques were used to characterise and differentiate between Kurun and Uro phosphate ores. Results of the the multivariate analysis indicated that the most abundant radionuclides in the Kurun and Uro phosphate are U-238, Ra-226, and Th-230. Hierarchical cluster analysis indicated that U-238 behave in a similar manner within the two types of phosphates. The most abundant radionuclides are U-234, Po-210, Ra-220, Th-230 and all belong to the uranium 238 decay series. (Majdi et al., 2011).

Discriminant analysis is a multivariate statistical technique to devise rules for assigning a new observation characterised by set of measured variables into a number of predefined groups. (Tatsuoka MM,1988). The discriminant statistical procedure that requires a series of steps, it allows for a consistent approach to processing and interpretation of the multi element geochemical data. The selection of appropriate samples that represent the barren and mineralized group is the most important step in the procedure. The assigning of the unknown samples with the one of the pre-defined training groups is another important step in terms of the allocation procedure.

Discriminant analysis has been used in geochemical exploration to distinguish target observation from background observation. This investigation showed that within the Egbe area, spessartine bearing amphibole/ micra schist co-occurs within known targets of rare metals. The mineralized pegmatites indicate the presences of spessartine-bearing amphibole, which was not indicated on the geologic sketch map. While in the Iregun and Wamba areas, the targets for the rare metals occur on the talc-schist and manganiferous gneisses (Siad et al., 1994).

The major and trace elements data was used in determining whether the MG2 and MG3 package resulted from a single or multiple magma pulses. This was done through the use of Spider diagrams that investigating the behaviour of the large ion lithophile elements (Rb, Ba and Sr), which are placed on the left of the diagram in order of incompatibility and the high field strength elements (HFSE; Th, U, Ce, Zr, Nb, Ti and Y) that are immobile elements arranged from right to left in order of increasing incompatibility. The results of the spider diagrams are presented in figure 5.16, 5.17, 5.18 and 5.19.

The downhole explorer was used to depict the various ratios such as SiO_2/Al_2O_3, Sr/Ba, Co/V and Mg# that were used by various authors to determine whether there was a change in the geochemistry of the magma or not.

4 Petrography

4.1 Introduction

The objectives of this work are to compare and contrast the geochemistry and the petrography of the MG3 package and MG2 package within the Critical Zone of the Bushveld Complex and to ascertain their origin from a single magma source or not. Petrography was used to determine the mineralogical composition of the different rocks types hosted in the MG2 package and MG3 package. Major rock forming minerals and accessory minerals contents were estimated and the texture of the rocks, alteration and grain size distribution described.

Two surface boreholes from Dwarsrivier Chrome Mine were used in this investigation namely DWR74 (drilled to a depth of 59.35m) and DWR172, (drilled to a depth of 234.14m). DWR 74 is situated on the far eastern side of the Dwarsrivier Chrome mine mining property, while DWR172 is on the far western side, with distance of 1150m separate the two boreholes.

The two boreholes intersected the following lithologies within the critical zone of Dwarsrivier Chrome mine as shown in figure 4.1. From the base there is the MG1 package, which is made up of the interlayering between the feldspathic pyroxenites and chromitites. The MG1 package is overlain by the MG2 package. Interlayering of chromitites and feldspathic pyroxenites but also occur in the MG2 package. The MG2 package is separated from the MG3 package by thick anorthosite layer (cumulus plagioclase). Interlayering between the chromitites and feldspathic pyroxenites also occurs in the MG3 package.

The Critical Zone carries huge deposits of chromitites within the lower (LG), middle (MG) and (UG) layers (Hatton and Von Gruenewalt, 1987; Schurmann et al.; 1998). Chromitite layers include the whole lower group (LG1 through LG7) along with the MG1 and MG2. The categorizing scheme was initially developed by Cousins and Feringina (1964) for the western limb. This zone displays spectacular layering of chromitite, pyroxenite, norite and anorthosite (Cameron, 1980, 1982).

The Middle Group contains four chromitite layers (MG1-4). The occurrence of plagioclase is between MG2 and MG3 in both the Western and Eastern limbs (Cawthorn et al.; 2006), the layers MG3 and MG4 already belong to the Upper Critical Zone.

The LG6 chromitite layer (economical seam) was found at shallower depths on the eastern side of the mining property within the DWR74 compared to DWR172, which is on the western side, where it's found at deeper depths.

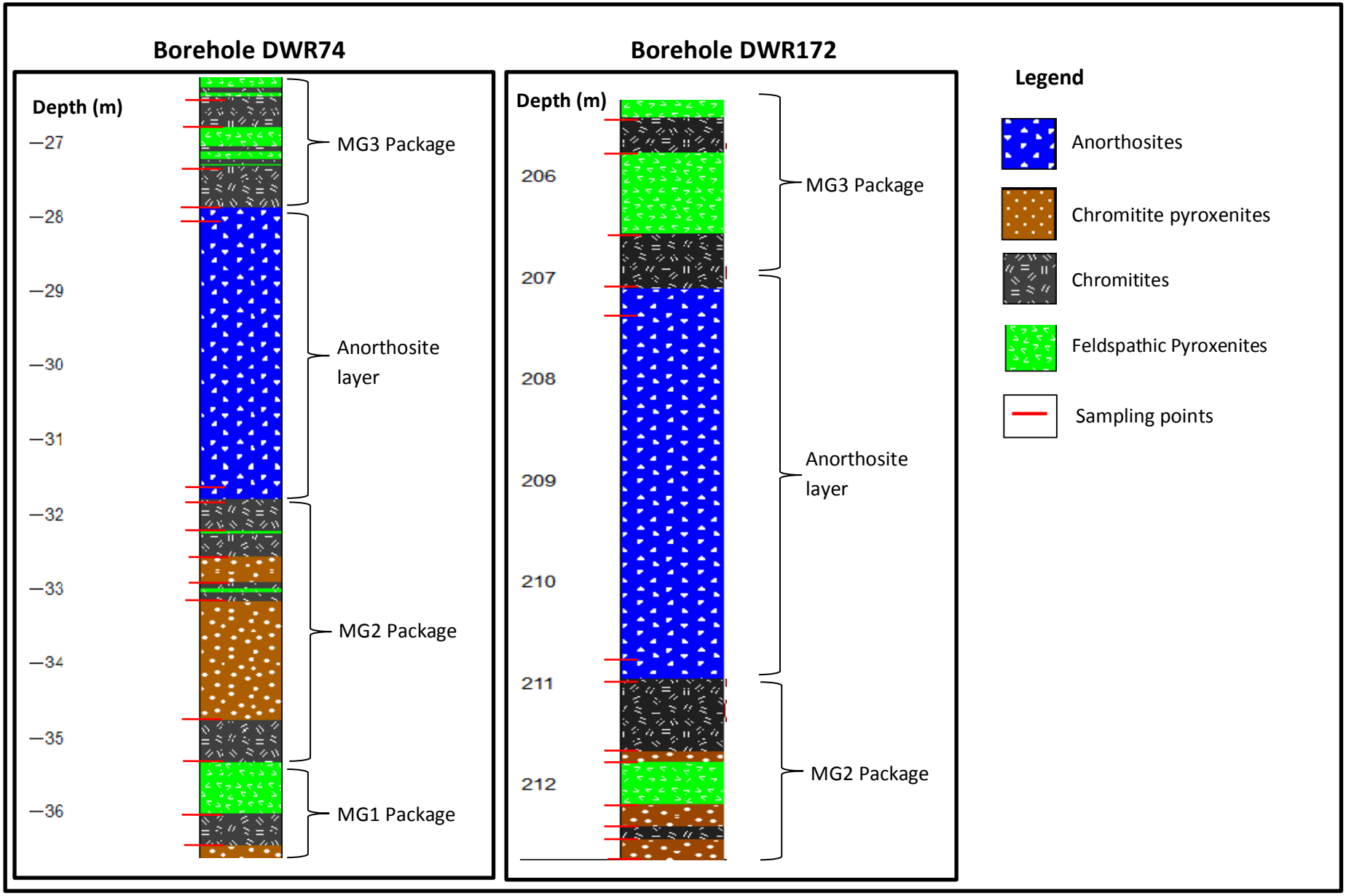

Figure 4.1: An illustration of the various rock types in boreholes DWR 74 and DWR 172

4.2 Core logging

4.2.1 Borehole DWR 74

The surface borehole DWR74 situated on the far eastern side of the mining property, the borehole consists of the following lithologies from the base. At the base of borehole DWR74 the MG1 package occurs between from 36.67m to 33.18m depth. It consist of a 0.21m chromitite pyroxenite layer at the base that is overlain by a chromitite pyroxenite layer, there is a 0.43m thick chromitite layer.

The contact between feldspathic pyroxenite layer and chromitite pyroxenite layer is gradational to a depth of 36.46m. Above the chromitite layer, there are three 0.19m to 0.33m thick chromitite and feldspathic pyroxenite layers that interlayered and extend to the top of the MG1 package. The contacts between the feldspathic pyroxenites and chromitite layers are sharp.

The MG2 package extends from 33.18m to 31.79m depth and the base consists of a 0.13 chromitite layer at a depth of 33.18m. From a depth of 33.05m to 31.79m, there is an interlayering of 0.03m to 0.21m feldspathic pyroxenite and chromitite. A relatively thicker chromitite pyroxenite occurs between 32.91m and 32.56m. The MG2 package is capped by a 0.21m thick chromitite layer and a 3.91m thick anorthosite layer. This anorthosite layer separates the MG3 package from MG2 package.

The MG3 package extends from a depth of 27.88m to 26.07m. The base of the MG3 package at depth of 27.88m, consist of a 0.57m chromitite layer that overlies the anorthosites layer. There is a sharp contact between the anorthosite and chromitite layers. This is followed by interlayering of feldspathic pyroxenite and chromitite layers, with thickness varying from 0.02m to 0.22m. The contacts between the feldspathic pyroxenite and chromitite layers are sharp.

4.2.2 Borehole DWR 172

The surface borehole DWR 172 is located on the far western side of the mining property. The MG2 package extends from a depth of 212.74m to 210.27m. A 0.20m thick chromitite pyroxenite occurs at the base of the MG2 package and is overlain by a 0.13m chromitite layer. The contact between the chromitite and chromitite pyroxenite layer is gradational.

Further up, 0.1m thick pegmatoidal pyroxenite, with disseminated chromite overlies the chromitite layer. The pegmatoidal pyroxenite with disseminated chromite is overlain by a 0.12m chromitite pyroxenite that has about 60% of disseminated chromite. The contact between the pegmatoidal pyroxenite with disseminated chromite and chromitite pyroxenite at a depth of 212.19m is a gradational contact.

Further up, a 0.42m thick feldspathic pyroxenite layer with a gradational contact overlies the chromitite pyroxenite layer. Upwards at 211.77m, a 0.10m chromitite pyroxenite overlies the feldspathic pyroxenite which is overlain by a 0.71m chromitite layer and then an anorthosite layer that is interlayered by a 3.55m thick feldspathic pyroxenite.

MG3 package occurs from 206.98m to 205.23m. The MG3 package, a 0.55m chromitite layer followed by an anorthosite layer, at a depth of 207.01m, followed upwards by a 0.69m chromitite and feldspathic pyroxenite layers. The latter is overlain by 0.35m chromitite layer. The MG3 package is capped by a 0.19m thick feldspathic pyroxenite. The contacts between the feldspathic pyroxenites and chromitite layers are sharp.

4.3 Rock Types

The four rock types were therefore identified during the core logging namely: feldspathic pyroxenites, chromitites, anorthosites and chromitite pyroxenites. The feldspathic pyroxenites, chromitites, chromitite pyroxenites and anorthosites occur in the MG2 and MG3 packages that were intersected by boreholes DWR74 and DWR172. Macroscopically these rock units have similarities in terms of colour and grain size. Under the microscope some differences become apparent in terms of modal mineral composition, grain size distribution, texture, ore minerals content and alterations features?

Abbreviations were used in the annotation of the various mineral names within the four rock types in the thin sections below. The following minerals have been identified and their abbreviations were used, Clinopyroxene (Cpx), orthopyroxene (Opx), Plagioclase (Plag) and Chromitite (Chr).

4.3.1 Feldspathic Pyroxenites

Macroscopically the feldspathic pyroxenites described are as light green to dark green with medium-grained pyroxene with white intercumulus coarse-grained feldspars as seen in plate 4.2. The term feldspathic pyroxenite is informally used to describe a lithology comprising of cumulus orthopyroxene with significant intercumulus feldspar (Kinnaird, 2005). The feldspathic pyroxenite consists of 35% clinopyroxene, 30% orthopyroxene, 20% plagioclase and 15% chromite.

The fine to coarse-grained clinopyroxenes and orthopyroxenes consist of subhedral to anhedral crystals, while the medium-grained plagioclases have subhedral crystals and occur interstitially between the orthopyroxenes and clinopyroxenes.

Within the feldspathic pyroxenite, the chromite occasionally occurs on top or along the pore spaces of orthopyroxene and clinopyroxene grains. The feldspathic pyroxenites show variable textures from ophitic, poikilitic to orthocumulate textures. There is evidence of alteration even though it is not that pervasive. The alteration occurs along the cracks and grain boundaries in the form of serpentinisation within the clinopyroxene and orthopyroxene grains illustrated by plate 4.3B, plagioclase commonly alters to sericite.

Macroscopically the feldspathic pyroxenites do not show any variation from the MG3 package to MG2 package. However in borehole DWR74 at a depth of 26.07m plagioclase decreases down the MG3 package, and changes from a cumulus to an intercumulus texture. Chromitites occurs as a minor constituent in the feldspathic pyroxenites MG3 and MG2 package. The shapes of the chromite vary from anhedral to subhedral crystals.

The MG3 feldspathic pyroxenites in borehole DWR172 show high content of plagioclase and chromite at 205.77m depth but a decrease in plagioclase and chromite content down the stratigraphy were the plagioclase occurs as an intercumulus mineral with little or no presences of chromite at 211.87m depth in the MG2 package.

The size of the orthopyroxene and clinopyroxene grains in borehole DWR74 vary from a fine – to-medium grained and then coarse grained between 26.79m and 27.05m depth in the MG3 package. Some orthopyroxene grains within the MG3 package exhibits bended exsolution lamellae in DWR172 at depths of 205.77m. In DWR74, feldspathic pyroxenites, the orthopyroxenes don't exhibits bended exsolution lamellae in both MG3 and MG2.

The chromites in the MG3 feldspathic pyroxenites at 205.87m depth occurs on top of the plagioclase, orthopyroxene and clinopyroxene grains while within the MG2 feldspathic pyroxenites at 212.07m depth, the chromites occur along the pore spaces or along boundaries of orthopyroxene and clinopyroxene as shown in plate 4.3B.

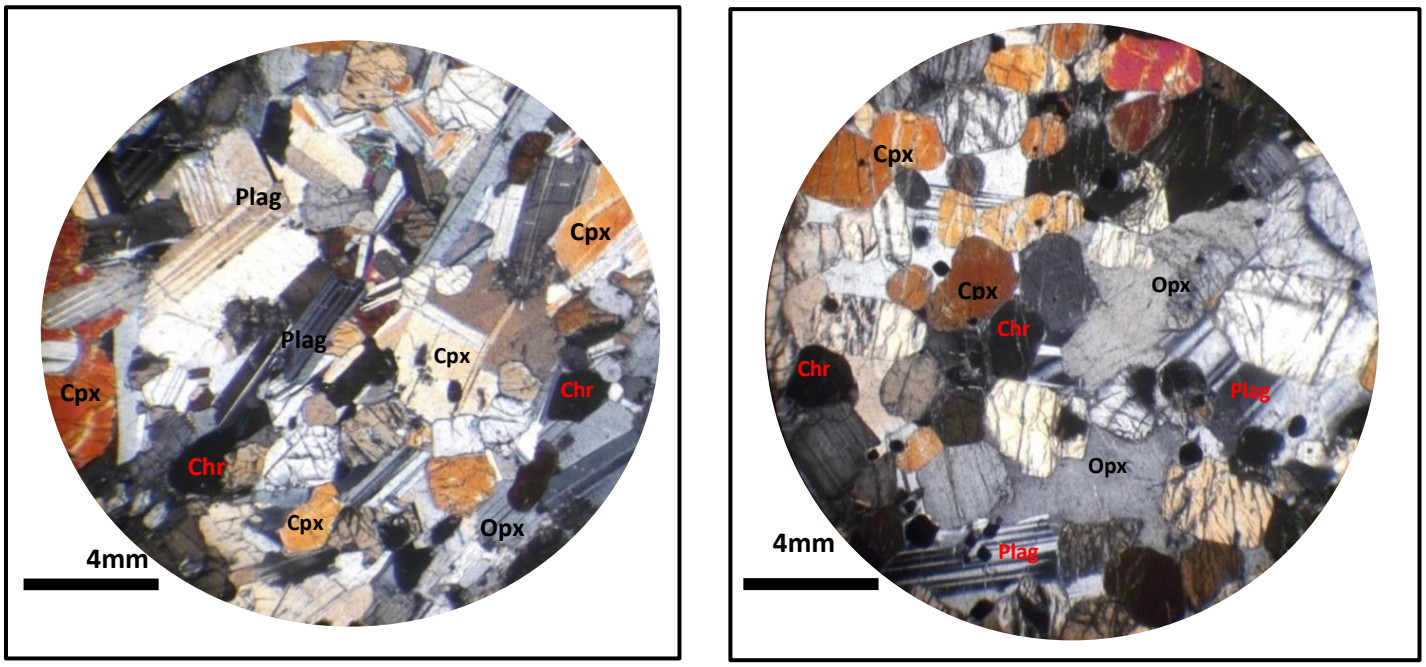

Plate 4.1: The feldspathic pyroxenite samples under a microscope. (A) Show the subhedral crystals shapes of the plagioclase. (B) Show orthopyroxenes and clinopyroxenes that exhibits alteration in the form of serpentinisation along the veins.

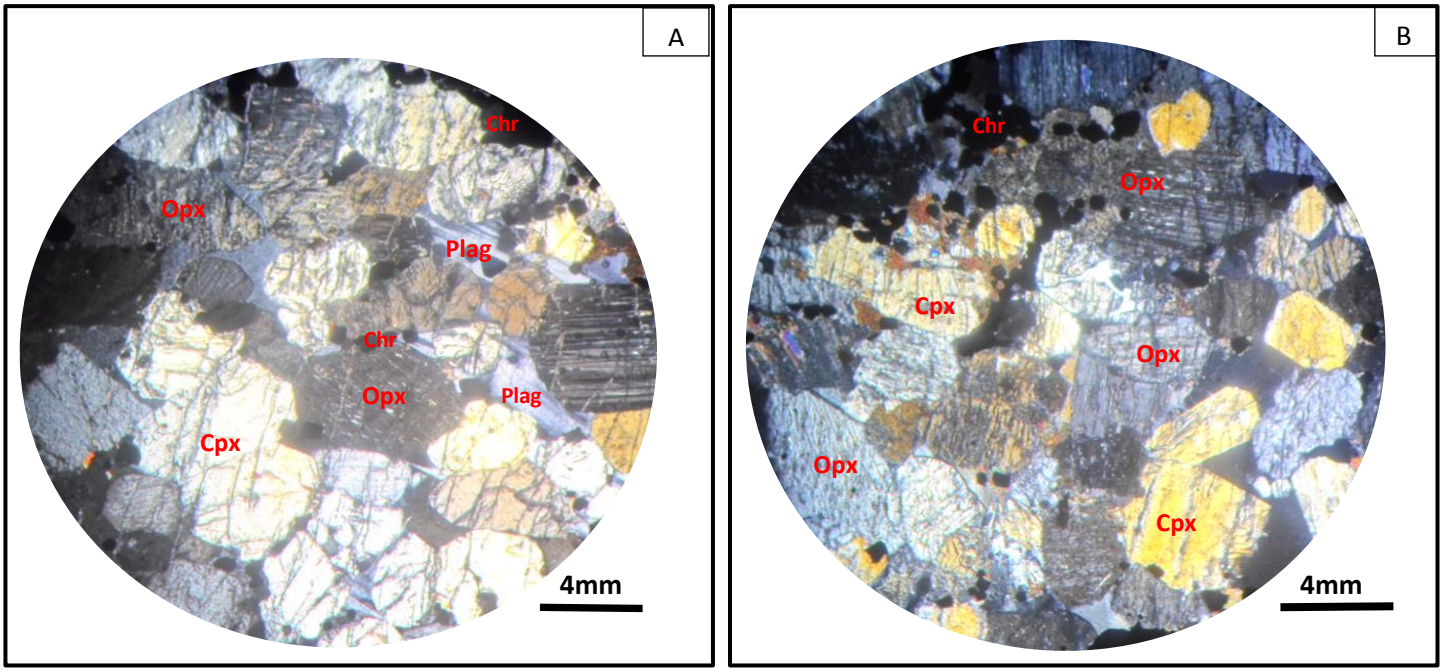

Plate 4.2: Feldspathic pyroxenite sample under a microscope. (A) The plagioclase content decrease, while the clinopyroxene and orthopyroxene content increases. (B) Chromitite grains occur as stains on the pyroxenes.

4.3.2 Chromitites

Macroscopically, chromitites are black to grayish black fine to medium-grained, with brown streak and metallic to greasy luster. The chromitites described as an igneous cumulate rock that which is mainly composed of chromite shown in Plate 4.5. Microscopically the chromitites consist of 60% chromite, 15% orthopyroxene, 20% clinopyroxene and 5% plagioclase. The fine to coarse-grained chromites consists of subhedral to anhedral crystal shape illustrated by plate 4.6A.

Plate 4.6A and 4.6B show medium to coarse grained, orthopyroxenes and fine to coarse-grained clinopyroxenes which are anhedral crystal in shape. Alteration occurs along the cracks of the orthopyroxene and clinopyroxene grains in the forms of serpentinisation. In places, alteration occurs along the cracks and grain boundaries of plagioclase and moderately alters it to sericite. Nevertheless, the alteration is not pervasive.

Macroscopically the chromitites in the MG2 package and MG3 package from both boreholes DWR 74 and DWR172 don't show any difference.

In borehole DWR74, the chromitites at depths of 26.27m in the MG3 package show higher content of clinopyroxene than those in the MG2 package at 32.26m. Chromitites in the MG3 package contain plagioclase and orthopyroxene. The contrary is the case in the in the MG2 package.

In borehole DWR172, at depths of 205.57m the clinopyroxene content in the MG3 package are lower than in the MG2 package at depths of 211.46m. Within the MG2 package orthopyroxene occurs, but is absent in the MG3 package. Both the MG3 package and MG2 package of borehole DWR172, in plate 4.6 B does not contain plagioclase.

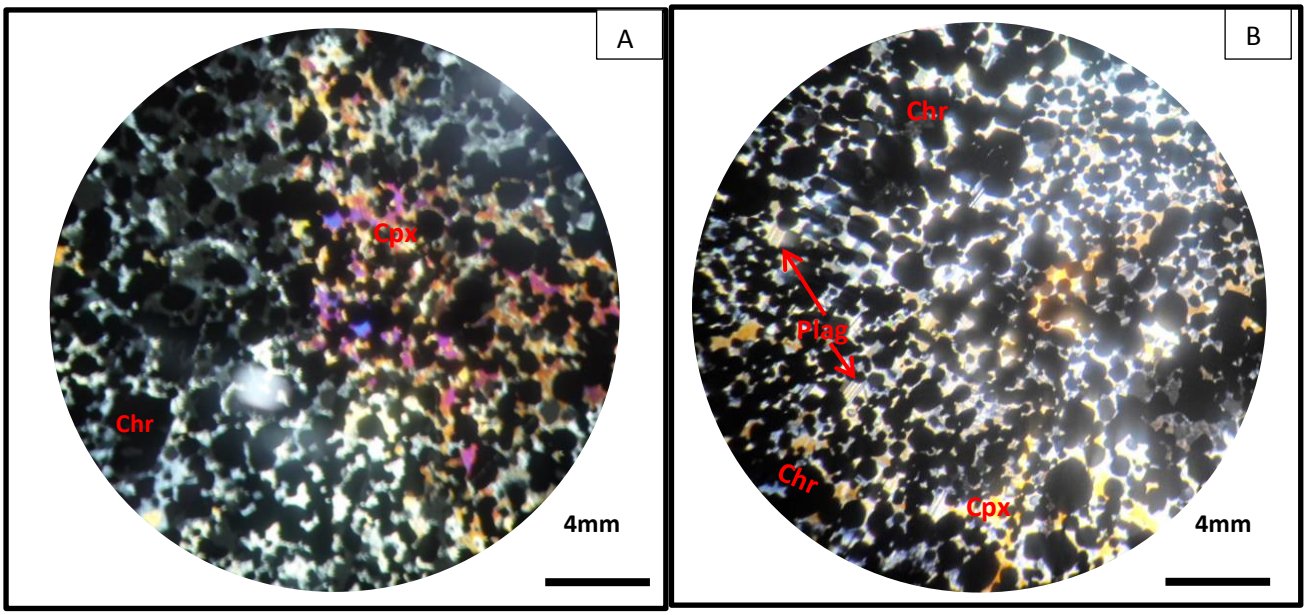

Plate 4.3: Chromitite samples under a microscope. (A) and (B) shows the orthopyroxene and clinopyroxene that occurs as an intercumulus mineral between the chromitite grains.

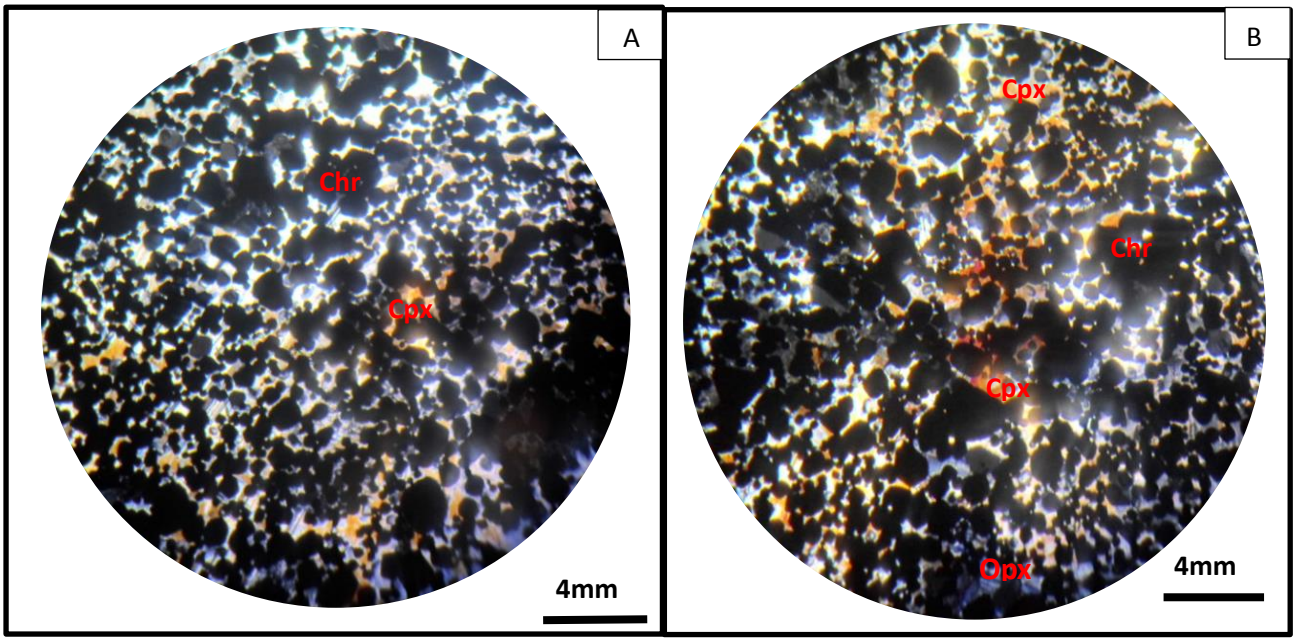

Plate 4.4: Chromitite samples under a microscope. (A) Shows fine to coarse-grained chromitites. (B) The absences of plagioclase, orthopyroxene and clinopyroxene are the dominant phase.

4.3.3 Anorthosites

Anorthosites are macroscopically composed of about 90 % of plagioclase interspersed by dark brown or greenish brown pyroxene as well as traces of disseminated chromitites (plate 4.8). The anorthosite is composed of 90% plagioclase, 2% chromitite, 3% orthopyroxene and 5% clinopyroxene. The fine to coarse orthopyroxene grains (Plate 4.9 A) and fine to medium-grained clinopyroxene grains are characterised by anhedral crystal shapes, while the fine-grained chromitites have a subhedral to anhedral crystals. The medium to coarse plagioclase grains exhibits a subhedral crystal shape. The anorthosites are characterised by adcumulate texture.
The plagioclase has repeated twining which results in the fine parallel bands in alternatively reserved positions called polysynthetic twining. The coarse-grained orthopyroxenes in plate 4.9B exhibits banded exsolution lamellae. Within the anorthosite, the fine to medium-grained chromitites occasionally occurs on top of or along the pore spaces between orthopyroxene and clinopyroxene grains. Sercitisation occurs in plagioclase grains and the orthopyroxene grains are serptinised.

Marcoscopically there are no marked differences in the anorthosites below MG3 package and those above the MG2 package. However in borehole DWR74 the plagioclase content below the MG3 package at depths of 27.88m increases towards the MG2 package at depths of 31.79m. Contrarily, the clinopyroxene and orthopyroxene content decreases. Furthermore clinopyroxenes change from a cumulus to an intercumulus mineral from the anorthosites below the MG3 package to those above the MG2 package. There is higher content of chromite in the anorthosites below the MG3 package compared to the MG2 package. The chromite in plate 4.9A occurs on the plagioclase, orthopyroxene and clinopyroxene in the anorthosites below the MG3 package, while those in the anorthosites above the MG2 package, occur along boundary of the orthopyroxene and plagioclase.

Borehole DWR172 shows an increase in the plagioclase content and decrease in the clinopyroxene and orthopyroxene content in the anorthosite layer. The size of the clinopyroxene changes from a coarse grain to a fine to medium grain size. There is a slight increase in chromite contents, in the anorthosites below the MG3 package relative to the anorthosites above the MG2 package. The chromite in both MG3 package and MG2 package occur along the boundaries between plagioclase and orthopyroxene grains.

The grain sizes of the orthopyroxenes and clinopyroxenes within the MG3 package at depths of 27.88m within the anorthosite layer are medium to coarse-grained. In the lower parts of the stratigraphy (31.79m), the clinopyroxene have fine to medium grains and the orthopyroxene are

medium to coarse-grained. In borehole DWR172, the chromites in the anorthosites above the MG2 package changes from fine to medium size.

The chromitites in borehole DWR74 within the anorthosites above the MG2 package at depth of 31.79m have an anhedral crystal shape. While the chromitites within the anorthosites below the MG3 chromitites at depths of 27.98m have, a subhedral to anhedral crystal shape.

Some orthopyroxene grains within the MG2 and MG3 package of borehole DWR172 exhibits banded exsolution lamellae, while plate 4.9B below the orthopyroxene grains with DWR74 don't exhibit banded exsolution lamellae.

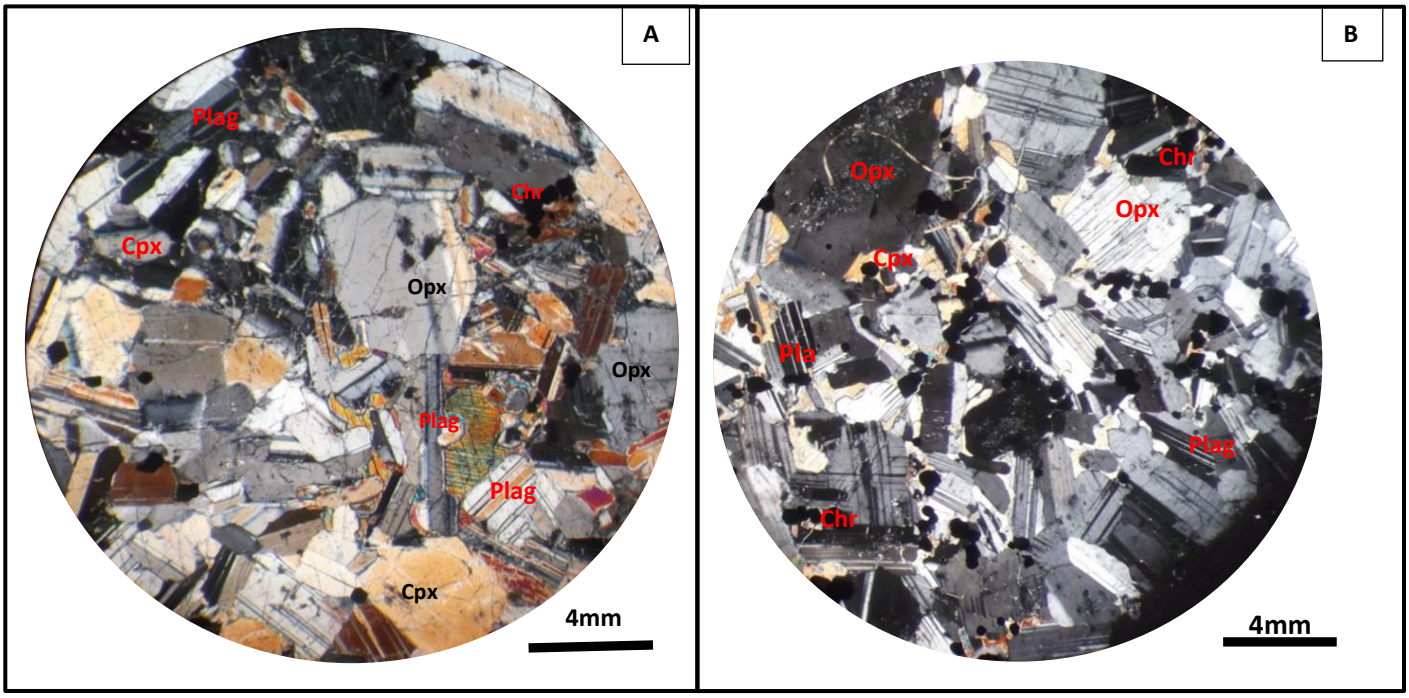

Plate 4.5: Anorthosite samples under a microscope. (A) Shows a coarse-grained orthopyroxene surrounded by fine grained plagioclase and (B) Some of the orthopyroxene grains shows banded exsolution lamellae.

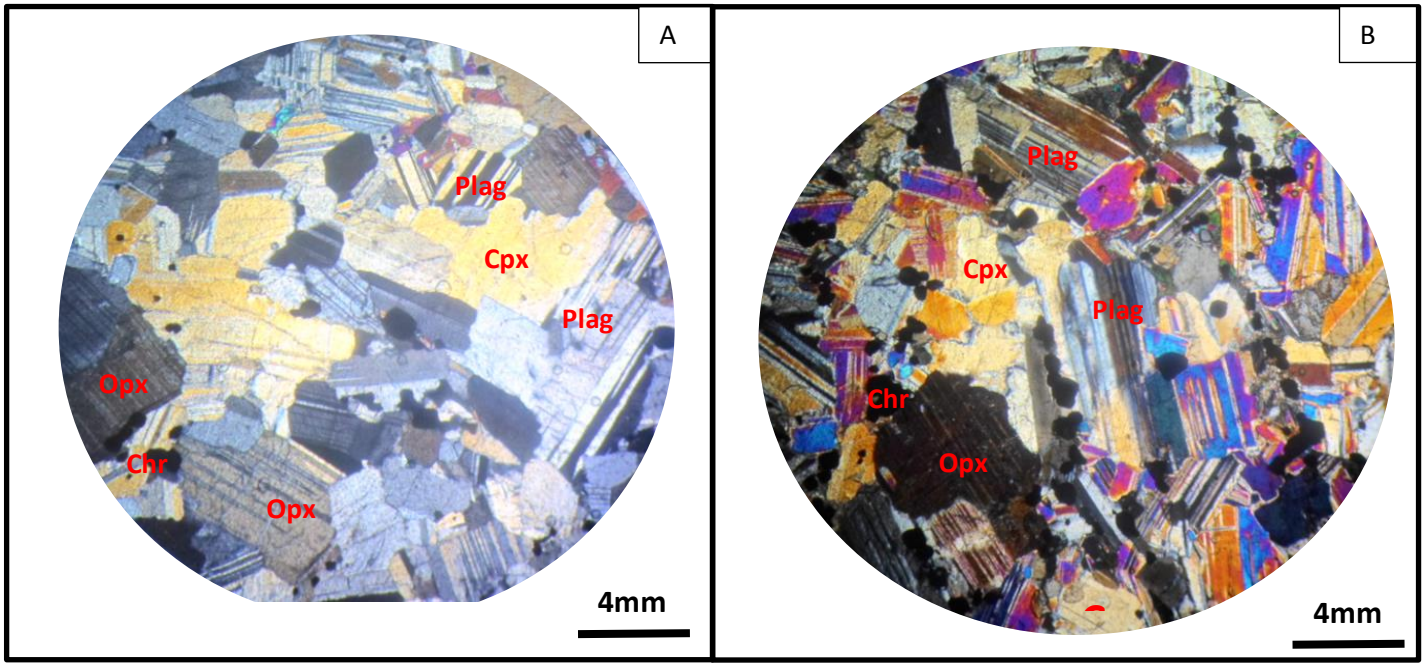

Plate 4.6: Anorthosite sample under a microscope. (A) Disseminated fine-grained chromitites occurring as stains on plagioclase, orthopyroxene and clinopyroxene. (B) A coarse grained orthopyroxene gain exhibiting banded exsolution lamellae.

A chromitite pyroxenite is macroscopically greenish brown to brown medium to coarse-grained feldspathic pyroxenite which consists of approximately 40% of fine to medium-grained disseminated chromite (plate 4.11). The chromitite pyroxenites consist of 30% orthopyroxene, 35% clinopyroxene, 15% chromitite and 20% plagioclase. The medium to coarse-grained orthopyroxenes and clinopyroxenes in the chromitite pyroxenite possess anhedral crystal shape (plate 4.12). Plagioclase occurs as an intercumulus mineral between the pyroxene grains. Plagioclase grains exhibits polysynthetic twining. The chromitite pyroxenites have an ophitic texture.

The clinopyroxene grains are serpentinised along the veins or cracks. This form of alteration is more extensive within the chromitite pyroxenites than in the feldspathic pyroxenites and anorthosites. There are those orthopyroxene grains that exhibit banded exsolution lamellae.

The chromitite pyroxenites are only found within the MG2 package and were sub divided into the upper and lower chromitite pyroxenites. The size of the chromite grains in the MG2 upper chromitite pyroxenites change from a medium to coarse sized, while the MG2 lower chromitite pyroxenites have fine to medium grains (plate 4.12 B). In both the MG2 upper and lower chromitite pyroxenites, plagioclase occurs as an intercumulus mineral.

The concentration of the plagioclase decreases in the upper chromitite pyroxenites and the size of the clinopyroxenes change from coarse grained to medium grained.

Occasionally in DWR74 there are the fine-grained plagioclase grains that occur as stains on clinopyroxene grains at depths of 33.18m to 34.58m within the MG2 package.

The chromitites grains in the MG2 package at depths of 33.18m have a subhedral to anhedral crystal shape and are fine to medium grain in size as illustrated in plate 4.12 B.

The MG2 package is not homogeneous in terms of mineral constituents. Plagioclase occurs as an intercumulus mineral within the chromitite pyroxenites at depths of 32.56m, while those at depths of 33.18m. At depth of 33.18m the concentration of the plagioclase decreases within the chromitite pyroxenite. The size of the clinopyroxenes change from coarse grained to medium grained at depth of 33.18m within the MG2 package.

The chromite within the chromitite pyroxenites borehole DWR172 at depths of 212.22m occur on top of the plagioclase, orthopyroxene and clinopyroxene grains, while at depths of 212.64m the chromitites within the MG2 package occur along the pore spaces or mineral boundaries of orthopyroxene and clinopyroxene grains as (plate 4.13) .

The chromites within the MG2 package in borehole DWR172 change from disseminated grains (Plate 4.13) at a depth of 215.54m to predominately closely packed medium to coarse grains (Plate 4. 12B) at depth of 212.74m.

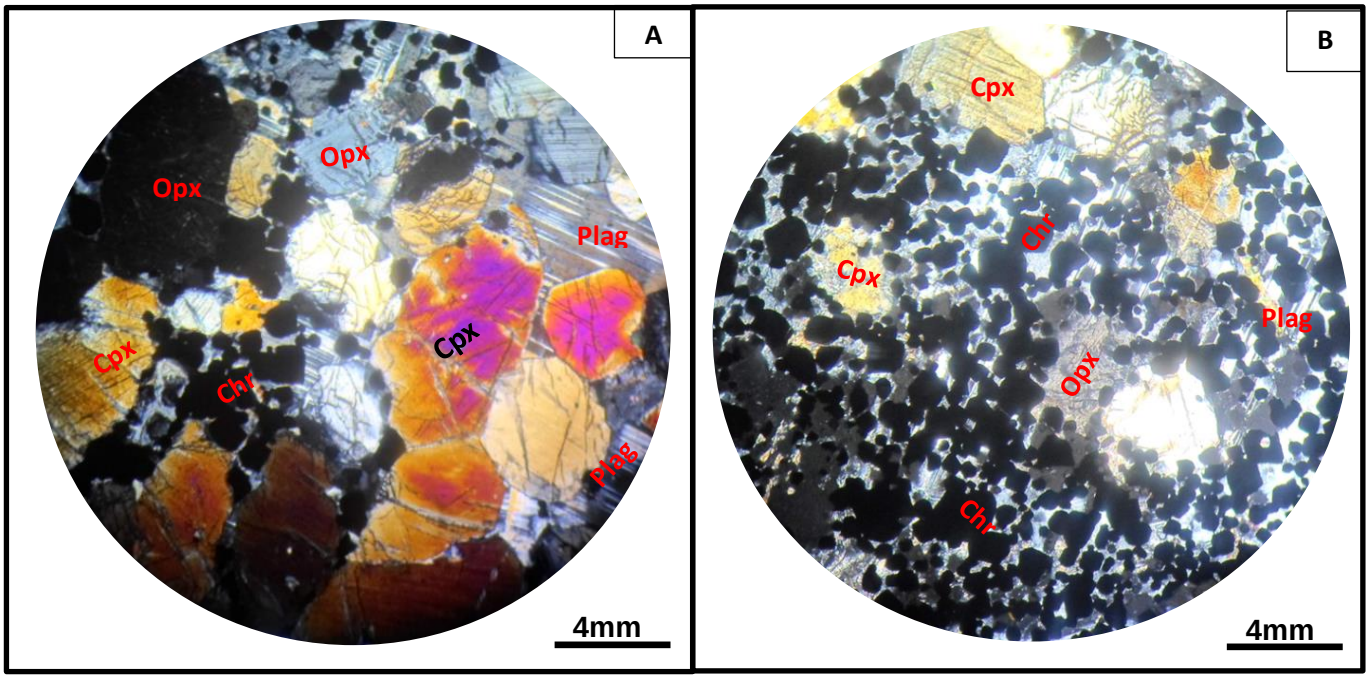

Plate 4.7: Chromitite pyroxenite samples under a microscope. (A) Show the coarse grained clinopyroxene, while (B) shows the fine to medium grained chromitites.

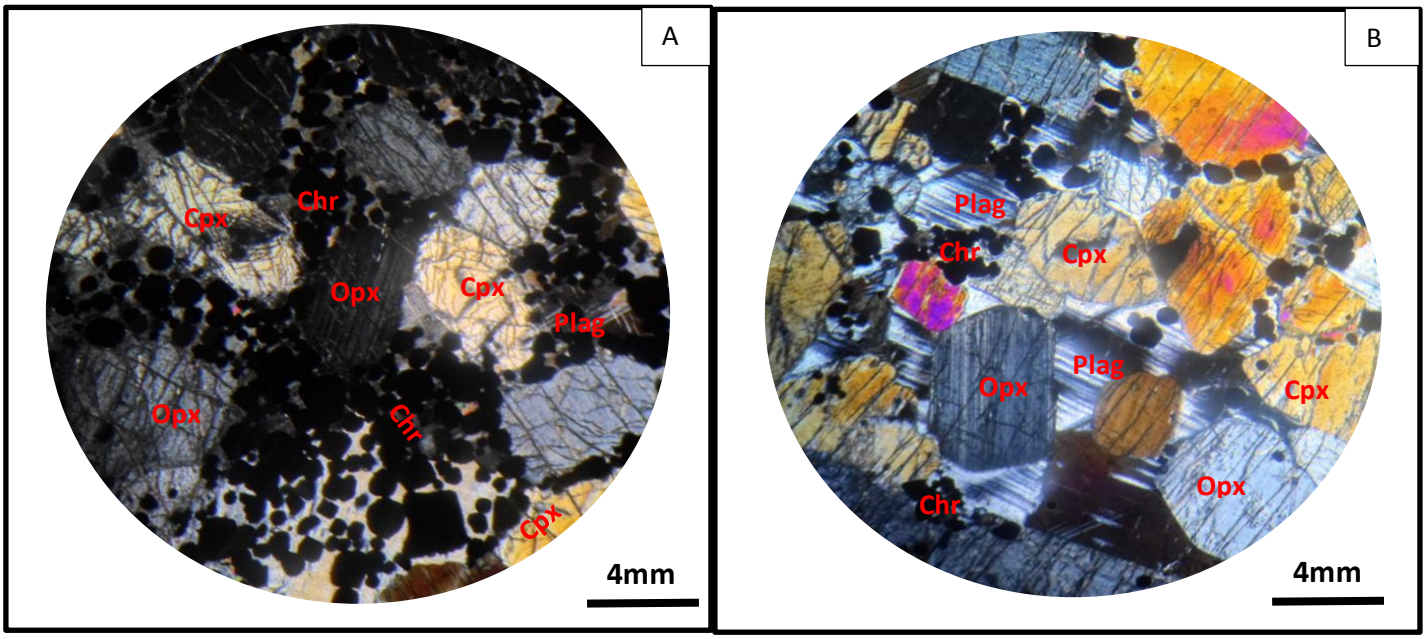

Plate 4.8: Chromitite pyroxenite samples under a microscope. Chromitite grains mainly occur predominately on the plagioclase or pore spaces. (B) The amount of chromitite within the MG3 package decreases, but an increase in the content of plagioclase.

4.3.5 Anorthite content of feldspathic pyroxenites, anorthosites and chromitite pyroxenites

The anorthite content within the various rock types was determined using Michel Levy method (Nesse, 2000) for boreholes DWR74 and DWR172.

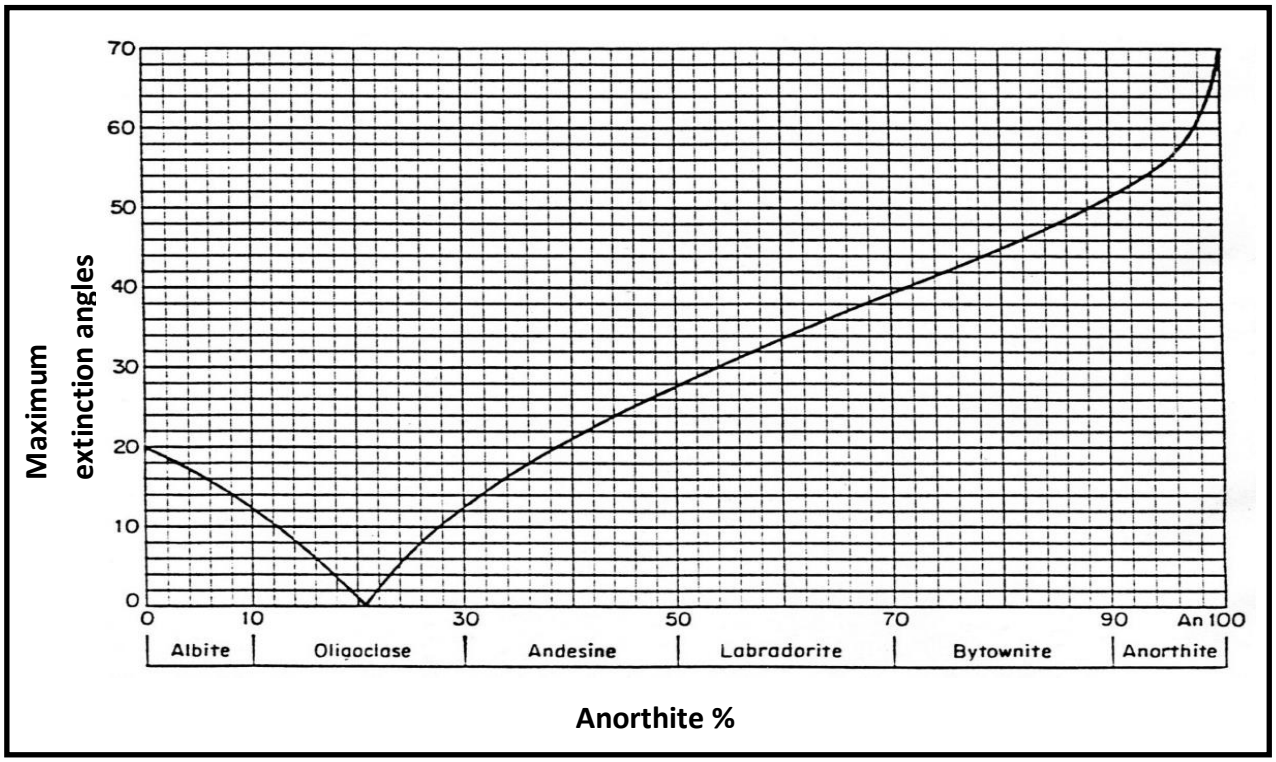

Figure 4.2: Michel Levy graph that shows the maximum extinction angle versus anorthite content (%).

The feldspathic pyroxenites in the MG3 package at a depth between 25.6m to 26.1m are labradorite, consisting of >50% calcium, while the feldspathic pyroxenites at a depth between 26.6m to 27.1m are andesine consisting of <50% calcium. A similar trend seen in the MG2 feldspathic pyroxenites at a depth of 32.1m are labradorite, while those at a depth of 33.1m are andesine. The chromitite pyroxenites in the MG2 package are labradorite, but consist of a higher calcium percentage (> 55%) than the MG2 feldspathic pyroxenites. The petrographic study showed decrease in the anorthite content from the MG3 package to the MG2 package and change in the texture from a cumulus to intercumulus texture.

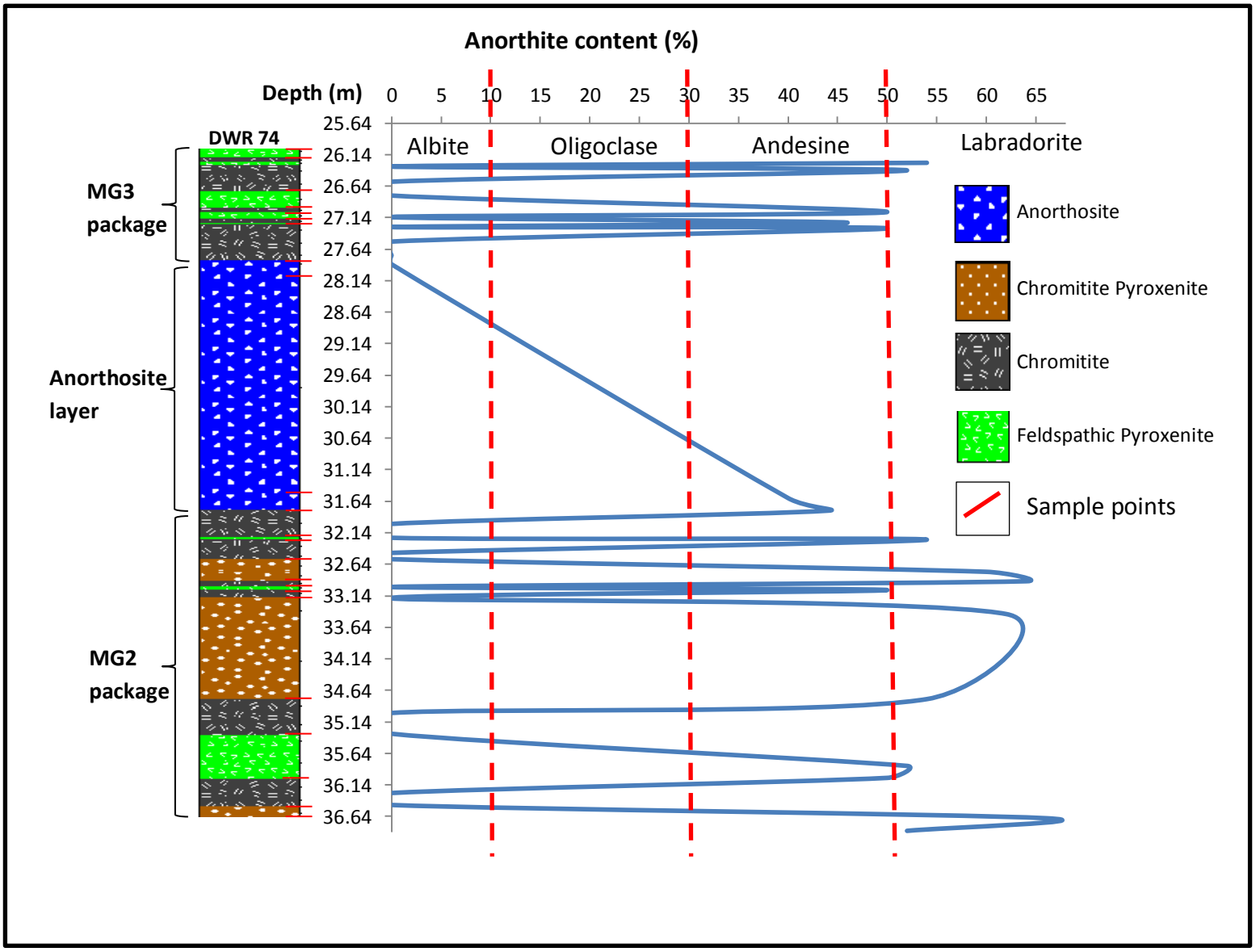

Figure 4.3: Illustration of the anorthite content within the various rocks of borehole DWR 74

In figure 4.4 the MG3 feldspathic pyroxenites at a depth between 205m to 206.5m are labradorite with > 50% calcium, but the MG2 feldspathic pyroxenite at a depth between 212m to 212.5m show slightly higher calcium content relative to the MG3 feldspathic pyroxenites. Although the chromitite pyroxenites in the MG2 package are labradorite, they have slightly higher calcium content as compared to the MG2 and MG3 feldspathic pyroxenites.

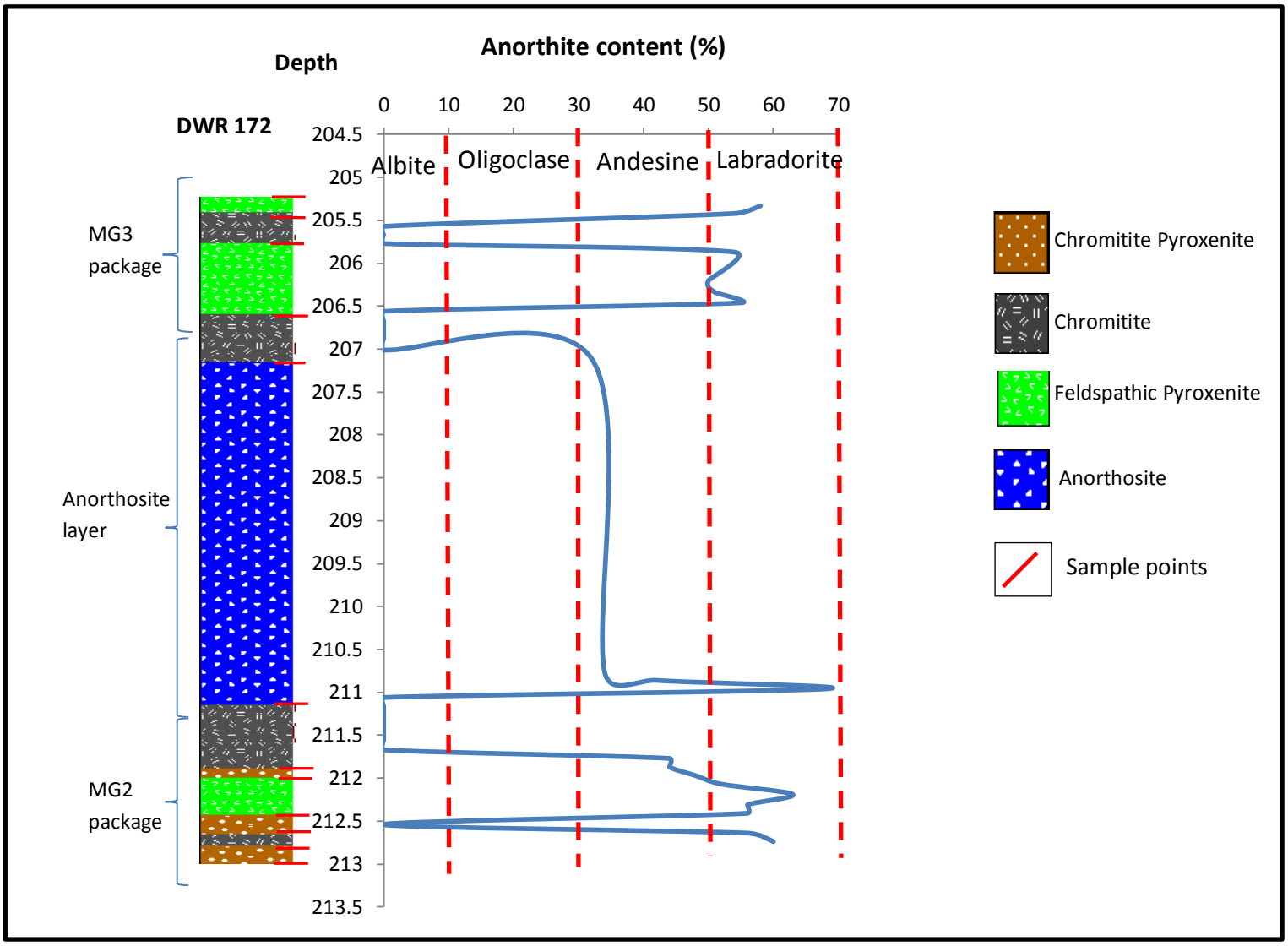

Figure 4.4: Illustration of the anorthite content within the various rock types of borehole DWR 172

4.4 Summary of the various rock types

Table 4.1: Major petrographic features in rock types of the MG3 package at Dwarsrivier chrome mine.

Rock Types	Alteration	Texture	Modal Composition
Feldspathic pyroxenites	Sercitisation (low) Serpentinisation (low)	Sub-ophitic texture	Clinopyroxene (35%), Orthopyroxene (30%), Plagioclase (20%) and chromites (15%)
Chromitites	Serpentinisation (low)	Cumulate texture	Chromites (60%), Clinopyroxene (20%) Orthopyroxene (15%) and Plagioclase (5%)
Anorthosites (below MG3 package)	Sercitisation (low) Serpentinisation (low)	Adcumulate texture	Plagioclase (70%) Clinopyroxene (10%) Orthopyroxene (10%) and chromites (10%)

Table 4.2: Major petrographic features in rock types of the MG2 package at Dwarsrivier chrome mine.

Rock Types	Alteration	Texture	Modal Composition
Feldspathic pyroxenites	Sercitisation (low) Serpentinisation (low)	Ophitic texture	Clinopyroxene (40%), Orthopyroxene (45%), Plagioclase (10%) and chromites (5%)
Chromitites	Serpentinisation (low)	Cumulate texture	Chromites (50%), Clinopyroxene (20%) Orthopyroxene (20%) and Plagioclase (10%)
Anorthosites **(Above the MG2 package)**	Sercitisation (low) Serpentinisation (low)	Adcumulate texture	Plagioclase (70%) Clinopyroxene (15%) Orthopyroxene (10%) and chromites (5%)
Chromitite pyroxenites **(lower)**	Serpentinisation (low)	Ophitic texture	Orthopyroxene (40%), Clinopyroxene (35%), Plagioclase (15%) and chromites (10%)
Chromitite pyroxenites **(upper)**	Serpentinisation (low)	Ophitic texture	Orthopyroxene (30%), Clinopyroxene (35%), Plagioclase (20%) and chromites (15%)

The summary of the differences between the various rocks types within the MG3 compared to the MG2 package are illustrated in table 4.1 and 4.2 are as follows:

In the MG3 feldspathic pyroxenites there is an increase in the chromite and plagioclase, but a decrease in the clinopyroxene and orthopyroxene content in the MG2 feldspathic pyroxenites. The orthopyroxene grains in the MG3 feldspathic pyroxenites exhibit banded exsolution lamellae, while it is absent in the MG2 feldspathic pyroxenites orthopyroxene grains. The chromite grains in the MG3 feldspathic pyroxenites occurs as stains on the plagioclase, orthopyroxene and clinopyroxene, while in the MG2 feldspathic pyroxenites the chromites occur along the pore spaces or boundary.

In the chromitites, the MG3 chromitites contains higher chromite content relative to the MG2 chromitites. The MG2 package chromitites shows a decrease in orthopyroxene and plagioclase content up the stratigraphy but a slight increase in the chromite content. There is the absence of orthopyroxenes and plagioclase in some parts of the MG2 chromitites.

The anorthosites below the MG3 package towards the anorthosites above the MG2 package show a decrease in the chromite content and increase in the clinopyroxene content as the grains change from cumulus to intercumulus.

In the chromitite pyroxenites, the plagioclase content decreases in the upper chromitite pyroxenite and a change in the clinopyroxene grains from coarse to medium grain size. The lower chromitite pyroxenites consist of higher chromite content, but lower orthopyroxene content relative to the upper chromitite pyroxenite. Chromite grains change from disseminated grains in the lower chromitite pyroxenite to predominately closely packed medium to coarse grains in the upper chromitite pyroxenite.

5 .Whole rock geochemistry

The aim of the project is to use geochemical and petrographic to distinguish the various rock types within the MG2 and MG3 package. Then determine whether or not the transition boundary from the MG2 package to the MG3 package was as a result of a single or multiple magma pulses and suggest the most suitable layer for exploitation between the MG2 and MG3 chromitites.

From the petrographic studies, the differences and similarities between feldspathic pyroxenites, chromitites, anorthosites and chromitite pyroxenites within the MG2 package and MG3 package are as follows:

- The feldspathic pyroxenites shows a decrease in the plagioclase content down the MG3 package as the plagioclase changes from a cumulus mineral to an intercumulus mineral in both boreholes DWR 74 and DWR172.
- Low contents of chromite are associated with the MG2 feldspathic pyroxenites, and the chromite content increase in and towards the MG3 feldspathic pyroxenites.
- The chromite grains within the MG3 feldspathic pyroxenites occurs dispersed on plagioclase, orthopyroxene and clinopyroxene grains, while these fill intergranular pore spaces or mineral boundaries in the MG2 feldspathic pyroxenites.
- The MG3 chromitites show a higher content of clinopyroxene relative to those in the MG2 package. The MG3 chromitites contain little or no plagioclase and orthopyroxenes, while the MG2 chromitites in DWR 74 show the presences of plagioclase. The MG2 chromitites show the presences of orthopyroxenes, but none of these is seen within the MG3 package.
- The anorthosites below the MG3 package in borehole DWR 172 show higher chromite content compared to the anorthosites below the MG2 package.
- In DWR 74 the chromitite grains within the anorthosites above the MG2 package at depths of 31.79m have anhedral crystal shape, while the chromitites grains within the anorthosites below the MG3 package have a subhedral to anhedral crystal shape.
- Chromite within DWR 172 borehole within the MG2 package are disseminated and vary from fine to medium grain within the lower chromitite pyroxenites, to predominately closely packed medium to coarse grained within the upper chromitite pyroxenites.

The data, comprising of the major oxides and trace elements in sample, mainly from two boreholes, DWR 74 and DWR172 are presented in Appendix A and B. These geochemical data were used to determine whether there are any similarities or differences in terms of the various rock types. This was done along the following steps:

1. The geochemical data summary for all data and rock types in table 5.1 was compiled using SPSS statistical software. The geochemical data summary gives an overview of, range, geometric mean and standard deviation of oxides and trace elements within the samples from boreholes DWR 74 and DWR 172.

2. A combination of cluster and discriminant analysis was used to classify and characterise the various rock types, using the major rock forming elements.

3. Classification, oxides and trace elements will be used to validate the petrographic study. Cluster analysis results will show the different rock types in terms of groups; while discriminant analysis will ascertain which of these groups (rock types) are chromitites, anorthosites, feldspathic pyroxenites and chromitite pyroxenite. Discriminant analysis was applied to the core logging result and compared to the cluster and discriminant analysis results applied to the same samples, to determine which method is the most reliable, prescribed by table 5.50.

4. Classified samples were used to construct the spider diagrams. The spider diagrams in figure 5.16, 5.17, 5.18 and 5.19 were used to compare the behavior of the LILE (Large Ion Lithophile Elements) such as Sr, Rb and Ba and the High field strength elements (HFSE) such as Th, U, Ce, Zr, Nb, Ti and Y in the different rock types.

5. Ratios such as SiO_2/Al_2O_3, Sr/Ba, Co/V and Mg# that were used by various authors to determine whether the transition boundary from the MG2 package to MG3 package is due to a single or multiple magma pulses.

5.1 Geochemistry data summary

The table 5.1 and 5.2 below gives an overview of the summary of oxides and trace elements distribution in samples from boreholes DWR 74 and DWR172.

The anorthosites contains the highest Al_2O_3 content (24.9 wt. %) followed in decreasing order of Al_2O_3 content by chromitites (13.7 wt. %), chromitite pyroxenites (9.1 wt. %) and feldspathic pyroxenites (7.5 wt. %). Anorthosites also contain the highest CaO content (10.6 wt. %) and decreases in feldspathic pyroxenites (3.5 wt. %), chromitite pyroxenites (3.2 wt. %) and chromitite (2 wt. %).

The highest Na_2O content is seen within the anorthosites (1.4 wt. %) followed in decreasing order in the chromitite pyroxenites (0.7 wt. %), chromitites (0.6 wt. %) and feldspathic pyroxenites (0.5 wt. %).

The chromitites contain the highest Cr_2O_3 content (31.1 wt. %) accompanied in decreasing order of Cr_2O_3 content by chromitite pyroxenite (8.5 wt. %), feldspathic pyroxenites (4.8 wt. %) and anorthosites (1.5 wt. %). The chromitites also show highest content of Fe_2O_3 (21.1 wt. %) followed in decreasing order of Cr_2O_3 content by the chromitite pyroxenites (14.6 wt. %), feldspathic pyroxenites (13.9 wt. %) and anorthosites (3 wt. %). The highest TiO_2 is seen within the chromitites (0.7 wt. %) followed in decreasing order by the chromitite pyroxenites (0.4 wt. %), feldspathic pyroxenites (0.2 wt. %) and anorthosites (0.2 wt. %).

The feldspathic pyroxenites consist of the highest content of SiO_2 (44.4 wt. %), accompanied by anorthosites (41.7 wt. %), chromitite pyroxenites (38.8 wt. %) and chromitites (16.6 wt. %). The feldspathic pyroxenites also shows the highest content of MgO (18.7 wt. %), followed in decreasing order by chromitite pyroxenites (17.6wt. %), chromitites (11 wt. %) and anorthosites (2.3 wt. %).

Table 5.1: Geochemical summary table of major and trace elements of anorthosites and chromitites

	Anorthosites				Chromitites			
Variable	Std. deviation	Geometric mean	DWR74 (GM)	DWR172 (GM)	Std. deviation	Geometric mean	DWR74 (GM)	DWR172 (GM)
Al_2O_3 (wt %)	5.7	24.9	21.1	28.3	1.6	13.7	13.7	13.6
CaO	5.1	10.6	6.6	15	0.8	2	1.8	2.2
Cr_2O_3	11.8	1.5	3.5	0.8	5.2	31.1	29.8	32.4
Fe_2O_3	8.4	3	5.1	2	2.1	22.1	22.7	21.5
K_2O	0.1	0.2	0.2	0.2	0.1	0.1	0.1	0.1
MgO	0.6	2.3	5.1	1.2	2.3	11	12.4	9.7
MnO	0	0	0.1	0	0	0.2	0.2	0.2
Na_2O	13.6	1.4	1.1	1.7	0.2	0.6	0.5	0.6
P_2O_5	0.3	0	0	0	0	0	0	0
SiO_2	0	41.7	32.5	50.3	5.8	16.6	16.9	16.9
TiO_2	0.4	0.2	0.3	0.1	0.1	0.7	0.8	0.7
NiO	6.6	0	0	0	0	0.1	0.1	0.1
Ba (ppm)	45	0	0	97.3	36.9	0	0	0
Ce	0	0	0	Bdl	0.2	0	0	0
Cl	32.7	55.5	81.5	41.6	56.4	80.9	94.5	69.3
Co	112.8	39.8	195.7	12.1	70.3	171.3	126.9	231.1
Cr	134111.5	26185.8	191556	5887	96208.1	161660.1	103967.7	251366.5
Cu	13.8	0	0	15.8	811.2	0	0	0
Ga	183.1	25	33.7	20	15.9	36.9	28.5	47.7
La	11.4	0	21.2	0	6.6	16.1	13.9	18.6
Nb	0.7	2	2.6	1.7	1.9	4.3	3.2	5.9
Nd	0	0	0	0	3.2	0	0	0
P	57.3	56.4	50.6	61.1	167.7	69.8	61.5	79.1
Pb	4.7	8.4	11.9	6.4	3.7	0	0	0
Rb	2.2	7.1	7.5	6.9	3.6	0	0	5.4
Sr	1.2	143	38.7	381.5	88.4	56.1	66.8	47.1
Th	0	0	0	0	0	0	0	0
Ti	2033.6	1391	3708.1	666.8	1207	3669.2	3026.7	4448.2
S	18.9	16.3	18.3	15	72.2	0	0	36
V	759.5	244.4	1210.7	73.6	662.3	1222.5	826.2	1808.9
U	1.2	0	0	0	1.2	0	0	0
Y	0.7	0	0	0	2.5	0	0	0
Zn	3.2	86.9	448.3	25.4	221.3	421.3	291.2	609.6
Zr	10.2	23.6	18.4	28.5	8	24.4	20.3	29.4

Table 5.2: Geochemical summary table of major and trace elements of chromitite pyroxenites and feldspathic pyroxenites.

Rock type	Chromitite pyroxenites				Feldspathic pyroxenites			
Variable	Std. deviation	Geometric mean	DWR74 (GM)	DWR172 (GM)	Std. deviation	Geometric mean	DWR74 (GM)	DWR172 (GM)
Al2O3 (wt %)	2.1	9.1	9.2	3.1	3.1	7.5	7.4	7.6
CaO	1.1	3.2	3.1	1.5	1.5	3.5	3.6	3.3
Cr2O3	10	8.5	9.2	7.7	7.7	4.8	3.8	5.9
Fe2O3	3.4	14.6	14.5	14.8	2.8	13.9	13.2	14.9
K2O	0.1	0.1	0.1	0.1	0.1	0.2	0.1	0.2
MgO	3.5	17.6	20	15.4	3.9	18.7	20.6	17.1
MnO	0	0.2	0.2	0.2	0	0.2	0.2	0.2
Na2O	0.1	0.7	0.7	0.7	0.3	0.5	0.3	0.7
P2O5	0	0	0	0	0	0	0	0
SiO2	11.3	38.8	41.8	36	8.8	44.4	45	43.8
TiO2	0.2	0.4	0.4	0.4	0.2	0.3	0.3	0.4
NiO	0	0.1	0.1	0.1	bdl	0.1	0.1	0.1
Ba (ppm)	32.6	34.6	23.1	61.8	29.6	45.1	30.6	63.8
Ce	0	0	0	0	0	0	0	0
Cl	100.8	103.2	94.2	113	67.8	134.6	116.7	153
Co	69.4	140	144.9	135.3	56.8	128.1	139.3	118.9
Cr	119553.5	69380.6	68915	69849.3	93985.1	61418.1	88738.4	44102.4
Cu	12.8	0	0	0	519.9	0	0	0
Ga	19.3	16.2	16.4	16	15.8	17.2	23.2	13.2
La	10.4	0	0	0	8	0	10.9	0
Nb	1.5	4.2	3.2	5.5	1.3	4	3	5.3
Nd	0	0	0	0	2.1	0	0	0
P	119.7	57.6	42.9	77.3	117.9	135.9	93.6	190.2
Pb	3.9	5.3	5.6	5	3.4	0	0	0
Rb	5.5	6.1	5.9	6.2	4.2	4.9	2.7	8.1
Sr	23.5	40.2	27.7	58.3	32.8	56.3	62	51.6
Th	0	0	0	0	0	0	0	0
Ti	1482.9	2440	2581.9	2306	1246.4	2458.4	2784.5	2197.7
S	28.3	0	0	55.6	64.1	0	0	80.7
V	644.3	542.2	568.3	517.3	646.7	566	753.5	437.4
U	2.1	0	0	0	2	0	0	0
Y	3	0	0	2.9	2.9	0	0	0
Zn	241.8	232.9	252	215.2	215.9	222.4	283.3	178.9
Zr	28.4	26.8	19	37.7	11.2	29.3	22	37.9

5.1.1 Validation and geochemical characterization based on field classification

Multivariate statistical methods such as factor, cluster and discriminant analysis were used to characterise the chromitites, chromitite pyroxenites, feldspathic pyroxenites and anorthosites based on the oxide content. Cluster analysis was used to separate the geochemical samples into different rock types on the basis of similarities. Discriminant analysis was used to take the different groups or rock types and identify which of these are chromitites, chromitite pyroxenites, anorthosites and feldspathic pyroxenites based on their oxide content.

5.1.1.1 Geochemical characterisation of the various rock types.

Factor analysis was applied on the geochemical data from 68 samples. The factor scores from the samples of various lithologies in the study area were graphically represented in relation to the rock types.

Table 5.3: The total variance results of the different lithologies, in the study area.

Total Variance Explained

Component	Initial Eigenvalues			Extraction Sums of Squared Loadings			Rotation Sums of Squared Loadings		
	Total	% of Variance	Cumulative %	Total	% of Variance	Cumulative %	Total	% of Variance	Cumulative %
1	6.784	56.533	56.533	6.784	56.533	56.533	5.359	44.660	44.660
2	3.458	28.819	85.353	3.458	28.819	85.353	4.239	35.325	79.985
3	1.043	8.689	94.042	1.043	8.689	94.042	1.687	14.056	94.042
4	.403	3.355	97.396						
5	.143	1.190	98.586						
6	.059	.488	99.074						
7	.050	.413	99.487						
8	.029	.238	99.725						
9	.018	.150	99.875						
10	.010	.079	99.954						
11	.005	.046	100.000						
12	2.377E-017	1.981E-016	100.000						

Extraction Method: Principal Component Analysis.

Table 5.4: Rotated component matrix of the various lithologies in the study area.

Component Matrix[a]

	Component		
	1	2	3
NiO	.990		
Fe_2O_3	.977		
CaO	-.936		
TiO_2	.874	-.403	
Na_2O	-.838	-.434	
Cr_2O_3	.833	-.507	
SiO_2	-.809	.559	
MnO	.792	.557	
MgO		.939	
Al_2O_3	-.456	-.872	
K_2O	-.488		.657
P_2O_5		.576	.657

Extraction Method: Principal Component Analysis.

a. 3 components extracted.

Table 5.4 above presents the results for the three factors explaining 94% of the total variance in the geochemical data. In table 5.5 factor one is positively loaded with Cr_2O_3, Fe_2O_3, TiO_2 and NiO. These oxides can be used to characterise the chromitites type of rocks. The negatively loaded factor two consist of SiO_2, CaO and Na_2O, these represent the feldspathic pyroxenites. Figure 5.1 is a graphical representation of the factor scores (table 5.5) that characterise the chromitites and feldspathic pyroxenites. The y-axis represents the positive and negative scores, while the x-axis represents the sample names. In figure 5.1, there are two feldspathic pyroxenite samples that can be defined by the presences of Cr_2O_3, Fe_2O_3, TiO_2, and NiO and a few chromitite samples which show high content of Al_2O_3, CaO and Na_2O. This suggests the presences of two types of feldspathic pyroxenites and chromitites.

The graphical representation of the factor score (table 5.5) in figure 5.2 that characterise the chromitite pyroxenites and anorthosites, with the x-axis represent the positive and negative factor scores and the y-axis represent the sample names. Factor two in figure 5.2 below is positively loaded with oxides NiO, MgO and MnO which represents the chromitite pyroxenites, while the negatively loaded oxides Al_2O_3, CaO and Na_2O represent the anorthosites.

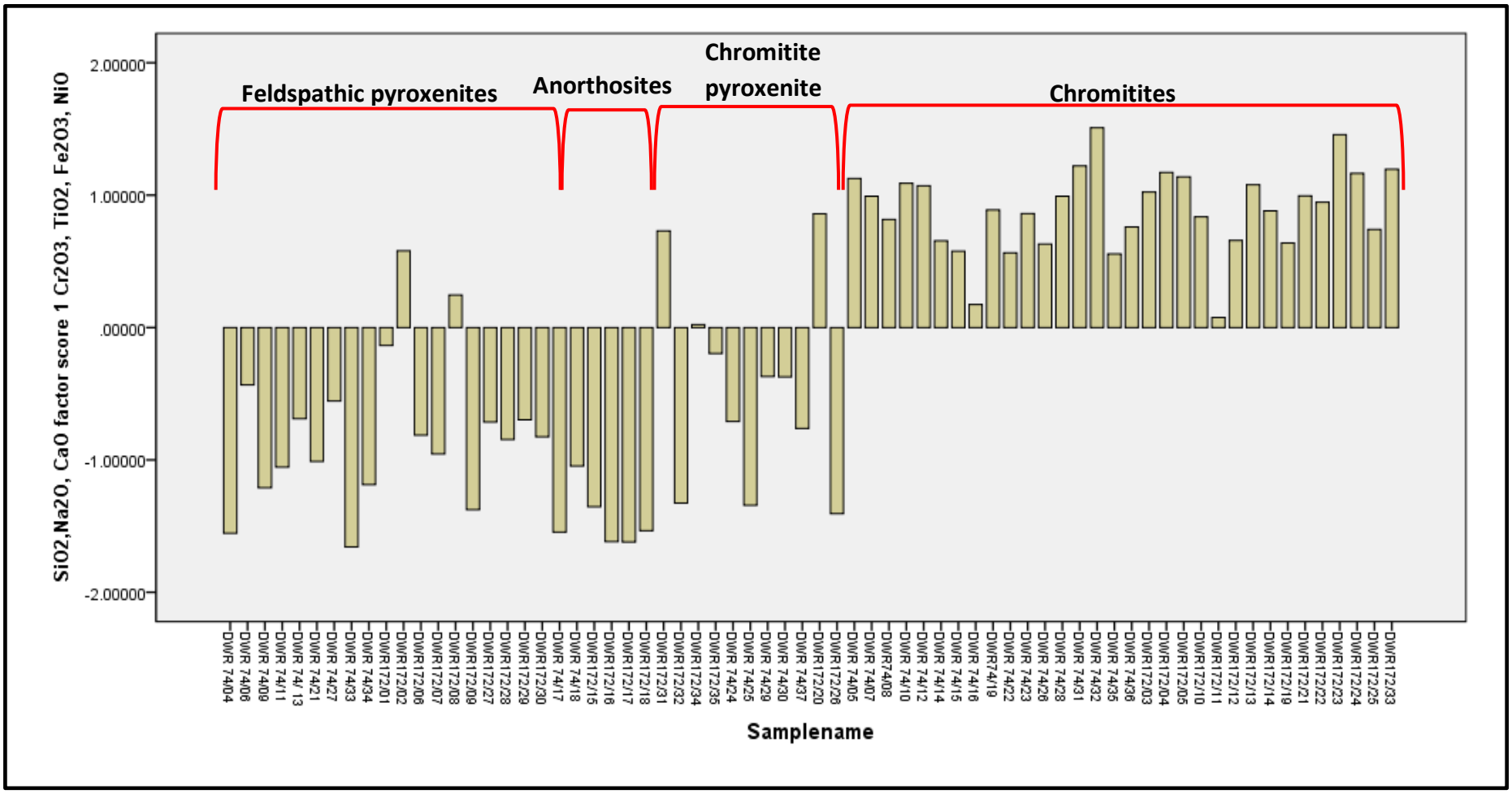

Figure 5.1: Graphical representation that shows the samples characterised as chromitites (positively loaded) and feldspathic pyroxenites (negatively loaded).

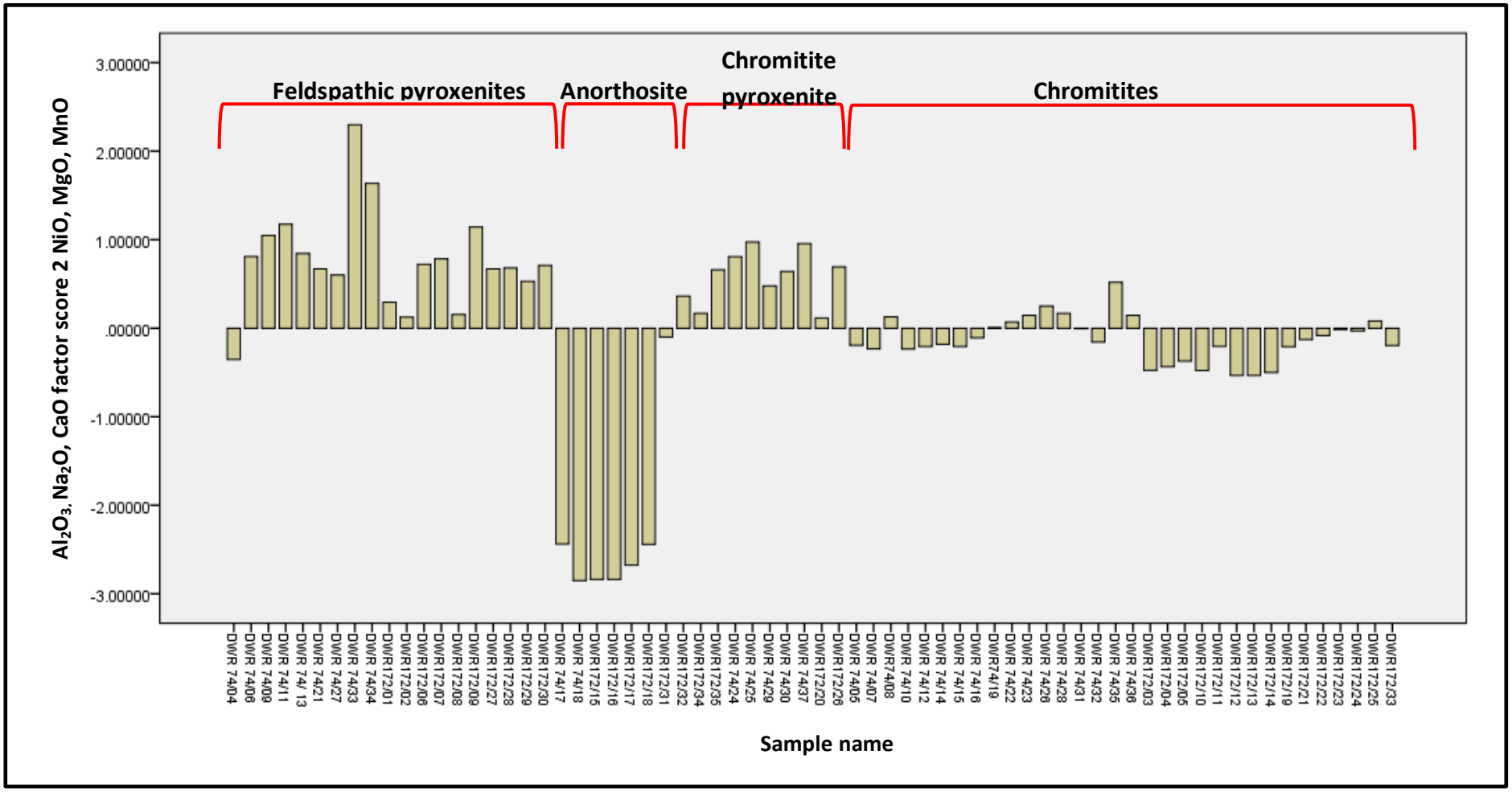

Figure 5.2: Graphical representation that shows the samples characterised as chromitite pyroxenites (positively loaded) and anorthosites (negatively loaded).

5.1.1.2 Geochemical characterisation of the MG3 package

In the previous section 5.1.1.1 factor scores illustrated the oxides that were used to differentiate the various rock types. In this section the factor scores will illustrate the major elements which can associated with the rock types in the MG3 package, Factor analysis was used on the feldspathic pyroxenites and chromitites within the MG3 package and anorthosites below the MG3 package that were identified in the field. The factor scores from the factor analysis illustrate the oxides that can be used to differentiate the various rock types within the MG3 package.

Table 5.5: The total variance results of the MG3 package.

Total Variance Explained

Component	Initial Eigenvalues			Extraction Sums of Squared Loadings			Rotation Sums of Squared Loadings		
	Total	% of Variance	Cumulative %	Total	% of Variance	Cumulative %	Total	% of Variance	Cumulative %
1	7.279	60.658	60.658	7.279	60.658	60.658	6.429	53.571	53.571
2	3.781	31.512	92.170	3.781	31.512	92.170	4.632	38.599	92.170
3	.534	4.452	96.623						
4	.283	2.355	98.977						
5	.044	.370	99.347						
6	.032	.265	99.612						
7	.018	.147	99.759						
8	.012	.098	99.857						
9	.010	.086	99.943						
10	.004	.033	99.975						
11	.003	.025	100.000						
12	-2.018E-016	-1.682E-015	100.000						

Extraction Method: Principal Component Analysis.

Table 5.6 above illustrates results for the two factors explaining 92.1% of the total variance. Table 5.7 factor one is positively loaded with Cr_2O_3, Fe_2O_3, TiO_2, NiO and MnO. These oxides characterise the MG3 chromitites, while SiO_2, CaO, Na_2O, K_2O and P_2O_5 are negatively loaded and considered to characterise the MG3 feldspathic pyroxenites, but there is a sample that consist of Cr_2O_3, Fe_2O_3, TiO_2, NiO and MnO.

Table 5.6: Rotated component matrix for the MG3 package.

Rotated Component Matrix[a]

	Component	
	1	2
SiO_2	-.987	
Cr_2O_3	.983	
TiO_2	.972	
Fe_2O_3	.911	
NiO	.845	.522
K2O	-.814	0
P_2O_5	-.646	.531
Al_2O_3		-.986
MgO		.923
MnO	.411	.894
Na_2O	-.457	-.866
CaO	-.666	-.735

Extraction Method: Principal Component Analysis.

Rotation Method: Varimax with Kaiser Normalization.

a. Rotation converged in 3 iterations.

The graphical representation of the factor scores for the different rock types in the MG3 package are represented by figure 5.3 which characterise feldspathic pyroxenites and chromitites and figure 5.4, characterise the chromitite pyroxenites and anorthosites. Figure 4.3 and 5.4 consist of y-axis represent the sample names and x-axis that represents the negative and positive factors. In figure 5.4, there are chromitites samples can be associated with Al_2O_3, CaO and Na_2O. This suggest the presences of two types of chromitites, while in figure 4.3 there are feldspathic pyroxenites that are defined by the presences of Cr_2O_3, Fe_2O_3, TiO_2 and NiO. This corresponds to results of the petrographic study, which indicate that the MG3 chromitites and MG3 feldspathic pyroxenites showed higher content of chromite relative to the MG2 feldspathic pyroxenites and MG2 chromitites. The MG2 chromitites and feldspathic pyroxenites showed lower content of chromite, but higher content of clinopyroxene and orthopyroxenes as compared to the MG3 chromitites and feldspathic pyroxenites. Although the petrographic study of the anorthosites below the MG3 package indicated the presences chromite, the factor analysis results doesn't consist of Cr_2O_3 and Fe_2O_3 as the major elements that can be associated with these anorthosites.

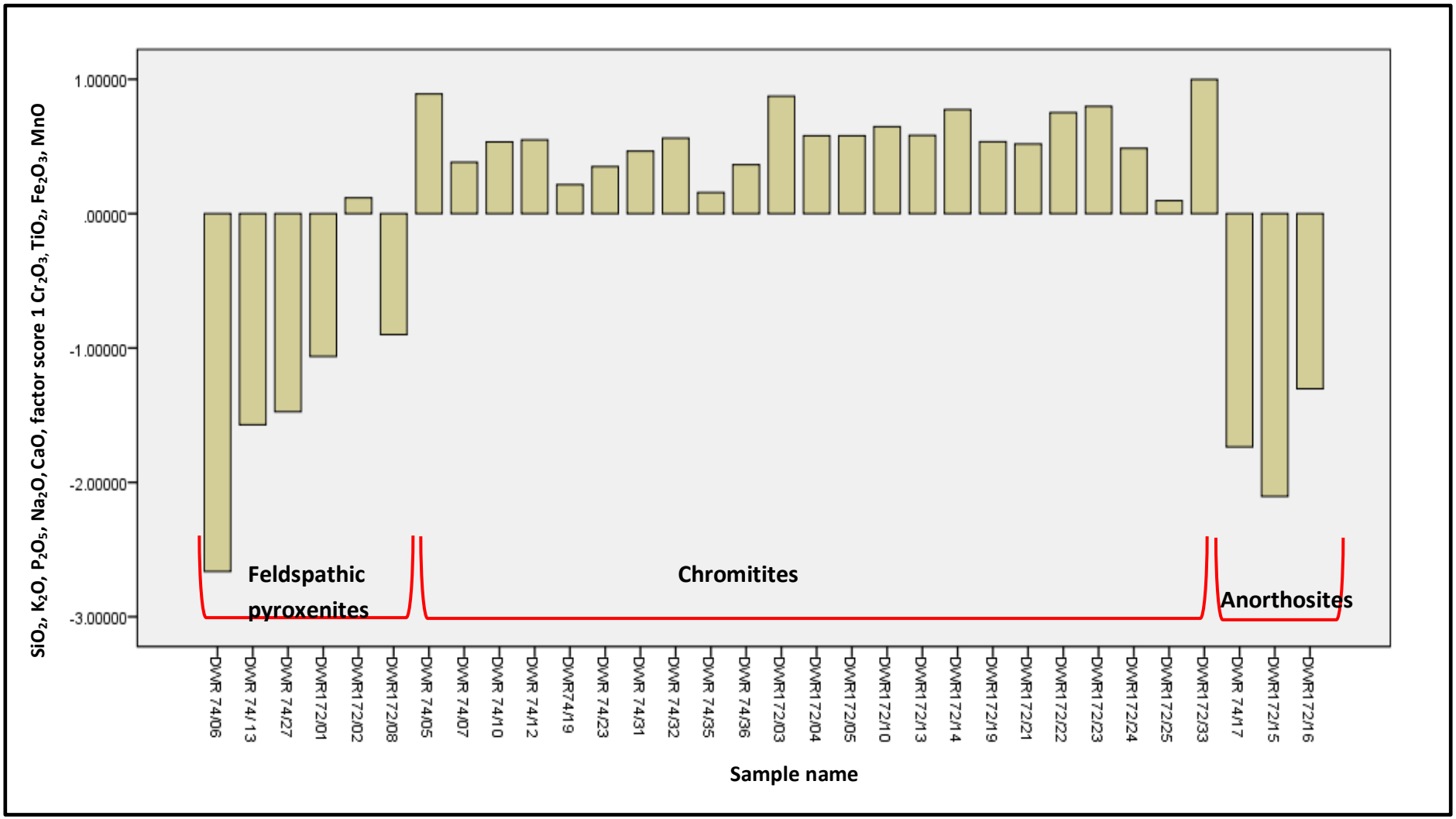

Figure 5.3: Graphical representation that show the samples characterised as chromitites (positively loaded) and feldspathic pyroxenites (negatively loaded) within the MG3 package

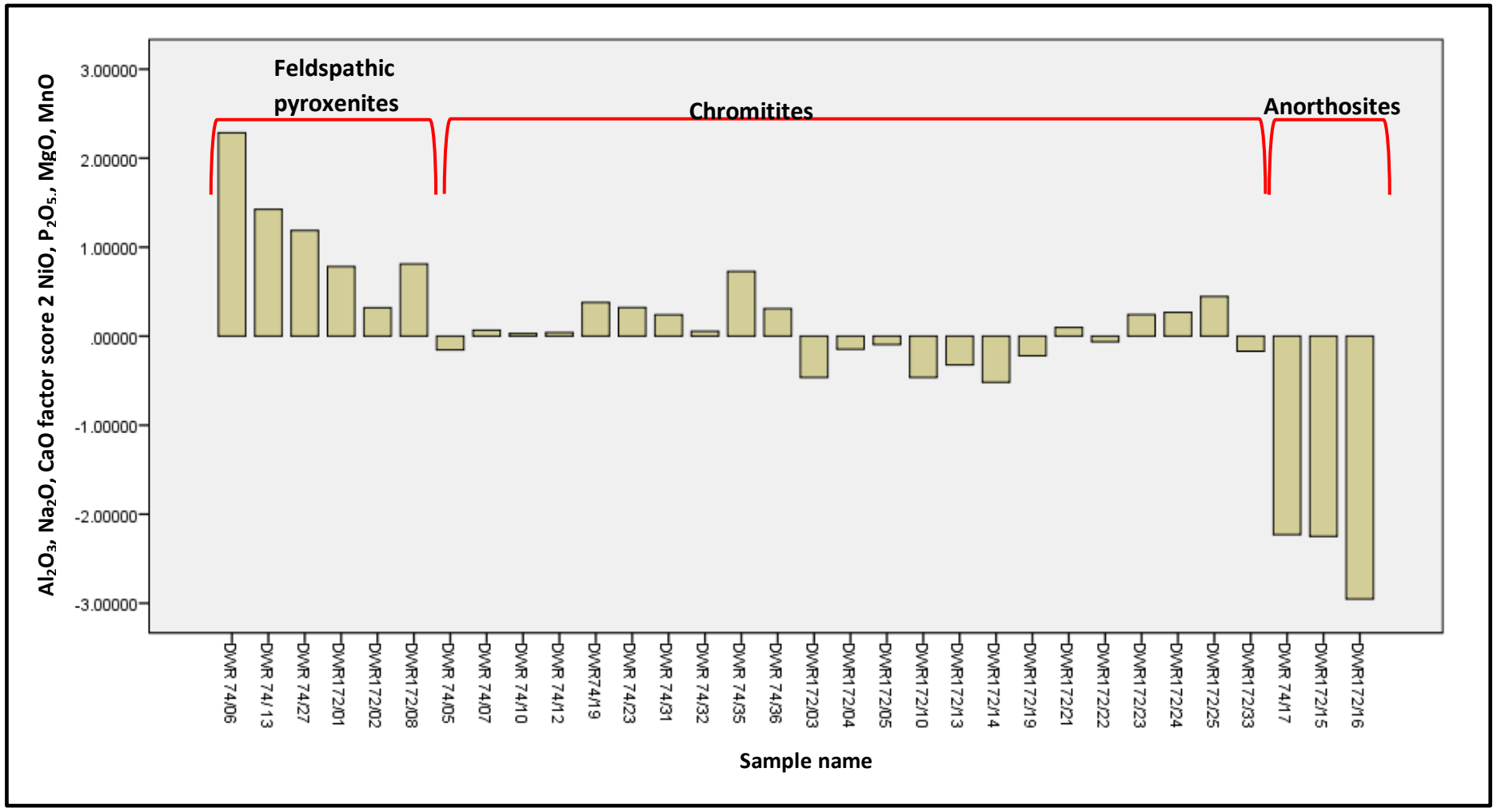

Figure 5.4: Graphical representation that shows the samples characterised as chromitite pyroxenites (positively loaded) and anorthosites (negatively loaded) within the MG3 package

5.1.1.3 Geochemical characterisation of the MG2 package

Multi element data from the feldspathic pyroxenites, chromitites anorthosites and chromitite pyroxenites based on core logging within the MG2 package were analyzed using factor analysis. The factor scores of these samples where represented graphically as factor scores against sample identification numbers (Fig 5.5 and 5.6). This allowed identification of the distinctive geochemical index that can be used to distinguish the different rock groups within the MG2 package.

Table 5.7: The total variance results of the MG2 package.

Total Variance Explained

Component	Initial Eigenvalues			Extraction Sums of Squared Loadings			Rotation Sums of Squared Loadings		
	Total	% of Variance	Cumulative %	Total	% of Variance	Cumulative %	Total	% of Variance	Cumulative %
1	6.669	55.576	55.576	6.669	55.576	55.576	5.530	46.085	46.085
2	3.281	27.343	82.918	3.281	27.343	82.918	4.018	33.483	79.568
3	1.249	10.407	93.325	1.249	10.407	93.325	1.651	13.757	93.325
4	.425	3.545	96.869						
5	.178	1.486	98.355						
6	.078	.649	99.004						
7	.060	.504	99.508						
8	.033	.275	99.783						
9	.014	.114	99.896						
10	.008	.066	99.962						
11	.005	.038	100.000						
12	5.527E-017	4.606E-016	100.000						

Extraction Method: Principal Component Analysis.

Table 5.8: Rotated component matrix of the MG2 package.

Rotated Component Matrix[a]

	Component		
	1	2	3
Cr_2O_3	.976		
TiO_2	.970		
SiO_2	-.966		
Fe_2O_3	.929		
NiO	.880	.431	
Al_2O_3		-.973	
MgO		.935	
MnO		.876	
CaO	-.641	-.751	
Na_2O	-.586	-.713	
P_2O_5			.872
K_2O			.849

Extraction Method: Principal Component Analysis.

Rotation Method: Varimax with Kaiser Normalization.

a. Rotation converged in 4 iterations.

Table 5.8 above presents the results for the three factors explaining 93.3% of the total variance. In table 5.9 factor one is positively loaded with Cr_2O_3, Fe_2O_3, TiO_2 and NiO. These oxides can be used to characterise the chromitite samples, but there are two chromitite samples that contain high content of SiO_2, CaO and Na_2O. Calcium oxide, SiO_2, and Na_2O are negatively loaded and are considered to characterise the feldspathic pyroxenites (figure 5.5). Majority of the feldspathic pyroxenites are defined by Cr_2O_3, Fe_2O_3, TiO_2 and NiO.

In figure 5.6, factor two is positively loaded with NiO, MgO and MnO. These represent the chromitite pyroxenites, but there are those chromitite pyroxenite samples that consist of Al_2O_3, CaO and Na_2O. The negatively loaded with oxides such Al_2O_3, CaO and Na_2O characterise the anorthosites rock types. The third factor is positively loaded with P_2O_5 and K_2O.

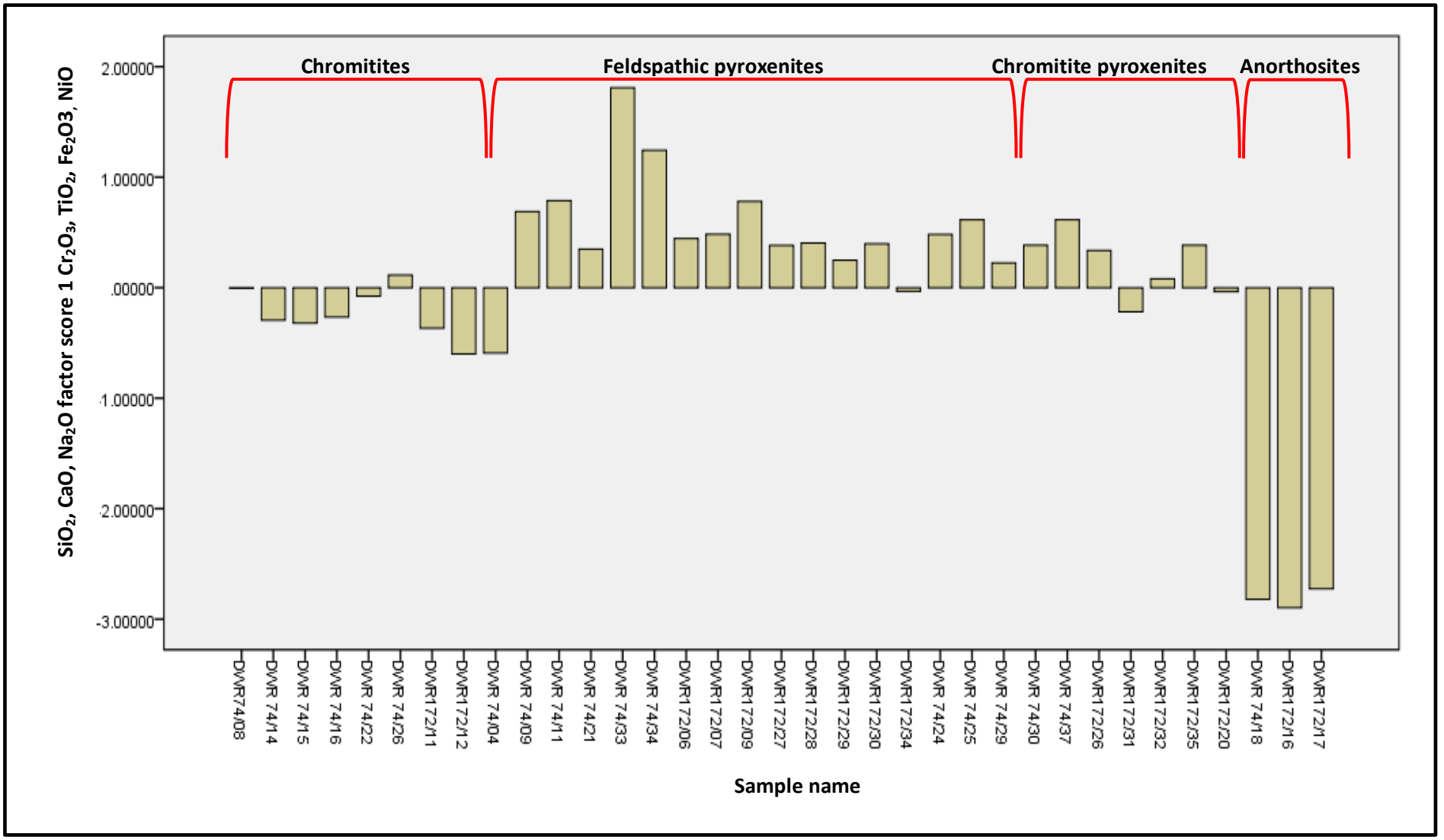

Figure 5.5: Graphical representation that shows the samples characterised as chromitites (positively loaded) and feldspathic pyroxenites (negatively loaded) within the MG2 package.

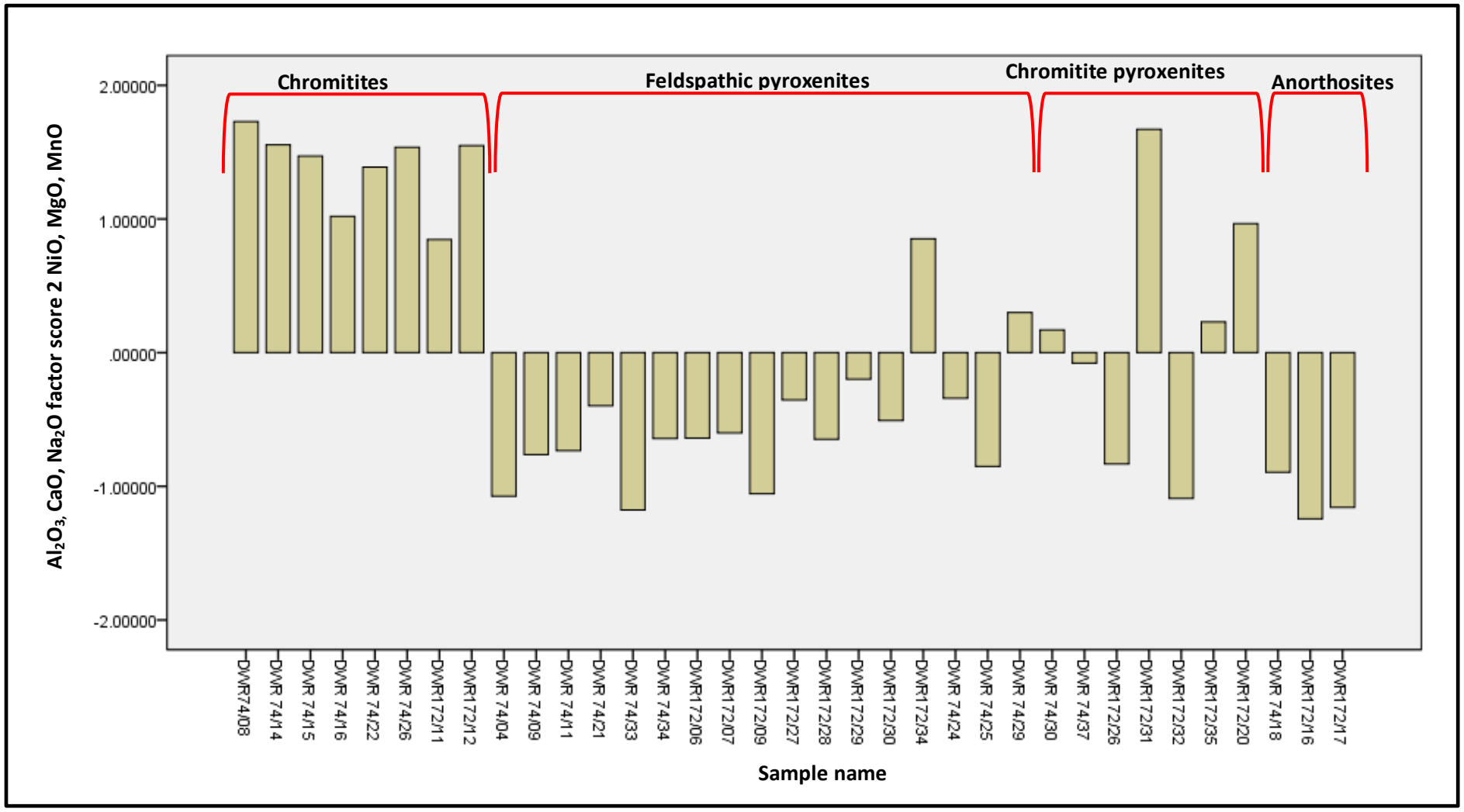

Figure 5.6: Graphical representation that shows the samples characterised as chromitite pyroxenites (positively loaded) and negatively loaded within the MG2 package.

In summary, the most important to note in the geochemical characterisation are:

- The various rock types from both the MG3 package and MG2 package were differentiated based on oxide content. The chromitites are defined by Cr_2O_3, Fe_2O_3, TiO_2 and NiO while SiO_2, CaO, Na_2O, K_2O and P_2O_5 characterise the feldspathic pyroxenites. The anorthosites are characterised by Al_2O_3, CaO and Na_2O, while NiO, P_2O_5, MgO and MnO characterise the chromitite pyroxenites. Petrographic studies revealed two types of chromitites, feldspathic pyroxenites, anorthosites and chromitite pyroxenites based on the modal composition, while factor analysis revealed only one type of anorthosite.

- The chromitites from the MG3 package show high content of Cr_2O_3, Fe_2O_3, TiO_2, NiO and MnO but there are a few chromitites samples that have high content of SiO_2, CaO and Na_2O. This suggests that there are two types of chromitites which was also seen within in the petrographic studies. Petrographic studies and factor analysis revealed two types of feldspathic pyroxenites and chromitites. The feldspathic pyroxenite samples which contain high content of chromite, factor analysis showed that they contain high content of Cr_2O_3, Fe_2O_3, TiO_2, NiO and MnO, while there are feldspathic pyroxenites samples which contain SiO_2, CaO, Na_2O, K_2O and P_2O_5. Based on the petrographic studies these are the samples which consist of high content of clinopyroxene and orthopyroxene.

- The chromitites within MG2 package are mainly composed of SiO_2, CaO and Na_2O but there are a few chromitites samples that consist of high content of Cr_2O_3, Fe_2O_3, TiO_2 and NiO. The feldspathic pyroxenites in the MG2 package consist of Cr_2O_3, Fe_2O_3, TiO_2 and NiO and there are other feldspathic pyroxenite samples that are defined by SiO_2, CaO and Na_2O. There are two types of chromitite pyroxenites that were identified in the petrographic study and factor analysis. The first group consist of high content of chromite were defined by NiO, MgO and MnO, while the second group consist of high content of orthopyroxene and plagioclase, were defined by Al_2O_3, CaO and Na_2O. Factor analysis revealed only one type of anorthosite from the anorthosites above the MG2 package. These are defined by high content of Al_2O_3, CaO and Na_2O. Petrographic study indicated two types of anorthosites, above the MG2 package and below the MG3 package.

5.1.2 Rock classification and characterisation by cluster and discriminant analysis.

In the previous section, factor analysis was used to determine oxides, in the various rock types identified during core logging. In this section, a different approach will be taken and then the two different methods will be compared to determine the most reliable method. Cluster analysis will identify the different groups or the rock types while discriminant analysis will identify which of these samples firstly belong to which rock type and secondly to which package, either the MG3 package or MG2 package.

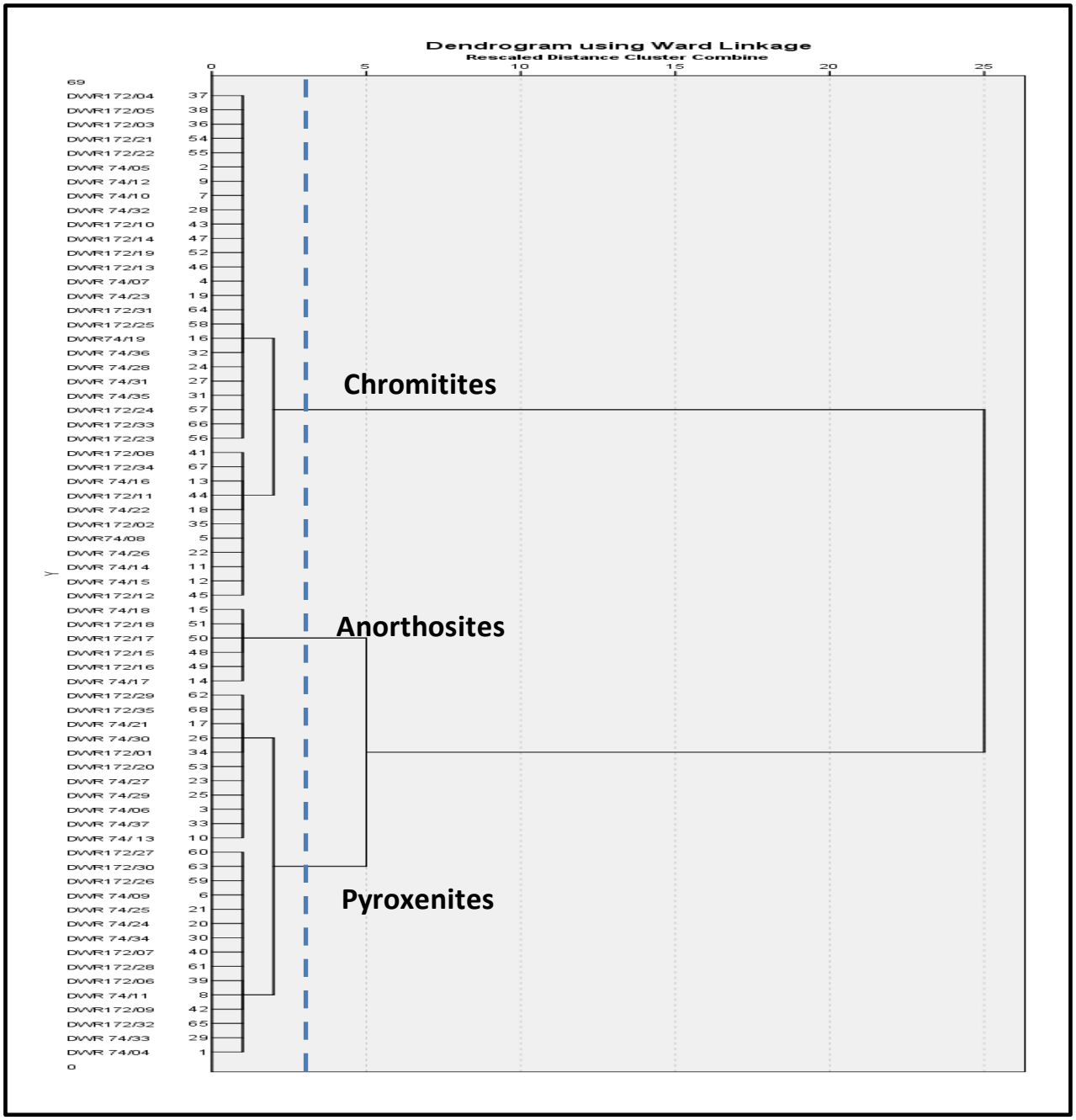

Figure 5.7: Dendrogram for sample points cluster identification of Dwarsrivier chrome mine data.

Figure 5.7 illustrates the cluster analysis results in the form of a dendrogram and it defined three clusters (Chromitites, anorthosites and pyroxenites), but the pyroxenites can be sub-divided into two groups. The pyroxenites samples where then analysed again using cluster analysis and two main groups were identified as illustrated by figure 5.8 below. The two groups emerged within the pyroxenites which are the feldspathic pyroxenites and chromitite pyroxenites.

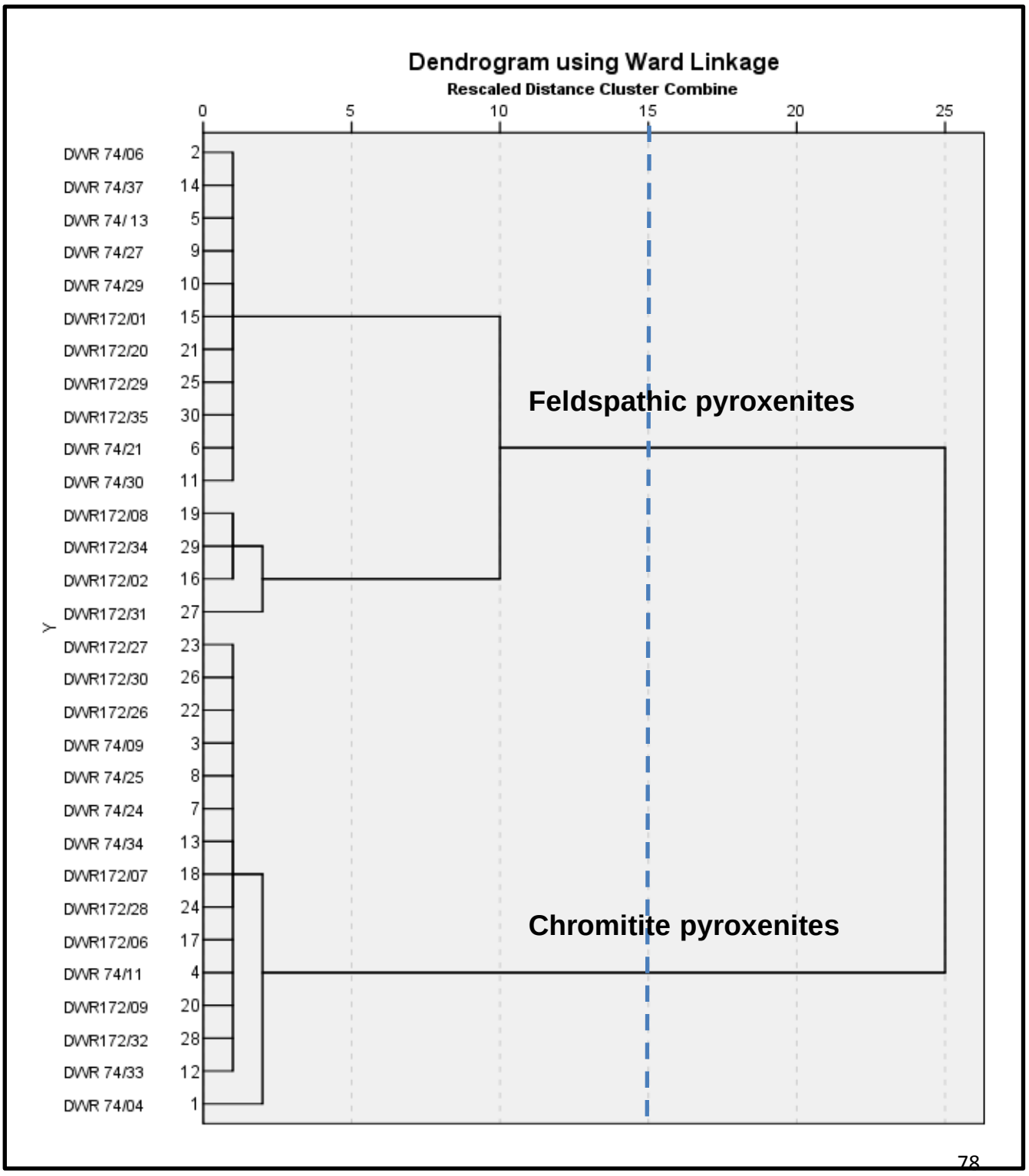

Figure 5.8: Dendrogram for sample points cluster identification of the two main groups of pyroxenites.

The combination of table 5.10 and table 5.11 shows the major elements which separate the chromitites from feldspathic pyroxenites in the first function in table 5.10. Oxides such as Fe_2O_3, NiO, TiO_2 and Cr_2O_3 characterise the chromitites, while the feldspathic pyroxenites are characterised by major elements such as SiO_2, CaO and K_2O. In function two the oxides which differentiate the anorthosites from chromitite pyroxenites are Al_2O_3 which characterise the anorthosites and chromitite pyroxenites are characterised by MgO. Manganese (IV) oxide and Na_2O didn't play a crucial role, thus they were excluded in the analysis.

Table 5.9: Three function discriminant structure matrix

Structure Matrix

	Function		
	1	2	3
Fe_2O_3	-.838*	-.070	.452
NiO	-.784*	-.212	.232
TiO_2	-.767*	.253	-.038
SiO_2	.723*	-.442	-.345
CaO	.660*	.576	.096
Cr_2O_3	-.656*	.330	.233
K_2O	.109*	-.037	.039
P_2O_5[b]	.064*	-.043	-.033
Al_2O_3	.149	.778*	.248
MgO	.007	-.593*	-.298
MnO[b]	-.349	-.457*	.112
Na_2O[b]	.268	.290*	-.094

Pooled within-groups correlations between discriminating variables and standardized canonical discriminant functions

Variables ordered by absolute size of correlation within function.

Table 5.10: Functions at group centroid.

Functions at Group Centroids

Predicted Group for Analysis 1	Function		
	1	2	3
Feldspathic pyroxenites	4.453	-4.588	.530
Chromitites	-4.278	1.441	.204
Chromitite Pyroxenites	.484	-1.790	-1.052
Anorthosites	11.266	7.721	.008

The results of the discriminant analysis are illustrated in figure 5.9 below in the form of a two-function discriminant plot that shows high content of the various oxides in each rock type.

Figure 5.9 below is discriminant plot representing the first two functions from the combination of discriminant and cluster analysis. On the y-axis, the first discriminant function has negative weights for Fe_2O_3, NiO, TiO_2 and Cr_2O_3 and Al_2O_3 and positive weights for CaO, SiO_2 and K_2O. On the x-axis, the second discriminant function has negative weights for MgO and positive weights for Al_2O_3.

Tables 5.10 and table 5.11 were used to characterise the various rock types based on the oxides content in the study area. The feldspathic pyroxenites are defined by CaO, SiO_2, K_2O and MgO, while the chromitites are characterised by Fe_2O_3, NiO, TiO_2 and Cr_2O_3 and Al_2O_3. Calcium oxide, SiO_2, K_2O and Al_2O_3 characterise the anorthosite samples, while the chromitite pyroxenites are characterised by CaO, SiO_2, K_2O, Fe_2O_3, NiO, TiO_2 and Cr_2O_3 and Al_2O_3.

Figure 5.9 also demonstrates the process of fractional crystallisation from the chromitites through to the feldspathic pyroxenites. There is high iron and chromium content within the chromitites (negatively loaded). As the heavy elements start crystallising, the chromium and iron content in the magma decreases. This is seen by the lower chromium and iron content within the chromitite pyroxenites and in the MG2 package from the MG3 package.

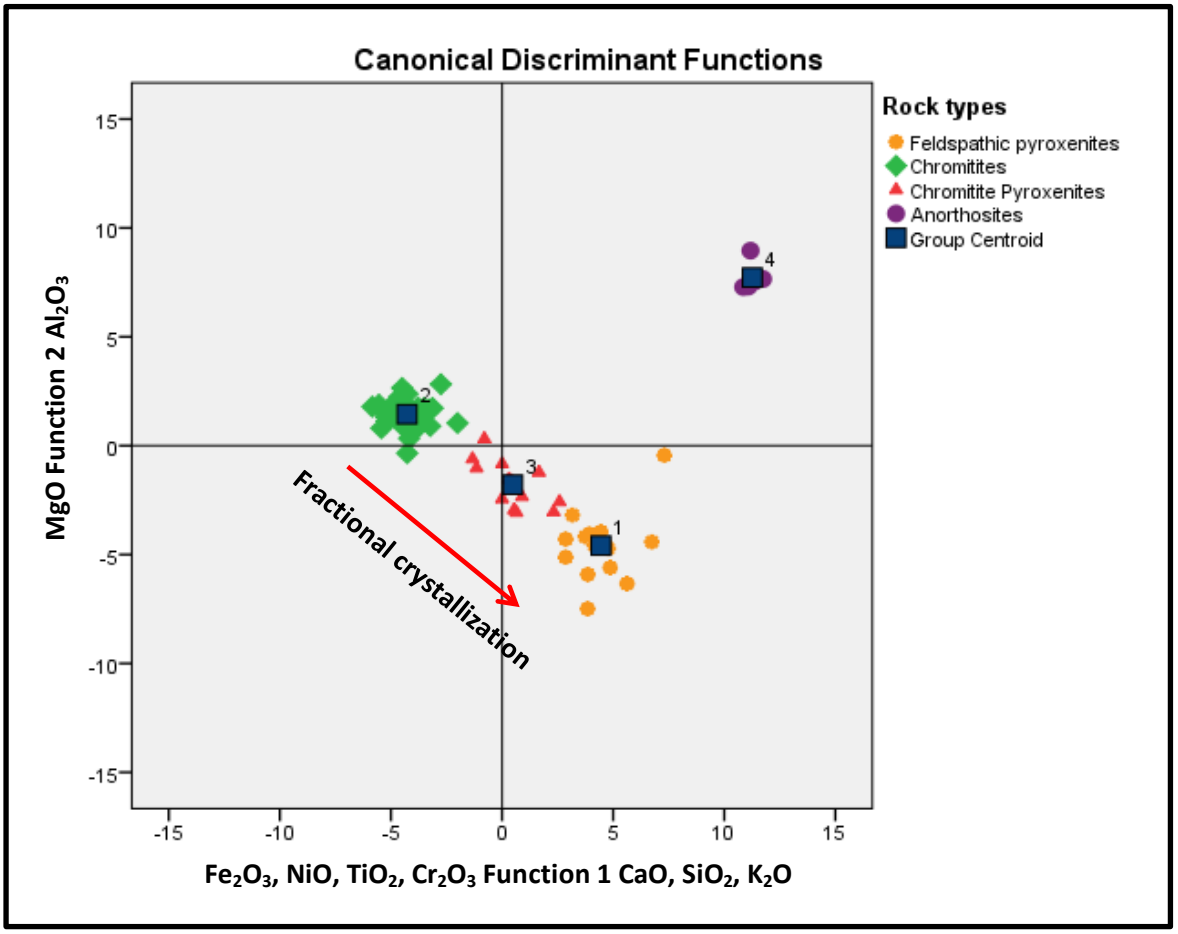

Figure 5.9: Two-function discriminant plot showing the abundance of oxides in each rock type from Dwarsrivier chrome mine.

Table 5.11 shows that the four rock types have been classified correctly by 100%. From the 68 samples collected in the field, 15 samples are feldspathic pyroxenites, 36 samples are chromitites, 11 samples are chromitite pyroxenites and 6 samples are anorthosites.

Table 5.12 present oxides which can be used to distinguish the four rock types within the MG2 and MG3 package of the Dwarsrivier Chrome mine. Stepwise discriminant analysis was used to evaluate these major elements that distinguish the four rock types. The results table 5.11 gave 100% of the original grouped cases to be correctly classified. The results gave 100% difference across the four rock types within the Dwarsrivier Chrome mine, with Fe_2O_3 giving the highest percentage difference at 95.6%, SiO_2 and CaO giving the second highest at 2.9% and TiO_2 being the lowest differentiator at 1.8%. A summary of the results is given in table 5.12.

Table 5.11: Classification results for the four rock types at Dwarsrivier chrome mine.

Classification Results[a]

		Ward Method	Predicted Group Membership				Total
			1	2	3	4	
Original	Count	Feldspathic Pyroxenites	15	0	0	0	15
		Chromitites	0	36	0	0	36
		Chromitite pyroxenites	0	0	11	0	11
		Anorthosites	0	0	0	6	6
	%	Feldspathic pyroxenites	100.0	.0	.0	.0	100.0
		Chromitites	.0	100.0	.0	.0	100.0
		Chromitite pyroxenites	.0	.0	100.0	.0	100.0
		Anorthosites	.0	.0	.0	100.0	100.0

a. 100.0% of original grouped cases correctly classified.

Table 5.12: the percentage difference of oxides that distinguishes the four rock types within Dwarsrivier chrome mine.

Major element	**Percentage difference**
Fe_2O_3	95.6%
SiO_2 and CaO	98.5%
TiO_2	100%
Total	100%

5.1.2.1 Elements which distinguish the major rock types in the MG2 package from those in the MG3 package.

The 68 samples collected from the study area in the field consist of 19 samples of feldspathic pyroxenites, 32 samples of chromitites, 6 samples of anorthosites and 11 samples of chromitite pyroxenites, but which of these samples from the various rock samples belong to the MG2 package and MG3 package?

In this section cluster analysis was applied to the 68 samples, which grouped them into four groups. These four groups are chromitites, feldspathic pyroxenites, chromitite pyroxenites and anorthosites.

Cluster analysis was again applied in each group to ensure that its only one group exists and then discriminant analysis was applied, that resulted in each group consisting of one function that is negatively loaded and the other being positively loaded with various elements. These elements will be used to distinguish the major rock types in the MG2 package to those in the MG3 package.

5.1.2.1.1 Feldspathic pyroxenites

A combination of cluster and discriminant analysis was used on the 18 feldspathic pyroxenites geochemical data.

In table 5.14 function one is negatively loaded with K_2O, MgO, CaO, P_2O_5, MnO and Na_2O. These oxides can be used to characterise the MG2 feldspathic pyroxenites, while Cr_2O_3, NiO, TiO_2, Fe_2O_3 and Al_2O_3 are negatively loaded and is therefore considered to characterise the feldspathic pyroxenites within the MG3 package. The structure matrix in table 5.13 below shows that SiO_2 didn't play a significant role in the analysis that is why it was not part of the analysis.

Table 5.15 shows the classification results for the feldspathic pyroxenites within the MG2 and MG3 package. It shows that the originally grouped cases of feldspathic pyroxenites were 100% classified and that from the 18 feldspathic pyroxenites samples, 13 samples are MG2 feldspathic pyroxenites and 6 samples are MG3 feldspathic pyroxenites.

Table 5.13: One function discriminant structure matrix and function group centroids for the MG2 and MG3 feldspathic pyroxenites.

Structure Matrix

	Function
	1
SiO_2[a]	-.648
Cr_2O_3	.573
NiO	.456
TiO_2	.454
Fe_2O_3	.439
K_2O	-.178
MgO	-.176
CaO	-.170
Al_2O_3	.164
P_2O_5	-.120
MnO	-.116
Na_2O	-.027

Pooled within-groups correlations between discriminating variables and standardized canonical discriminant functions

Variables ordered by absolute size of correlation within function.

a. This variable not used in the analysis.

Functions at Group Centroids

Ward Method	Function
	1
MG2 Feldspathic Pyroxenites	-1.842
MG3 Feldspathic Pyroxenites	3.991

Unstandardized canonical discriminant functions evaluated at group means

Table 5.14: Classification results for the MG2 and MG3 feldspathic pyroxenites.

Classification Results

		Ward Method	Predicted Group Membership		Total
			1	2	
Original	Count	MG2 Feldspathic pyroxenites	13	0	13
		MG3 Feldspathic pyroxenites	0	6	6
	%	MG2 Feldspathic pyroxenites	100.0	.0	100.0
		MG3 feldspathic pyroxenites	.0	100.0	100.0

a. 100.0% of original grouped cases correctly classified.

Stepwise discriminant analysis was used to determine the major elements which can be used to differentiate the MG2 feldspathic pyroxenites from the MG3 feldspathic pyroxenites.

SiO_2 didn't play a significant role in the analysis, that why it was not part of the analysis as illustrated by table 5.14.

The oxides which differentiates the two feldspathic pyroxenites was Cr_2O_3. Therefore chromium (III) oxide and SiO_2 were then removed from the analysis to again determine if there are other oxide(s) than chromium (III) oxide that can be used to differentiate the two feldspathic pyroxenites. This revealed NiO and MnO are the two oxides that differentiate the feldspathic pyroxenites within the MG2 and MG3 package (table 5.15). Both NiO and MnO gave a 94.7% that the original grouped cases where correctly classified as presented by table 5.16. Thus these results can be used with high level of confidence.

Table 5.15: oxides used to distinguish the MG3 feldspathic pyroxenites and MG2 feldspathic pyroxenites.

Variables Entered/Removed

Step	Entered	Wilks' Lambda							
		Statistic	df1	df2	df3	Exact F			
						Statistic	df1	df2	Sig.
1	NiO	.370	1	1	17.000	28.997	1	17.000	.000
2	MnO	.231	2	1	17.000	26.567	2	16.000	.000

At each step, the variable that minimizes the overall Wilks' Lambda is entered.

a. Maximum number of steps is 20.

b. Minimum partial F to enter is 3.84.

c. Maximum partial F to remove is 2.71.

d. F level, tolerance, or VIN insufficient for further computation.

Table 5.16: Classification results for the MG2 and MG3 feldspathic pyroxenites samples using stepwise discriminant analysis.

Classification Results

		Ward Method	Predicted Group Membership		Total
			1	2	
Original	Count	MG3 Feldspathic pyroxenites	12	1	13
		MG2 Feldspathic pyroxenites	0	6	6
	%	MG3 Feldspathic pyroxenites	92.3	7.7	100.0
		MG2 Feldspathic pyroxenites	.0	100.0	100.0

a. 94.7% of original grouped cases correctly classified.

The scatter plot of NiO vs MnO for the MG feldspathic pyroxenites is presented in Fig 5.10. Stepwise discriminant analysis shows that Nickel (II) oxide and MnO could be used to distinguish MG2 feldspathic pyroxenites from the MG3 feldspathic pyroxenites (table 5.16). The scatter plot below shows that the MG3 feldspathic pyroxenites have higher concentration of NiO relative to lower content of NiO within the MG2 package. There are those MG2 feldspathic pyroxenites that show higher concentration of MnO. This is due to the presences of higher content of orthopyroxene, relative to the higher plagioclase content within the MG3 feldspathic pyroxenites. The higher presences of NiO may attribute to possible sulphide or chromite control.

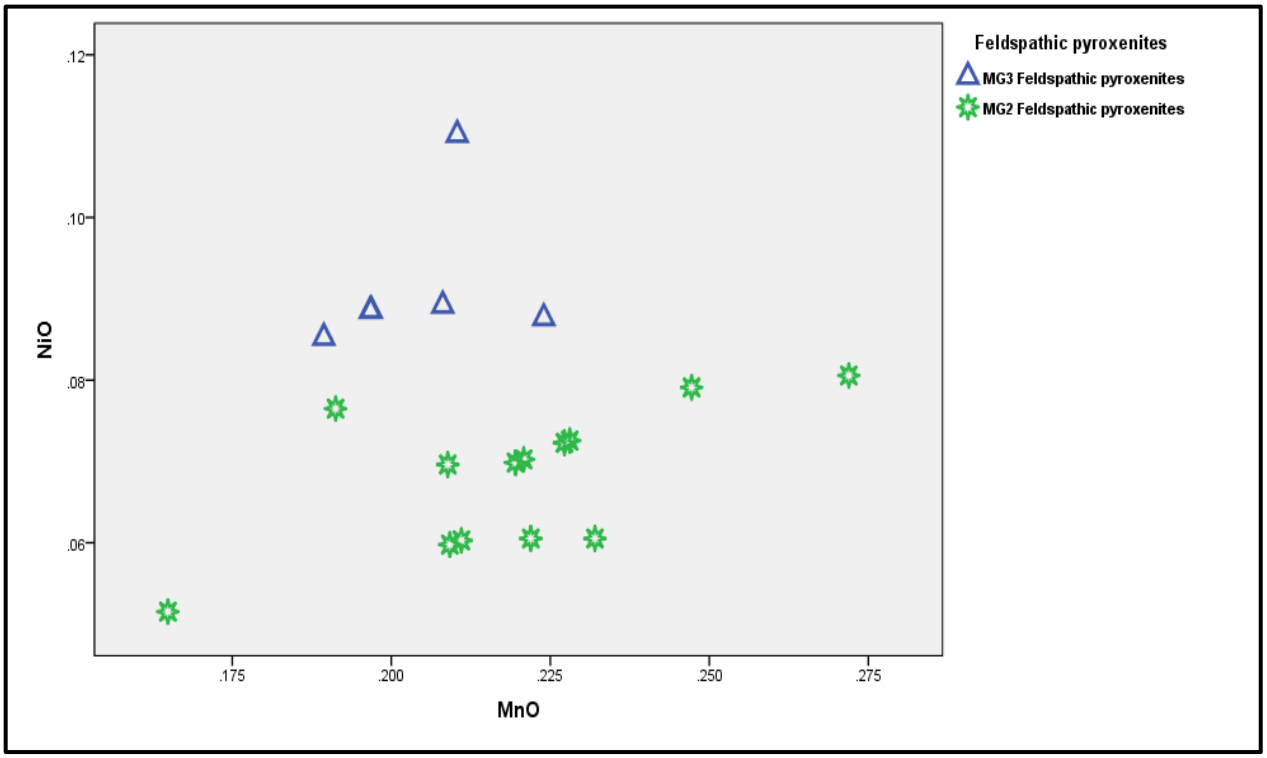

Figure 5.10: Scatter plot of the whole rock NiO versus whole rock MnO for the feldspathic pyroxenites.

5.1.2.1.2 Chromitites

The geochemical data of thirty two chromitite samples were analyzed using cluster and discriminant analysis. The thirty two chromitite samples were sub-divided into two groups, which are the MG2 chromitites and MG3 chromitites. The discriminant analysis was used to establish which oxides can be used to distinguish the two types of chromitites.

Table 5.17: One function discriminant structure matrix and function group centroids for the MG2 and MG3 chromitites

Structure Matrix

	Function
	1
SiO_2[a]	-.690
Cr_2O_3	.645
Fe_2O_3	.531
NiO	.354
CaO	-.289
MnO	.242
TiO_2	.210
MgO	-.206
P_2O_5	-.186
Na_2O	-.177
K_2O	.084
Al_2O_3	-.031

Pooled within-groups correlations between discriminating variables and standardized canonical discriminant functions

Variables ordered by absolute size of correlation within function.

a. This variable not used in the analysis.

Functions at Group Centroids

Ward Method	Function
	1
MG3 Chromitites	.972
MG2 Chromitites	-2.916

Unstandardized canonical discriminant functions evaluated at group means

Table 5.17 demonstrates that function one is positively loaded with Cr_2O_3, Fe_2O_3, NiO, MnO and TiO_2. These oxides can be used to characterise the MG3 chromitites, while CaO, MgO, P_2O_2, Na_2O and Al_2O_3 are negatively loaded and therefore characterise the MG2 chromitites.

Table 5.18 shows the chromitite samples have been correctly classified into the MG3 chromitites and MG2 chromitites by 100%, indicating that the percentage of accurate analysis is high for distinguishing the MG3 chromitites from the MG2 chromitites. The MG3 chromitites consist of twenty four samples and eight samples are from the MG2 chromitites.

Table 5.18: Classification results for the MG2 and MG3 feldspathic pyroxenites.

Classification Results

		Ward Method	Predicted Group Membership		Total
			1	2	
Original	Count	MG3 Chromitites	24	0	24
		MG2 Chromitites	0	8	8
	%	MG3 Chromitites	100.0	.0	100.0
		MG2 Chromitites	.0	100.0	100.0

a. 100.0% of original grouped cases correctly classified.

Table 5.19: oxides used to distinguish the difference between the MG3 chromitites and MG2 chromitites

Variables Entered/Removed

Step	Entered	Removed	Wilks' Lambda							
			Statistic	df1	df2	df3	Exact F			
							Statistic	df1	df2	Sig.
1	NiO		.725	1	1	30.000	11.356	1	30.000	.002
2	MgO		.624	2	1	30.000	8.746	2	29.000	.001
3	CaO		.454	3	1	30.000	11.206	3	28.000	.000
4		NiO	.455	2	1	30.000	17.392	2	29.000	.000

At each step, the variable that minimizes the overall Wilks' Lambda is entered.

a. Maximum number of steps is 6.

b. Minimum partial F to enter is 3.84.

c. Maximum partial F to remove is 2.71.

d. F level, tolerance, or VIN insufficient for further computation.

The MG3 chromitites can be differentiated from the MG2 chromitites by using stepwise discriminant analysis. Table 5.19 above show Nickel (II) oxide, MgO and CaO can be used to distinguish the MG3chromitites from MG2 chromitites.

The stepwise discriminant revealed that three elements can be used to distinguish the MG3 chromitites from the MG2 chromitites, with an accuracy level of 96.9%.

Nickel (II) oxide gives the highest percentage difference of 78.1% while MgO, the lowest percentage difference of 3.1%. Table 5.20, shows the percentage difference of the oxides that distinguish the MG3 chromitites from the MG2 chromitites.

Table 5.20: Oxides with the percentage difference used to distinguish the MG2 and MG3 chromitites.

Major element	Percentage difference
NiO	78.1%
CaO	93.8%
MgO	96.9%
Total	96.9%

The stepwise discriminant analysis results (table 5.20) showed that NiO, MgO and CaO are the three oxides which could be used differentiate the MG3 chromitites from the MG2 chromitites. Table 5.20 shows that NiO and CaO have a percentage difference as compared to MgO. Figure 5.11 shows that the MG3 chromitites are characterised by higher NiO concentration relative to the MG2 chromitites. The high NiO content is associated with higher content of chromite within the MG3 chromitites as compared to the MG2 chromitites.

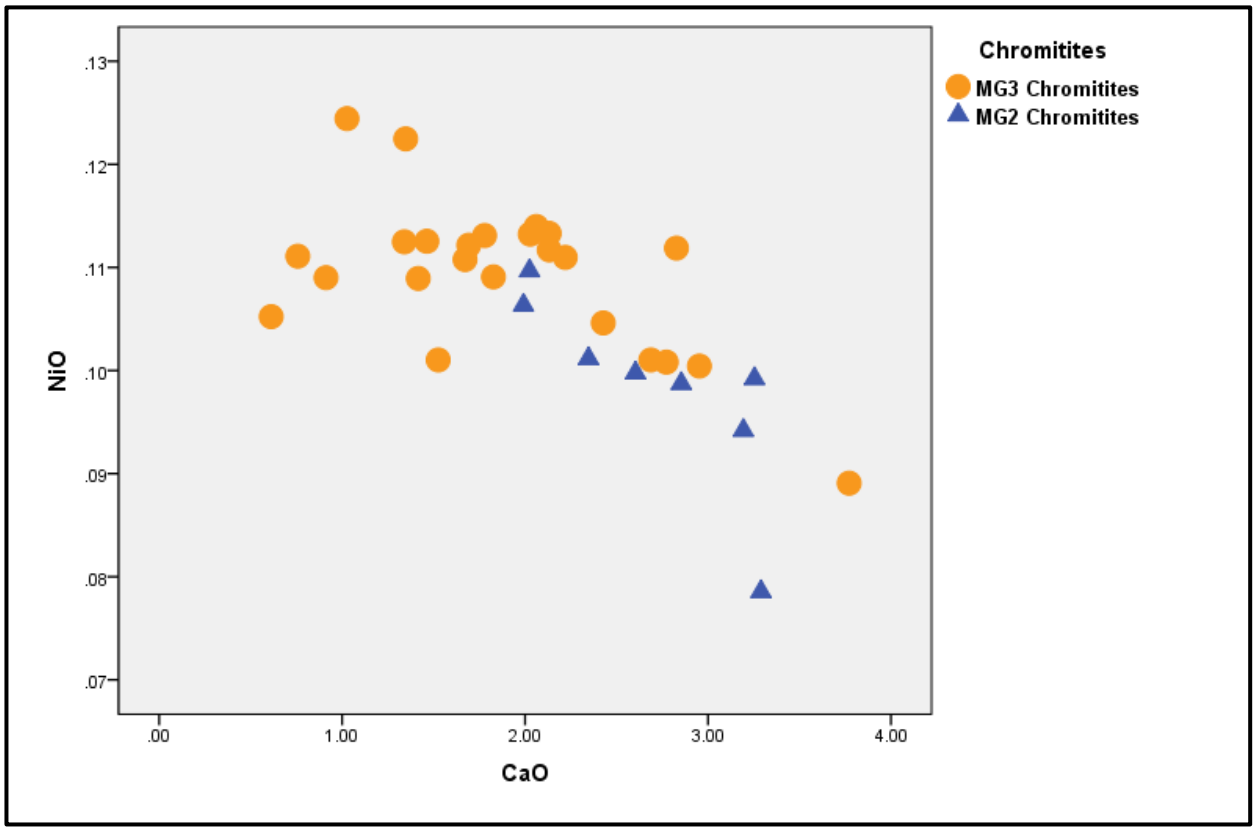

Figure 5.11: Scatter plot of the whole rock NiO versus whole rock CaO within the MG chromitites

5.1.2.1.3 Anorthosites

The anorthosite samples were sub-divided into two groups, after a combination of cluster and discriminant analysis was used to characterise the samples. Anorthosites where sampled from above the MG2 package and below the MG3 package.

The oxides P_2O_5, TiO_2, SiO2, K2O, MnO, MgO, NiO and Na_2O were not part of the analysis as illustrated by the structure matrix in table 5.21 below. In table 5.21 function one is negatively loaded with Fe_2O_3 and CaO. These oxides characterise the anorthosites below the MG3 package, while there are oxides that can be used to characterise the anorthosites above the MG2 package. Table 5.22 illustrates that the anorthosite samples have been correctly classified by 100%, with the anorthosites above the MG2 consisting of 3 samples and the other 3 samples belong to the anorthosites below the MG3 package.

Table 5.21: One function discriminant structure matrix and function group for the anorthosites above the MG2 package and below the MG3 package.

Structure Matrix

	Function
	1
P_2O_5[a]	-.915
TiO_2[a]	-.442
SiO_2[a]	-.410
K_2O[a]	-.177
Cr_2O_3	.150
MnO[a]	.144
MgO[a]	.120
NiO[a]	-.100
Al_2O_3	.080
Na_2O[a]	-.044
Fe_2O_3	.022
CaO	.002

Pooled within-groups correlations between discriminating variables and standardized canonical discriminant functions

Variables ordered by absolute size of correlation within function.

a. This variable not used in the analysis.

Functions at Group Centroids

Ward Method	Function
	1
Anorthosites below the MG3 package	-10.713
Anorthosites above the MG2 package	10.713

Unstandardized canonical discriminant functions evaluated at group means

Table 5.22: Classification results for the anorthosites below the MG3 package and anorthosites above the MG2 package.

Classification Results

		Ward Method	Predicted Group Membership		Total
			1	2	
Original	Count	Anorthosite below MG3 package	3	0	3
		Anorthosite above MG2 package	0	3	3
	%	Anorthosite below MG3 package	100.0	.0	100.0
		Anorthosite above MG2 package	.0	100.0	100.0

a. 100.0% of original grouped cases correctly classified.

Table 5.23: Oxides used to distinguish the difference between the anorthosites below the MG3 package and anorthosites above the MG2 package.

Variables Entered/Removed

Step	Entered	Wilks' Lambda							
		Statistic	df1	df2	df3	Exact F			
						Statistic	df1	df2	Sig.
1	NiO	.005	1	1	4.000	755.919	1	4.000	.000
2	K2O	.000	2	1	4.000	8171.596	2	3.000	.000
3	TiO_2	.000	3	1	4.000	60297.613	3	2.000	.000

At each step, the variable that minimizes the overall Wilks' Lambda is entered.

a. Maximum number of steps is 24.

b. Minimum partial F to enter is 3.84.

c. Maximum partial F to remove is 2.71.

d. F level, tolerance, or VIN insufficient for further computation.

The stepwise discriminant analysis was then done to determine the oxides which can be used to distinguish the anorthosites above the MG2 package from the anorthosites below the MG3 package.

Table 5.23 above show NiO, K_2O and TiO_2 can be used to distinguish the anorthosites above the MG2 package from the anorthosites below the MG3 package.

Table 5.24 below is stepwise discriminant classification results for the three oxides used can correctly distinguish the two types of anorthosites by 100%, indicating the percentage of accuracy for distinguishing the anorthosites above the MG2 package from the anorthosites below the MG3 package.

Table 5.24: Classification results for the anorthosites below the MG3 package and anorthosites above the MG2 package using stepwise discriminant analysis.

Classification Results

		Ward Method	Predicted Group Membership		Total
			1	2	
Original	Count	Anorthosite below the MG3 package	3	0	3
		Anorthosite above the MG2 package	0	3	3
	%	Anorthosite below the MG3 package	100.0	.0	100.0
		Anorthosites above the MG2 package	.0	100.0	100.0

a. 100.0% of original grouped cases correctly classified.

5.1.2.1.4 Chromitite pyroxenites

The geochemical data from eleven chromitite pyroxenite samples were analyzed using a combination of cluster and discriminant analysis. Two types of chromitite pyroxenites were identified through cluster analysis. Sodium (II) oxide, SiO_2, and NiO were not part of the analysis (table 5.25) of the structure matrix.

Table 5.25: One function discriminant structure matrix and function group centroids for the lower and upper chromitite pyroxenites.

Structure Matrix

	Function
	1
Cr_2O_3	-.282
MgO	.275
SiO_2[a]	.246
Al_2O_3	-.223
Fe_2O_3	-.218
Na_2O[a]	.143
TiO_2	-.141
CaO	.129
K_2O	.098
P_2O_5	.065
MnO	.061
NiO[a]	-.013

Pooled within-groups correlations between discriminating variables and standardized canonical discriminant functions

Variables ordered by absolute size of correlation within function.

a. This variable not used in the analysis.

Functions at Group Centroids

Ward Method	Function
	1
Upper chromitite pyroxenites	2.296
Lower chromitite pyroxenites	-10.331

Unstandardized canonical discriminant functions evaluated at group means

In table 5.25, function one is positively loaded with MgO, CaO, K_2O, P_2O_5 and MnO. These oxides can be used to characterise the upper chromitite pyroxenites, while Cr_2O_3, Al_2O_3, Fe_2O_3 and TiO_2 are negatively loaded and therefore considered to characterise the lower chromitite pyroxenites. The upper chromitite pyroxenites which consist of nine samples and lower chromitite pyroxenites consist of two samples.

The results give a 100% difference between the upper chromitite pyroxenites from the lower chromitite pyroxenites. These results can be used with high level of confidence. A summary of the results is given in table 5.26.

Table 5.26: Classification results for upper and lower chromitite pyroxenites.

Classification Results[a]

		Ward Method	Predicted Group Membership		Total
			1	2	
Original	Count	Upper chromitite pyroxenites	9	0	9
		Lower chromitite pyroxenites	0	2	2
	%	Upper chromitite pyroxenites	100.0	.0	100.0
		Lower chromitite pyroxenites	.0	100.0	100.0

a. 100.0% of original grouped cases correctly classified.

Table 5.27: Oxides used to distinguish between the upper and lower chromitite pyroxenites.

Variables Entered/Removed

Step	Entered	Wilks' Lambda							
		Statistic	df1	df2	df3	Exact F			
						Statistic	df1	df2	Sig.
1	MgO	.313	1	1	9.000	19.794	1	9.000	.002
2	K_2O	.175	2	1	9.000	18.876	2	8.000	.001

At each step, the variable that minimizes the overall Wilks' Lambda is entered.

a. Maximum number of steps is 4.

b. Minimum partial F to enter is 3.84.

c. Maximum partial F to remove is 2.71.

d. F level, tolerance, or VIN insufficient for further computation.

Stepwise discriminant analysis was used to determine the major elements which can contrast the upper chromitite pyroxenites from the lower chromitite pyroxenites within the MG2 package. Table 5.27 shows MgO and K_2O can be used to separate the upper chromitite pyroxenites from the lower chromitite pyroxenites. The stepwise discriminant classification results for the two oxides used to distinguish the two types of chromitite pyroxenites which are correctly classified by 100% (Table 5.28).

Table 5.28: Classification results for the upper and lower chromitites, using stepwise discriminant analysis.

Classification Results[a]

		Ward Method	Predicted Group Membership		Total
			1	2	
Original	Count	Upper chromitite pyroxenites	9	0	9
		Lower chromitite pyroxenites	0	2	2
	%	Upper chromitite pyroxenites	100.0	.0	100.0
		Lower chromitite pyroxenites	.0	100.0	100.0

a. 100.0% of original grouped cases correctly classified.

Table 5.28, MgO and K_2O can distinguish the two types of chromitites pyroxenites within the MG2 package. The lower chromitite pyroxenites (lower parts of the MG2 package) show a higher concentration of MgO relative to the upper chromitite pyroxenites (upper parts of the MG2 package).

In summary, the elements that contrast the major rock types in the MG2 package from the MG3 package:

- Petrography revealed that the major rock types can be sub-divided into two; this was confirmed by the geochemical characterisation of the various rock types. The oxides that distinguish the chromitites, feldspathic pyroxenites, chromitite pyroxenites and anorthosites are Fe_2O_3, SiO2, CaO and TiO_2.
- The chromitites can be sub-divided into the MG3 chromitites and MG2 chromitites based on their association to certain elements. Nickel (II) oxide, MgO and CaO are the oxides that distinguish the MG3 chromitites from the MG2 chromitites.
- There are two types of feldspathic pyroxenites, namely the MG3 feldspathic pyroxenites and MG2 feldspathic pyroxenites. The MG2 feldspathic pyroxenites and MG2 feldspathic pyroxenites can be differentiated by using NiO and MnO.
- Nickel (II) oxide, K_2O and TiO_2 are the elements that can be used distinguish the anorthosites above the MG2 package from those below the MG3 package.
- The chromitite pyroxenites in the MG2 package can be sub-divided into two types. Magnesium oxide and K_2O are the elements used to differentiate the lower chromitite pyroxenites from the upper chromitites pyroxenites.

5.1.2.2 Trace elements that distinguish the major rock types in the MG2 package from those in the MG3 package.

In this section cluster analysis was applied on the trace elements geochemical data of the 68 samples, which grouped them into four groups which are the chromitites, feldspathic pyroxenites, chromitite pyroxenites and anorthosites. Cluster analysis was again applied in each group to ensure that its only one group exists and then discriminant analysis was applied, that resulted in each group consisting of one function that is negatively loaded and the other being positively loaded with various trace elements. These trace elements will be used to distinguish between the major rock types in the MG2 package to those in the MG3 package.

Table 5.29: Three function matrix and function at centroids for major elements.

Structure Matrix

	Function		
	1	2	3
Cr	.720*	.015	-.069
Zn	.686*	-.027	-.014
V	.552*	.039	.042
Ti	.512*	.488	.142
Ga	.459*	-.147	.089
Co	.398*	.182	.089
Ni	.246	.445*	.007
Sr	-.067	-.320*	.043
P	-.057	.253*	-.180
Zr	-.041	.252*	.062
Nd	-.037	-.198*	.009
Ba	-.138	-.155*	.051
Y	-.131	.133*	-.078
Pb	-.016	-.131*	-.052
Ce	-.021	-.113*	.005
S	-.052	.100*	.044
Cu	.003	-.095*	-.051
Nb	.033	.234	.538*
Cl	-.074	.342	-.342*
U	-.013	.002	-.308*
La	.142	.115	-.251*
Rb	-.028	.074	-.119*

Pooled within-groups correlations between discriminating variables and standardized canonical discriminant functions
Variables ordered by absolute size of correlation within function.

*. Largest absolute correlation between each variable and any discriminant function

Functions at Group Centroids

Average Linkage (Between Groups)	Function		
	1	2	3
Feldspathic pyroxenites	-9.236	-.643	.011
Chromitites	7.085	-.273	-.118
Chromitite pyroxenites	-3.615	1.723	-.384
Anorthosites	1.748	.825	1.941

Unstandardized canonical discriminant functions evaluated at group means

The combination of cluster and discriminant analysis was used to characterise the rock types from Dwarsrivier chrome mine. In table 5.29, function one in the structure matrix and the function groups at centroids characterise the chromitites. Function two; consist of chromitite pyroxenites and feldspathic pyroxenites. The results of the combination of cluster and discriminant analysis are illustrated in figure 5.14 in the form of a two-function discriminant plot. This shows the trace elements which distinguish the four rock types.

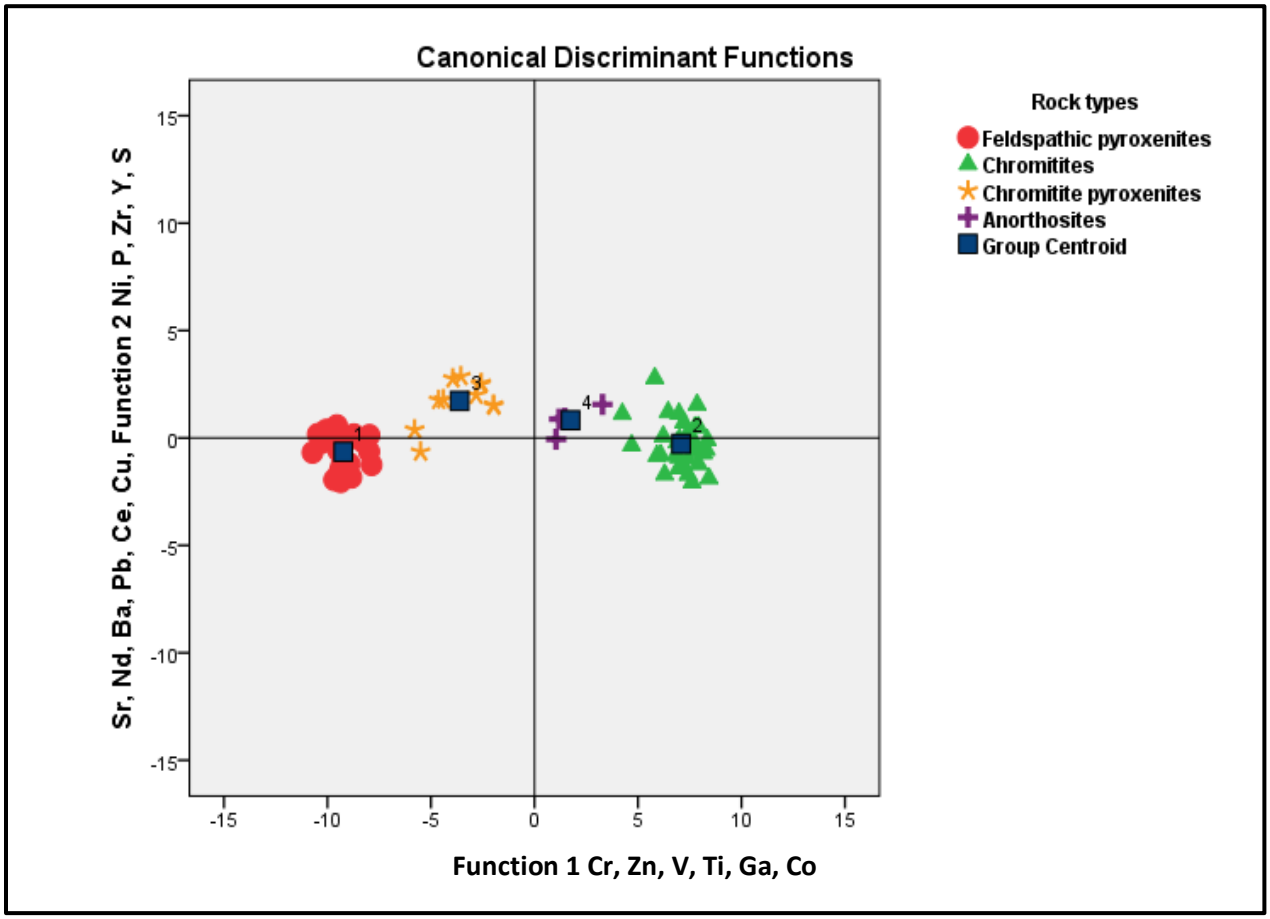

Figure 5.12: Two-function discriminant plot showing the abundance of trace elements in each rock type from the Dwarsrivier chrome mine.

In figure 5.12 is discriminant plot representing the first two functions from the combination of discriminant and cluster analysis. On the y-axis, the first discriminant function has positive weights for Cr, Zn, V, Ti, Ga and Co. On the x-axis, the second discriminant function has negative weights for Sr, Nd, Ba, Pb, Ce and Cu, while on the positive weights for Ni, P, Zr, Y and S.

Table 5.29 shows the structure matrix and functions at group centroids that characterise the various rock types based on the trace elements. The feldspathic pyroxenites can be associated with the following trace elements such as Sr, Nd, Ba, Pb, Ce, Cu, Ni, P, Zr, Y and S while the

chromitites with Cr, Zn, V, Ti Ga, Co, Ni, P, Zr, Y and S. Trace elements such as Cr, Zn, v, Ti, Ga, Co, Ni, P, Zr, Y and S are associated with the anorthosite samples while Ni, P, Zr, Y and S can be associated with the chromitite pyroxenites.

Table 5.30 shows the four rock types that have been classified correctly by 100%. From the 68 samples collected in the field, the combination of cluster and discriminant analysis shows that 21 samples are feldspathic pyroxenites, 32 samples are chromitites, 11 samples are chromitite pyroxenites and 4 samples are anorthosites.

Table 5.30: Classification results for the rock types at Dwarsrivier chrome mine based on the trace elements.

Classification Results[a]

		Average Linkage (Between Groups)	Predicted Group Membership				Total
			1	2	3	4	
Original	Count	Feldspathic pyroxenites	21	0	0	0	21
		Chromitites	0	32	0	0	32
		Chromitite pyroxenites	0	0	11	0	11
		Anorthosites	0	0	0	4	4
	%	Feldspathic pyroxenites	100.0	.0	.0	.0	100.0
		Chromitites	.0	100.0	.0	.0	100.0
		Chromitite pyroxenites	.0	.0	100.0	.0	100.0
		Anorthosites	.0	.0	.0	100.0	100.0

a. 100.0% of original grouped cases correctly classified.

Stepwise discriminant analysis was used to determine the trace elements which can be used to distinguish the four rock types within the MG2 and MG3 package. The results table 5.32 gave 97.1% of the original grouped cases to be correctly classified. Table 5.31 illustrates that trace elements Cr, Ga and Ti can be used to distinguish the four rock types at Dwarsrivier chrome mine.

Table 5.31: Trace elements used to distinguish the difference between the four rock types from Dwarsrivier chrome mine.

Variables Entered/Removed[a,b,c,d]

Step	Entered	Wilks' Lambda											
		Statistic	df1	df2	df3	Exact F				Approximate F			
						Statistic	df1	df2	Sig.	Statistic	df1	df2	Sig.
1	Cr	.034	1	3	64.000	614.580	3	64.000	.000				
2	Ga	.025	2	3	64.000	111.695	6	126.000	.000				
3	Ti	.019	3	3	64.000					68.971	9	151.042	.000

At each step, the variable that minimizes the overall Wilks' Lambda is entered.

a. Maximum number of steps is 46.

b. Minimum partial F to enter is 3.84.

c. Maximum partial F to remove is 2.71.

d. F level, tolerance, or VIN insufficient for further computation.

Table 5.32: Classification results for trace elements within the four rock types at Dwarsrivier Chrome mine, using stepwise discriminant analysis.

Classification Results[a]

		Average Linkage (Between Groups)	Predicted Group Membership				Total
			1	2	3	4	
Original	Count	Feldspathic pyroxenites	21	0	0	0	21
		Chromitites	0	30	0	2	32
		Chromitite pyroxenites	0	0	11	0	11
		Anorthosites	0	0	0	4	4
	%	Feldspathic pyroxenites	100.0	.0	.0	.0	100.0
		Chromitites	.0	93.8	.0	6.3	100.0
		Chromitite pyroxenites	.0	.0	100.0	.0	100.0
		Anorthosites	.0	.0	.0	100.0	100.0

a. 97.1% of original grouped cases correctly classified.

5.1.2.3 Trace element patterns in rock types within the MG2 and MG3 package

The combination of cluster and discriminant analysis was used to determine the trace elements that characterise the chromitites, feldspathic pyroxenites, chromitite pyroxenites and anorthosites within the MG2 package from those in the MG3 package.

Stepwise discriminant analysis was used to determine the trace element(s) which can distinguish the feldspathic pyroxenites and chromitites from the MG2 package from those in the MG3 package, anorthosites above the MG2 package to those anorthosites below the MG3 package and chromitite pyroxenites in the upperpart of the MG2 package to those in the lower part of the MG2 package.

5.1.2.3.1 Feldspathic pyroxenites

A combination of cluster and discriminant analysis was used to determine the trace elements used to characterise the MG3 feldspathic pyroxenites and MG2 feldspathic pyroxenites.

In table 5.33 function one is negatively loaded with Ba, Y, Pb, Cu, U, Zr, Nb, Sr and Rb. These trace elements characterise the MG2 feldspathic pyroxenites, while Ti, Ni, Ga, Co, Zn, Cr and La are positively loaded and characterise the feldspathic pyroxenites within the MG3 package. The structure matrix in table 5.33 above shows that trace elements V, P, Nd and S were not part of the analysis.

Table 5.33: One function discriminant structure matrix and function group centroids for the MG3 feldspathic pyroxenites and MG2 feldspathic pyroxenites.

Structure Matrix

	Function
	1
Ti	.177
Ni	.169
Ga	.163
Co	.137
Zn	.128
Cr	.123
V[a]	.110
Ba	-.109
P[a]	-.101
Nd[a]	-.094
Cl	-.088
Y	-.087
Pb	-.061
Cu	-.049
U	-.039
Zr	-.037
S[a]	-.022
Nb	-.015
Sr	-.013
La	.012
Rb	-.002

Pooled within-groups correlations between discriminating variables and standardized canonical discriminant functions

Variables ordered by absolute size of correlation within function.

a. This variable not used in the analysis.

Functions at Group Centroids

VAR00001	Function
	1
MG3 Feldspathic pyroxenites	4.801
MG2 Feldspathic pyroxenites	-2.216

Unstandardized canonical discriminant functions evaluated at group means

Table 5.34: Classification results for trace elements within the MG2 feldspathic pyroxenites and MG3 feldspathic pyroxenites.

Classification Results[a]

		VAR00001	Predicted Group Membership		Total
			1.00	2.00	
Original	Count	MG3 feldspathic pyroxenites	6	0	6
		MG2 feldspathic pyroxenites	0	13	13
	%	MG3 feldspathic pyroxenites	100.0	.0	100.0
		MG2 feldspathic pyroxenites	.0	100.0	100.0

a. 100.0% of original grouped cases correctly classified.

Table 5.35: Classification results for trace elements that distinguish the MG3 feldspathic pyroxenites from the MG2 feldspathic pyroxenites, using stepwise discriminant analysis.

Variables Entered/Removed[a,b,c,d]

Step	Entered	Wilks' Lambda							
		Statistic	df1	df2	df3	Exact F			
						Statistic	df1	df2	Sig.
1	Ga	.320	1	1	17.000	36.085	1	17.000	.000
2	U	.223	2	1	17.000	27.863	2	16.000	.000

At each step, the variable that minimizes the overall Wilks' Lambda is entered.

a. Maximum number of steps is 4.

b. Minimum partial F to enter is 3.84.

c. Maximum partial F to remove is 2.71.

d. F level, tolerance, or VIN insufficient for further computation.

Stepwise discriminant analysis was used to determine the trace elements which can be used to differentiate the MG2 feldspathic pyroxenites from the MG3 feldspathic pyroxenites. The trace element which differentiates the two feldspathic pyroxenites was Ti. Then Ti removed from the analysis to again determine if there were other trace element(s) other than Ti that can be used to differentiate the two feldspathic pyroxenites. Gallium and Uranium are the two trace elements that differentiate the feldspathic pyroxenites within the MG2 and MG3 package illustrated by the table 5.35 above.

Table 5.36 gave a 94.7% difference across the feldspathic pyroxenites with Ga depicting the highest percentage difference of 89.5% and U with the lowest percentage difference of 5.2%.

Table 5.36: The trace element percentage difference that differentiate the MG3 feldspathic pyroxenites from MG2 feldspathic pyroxenites.

Trace element	Percentage difference
Ga	89.5%
U	94.7%
Total	94.7%

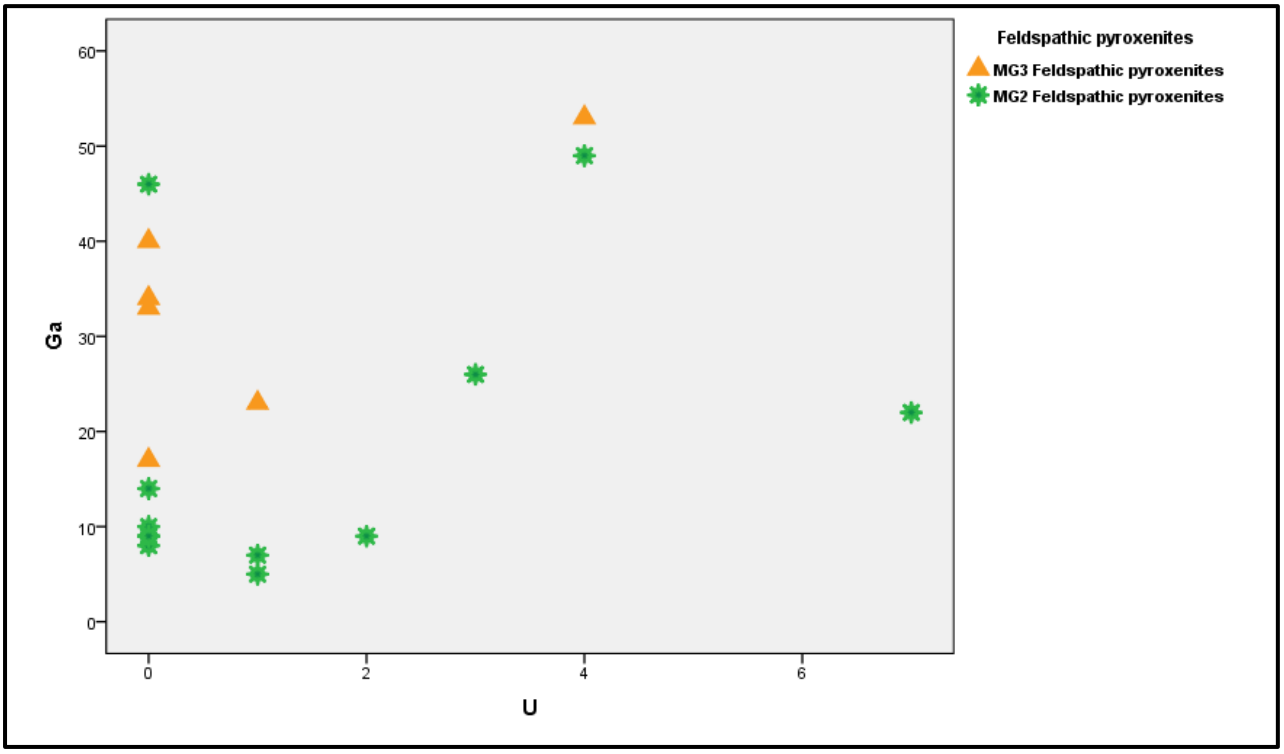

Figure 5.13: Scatter plot of the trace elements Ga versus U within the MG feldspathic pyroxenites.

Figure 5.1 above shows the scatter plot of trace elements Ga versus U within the feldspathic pyroxenites. The MG3 feldspathic pyroxenites show higher Ga content compared to the MG2 feldspathic pyroxenites. According Paktunc and Cabri (1995), the chromite grains show prominent amounts of Ni, Zn, Co and lower amounts of Ga were also detected. All these elements occur in sulphide, but their distribution are mainly controlled by the presences of chromite grains. This also corresponds to the higher chromite content seen within the within the MG3 feldspathic pyroxenites petrographic study.

5.1.2.3.2 Chromitites

The geochemical data of the chromitite samples were analyzed using cluster and discriminant analysis. The combination of cluster and discriminant analysis will reveal the trace elements that can be used to distinguish the types of chromitites.

Table 5.37: One function discriminant structure matrix and function at centroids for MG3 and MG2 chromitites.

Structure Matrix

	Function
	1
Co	.369
Cr	.347
Zn	.342
Ni	.339
Sr	-.329
V	.320
Ti	.291
Ba	-.247
Ga	.234
Cl	-.191
Ce	-.173
Y	-.132
Nd	-.121
La	.118
Pb	-.078
Zr	.073
Cu	.054
Nb	.044
U	-.040
P	.027
Rb	-.011
S	.008

Pooled within-groups correlations between discriminating variables and standardized canonical discriminant functions

Variables ordered by absolute size of correlation within function.

Functions at Group Centroids

VAR00001	Function
	1
MG3 Chromitites	1.059
MG2 Chromitites	-3.178

Unstandardized canonical discriminant functions evaluated at group means

In table 5.37 function one is positively loaded with Co, Cr, Zn, Ni, V, Ti, Ga, La, Zr, Cu, P and S.

These trace elements can be used to characterise the MG3 chromitites, while Sr, Ba, Cl, Ce, Y, Nd, Pb, Nb, U and Rb are negatively loaded and is considered to characterise the MG2 chromitites. Table 5.38 shows the chromitite samples have been correctly classified into the MG3 chromitites and MG2 chromitites by 100% indicating high level of confidence in the discrimination. The MG3 chromitites consist of 24 samples and 8 samples are from the MG2 chromitites.

Table 5.38: Classification for the element within the MG2 chromitites and MG3 chromitites**.**

Classification Results[a]

		VAR00001	Predicted Group Membership		Total
			1.00	2.00	
Original	Count	MG3 Chromitites	24	0	24
		MG2 Chromitites	0	8	8
	%	MG3 Chromitites	100.0	.0	100.0
		MG2 Chromitites	.0	100.0	100.0

a. 100.0% of original grouped cases correctly classified.

Table 5.39: Classification results for trace elements that distinguish the MG3 chromitites from the MG2 analysis.

Variables Entered/Removed[a,b,c,d]

Step	Entered	Wilks' Lambda							
		Statistic	df1	df2	df3	Exact F			
						Statistic	df1	df2	Sig.
1	Zn	.138	1	1	30.000	187.348	1	30.000	.000
2	Nb	.121	2	1	30.000	105.606	2	29.000	.000

At each step, the variable that minimizes the overall Wilks' Lambda is entered.

a. Maximum number of steps is 46.

b. Minimum partial F to enter is 3.84.

c. Maximum partial F to remove is 2.71

Table 5.38 shows trace elements Zn and Nb that distinguishes the MG3 chromitites from the MG2 chromitites. Stepwise discriminant analysis gave a 100% difference across the chromitites with Zn giving the highest percentage difference of 96.9% and Nb with the lowest percentage difference of 3.1%. A summary of the results is given in table 5.40.

Table 5.40: The trace elements percentage that distinguish the MG3 chromitites from MG2 chromitites

Trace element	**Percentage difference**
Zn	96.9%
Nb	3.1%
Total	100%

Table 5.41: Classification results for trace elements within the MG2 chromitites and MG3 chromitites, using stepwise discriminant analysis.

		Predicted Group for Analysis 1	Predicted Group Membership		Total
			1.00	2.00	
Original	Count	MG3 chromitites	25	0	25
		MG2 chromitites	0	7	7
	%	MG3 chromitites	100.0	.0	100.0
		MG2 chromitites	.0	100.0	100.0

a. 100.0% of original grouped cases correctly classified.

Figure 5.14 below shows the scatter plot of trace elements Zn versus Nb within the chromitites within the MG2 package and MG3 package. The MG3 chromitites show a higher concentration of Zn. Paktunc and Cabi (1995) suggested that the chromitites within the Eastern Bushveld complex have high content of Zn, Ni and Ga. This suggests that the high content of Zn is due to the presences of chromitite. The felsic rocks generally have high content of Nb. This means that the MG2 chromitites are more felsic in composition. This is seen by the high concentration of CaO, Na_2O and $Al_2O_{3,}$ which characterise the MG2 chromitites.

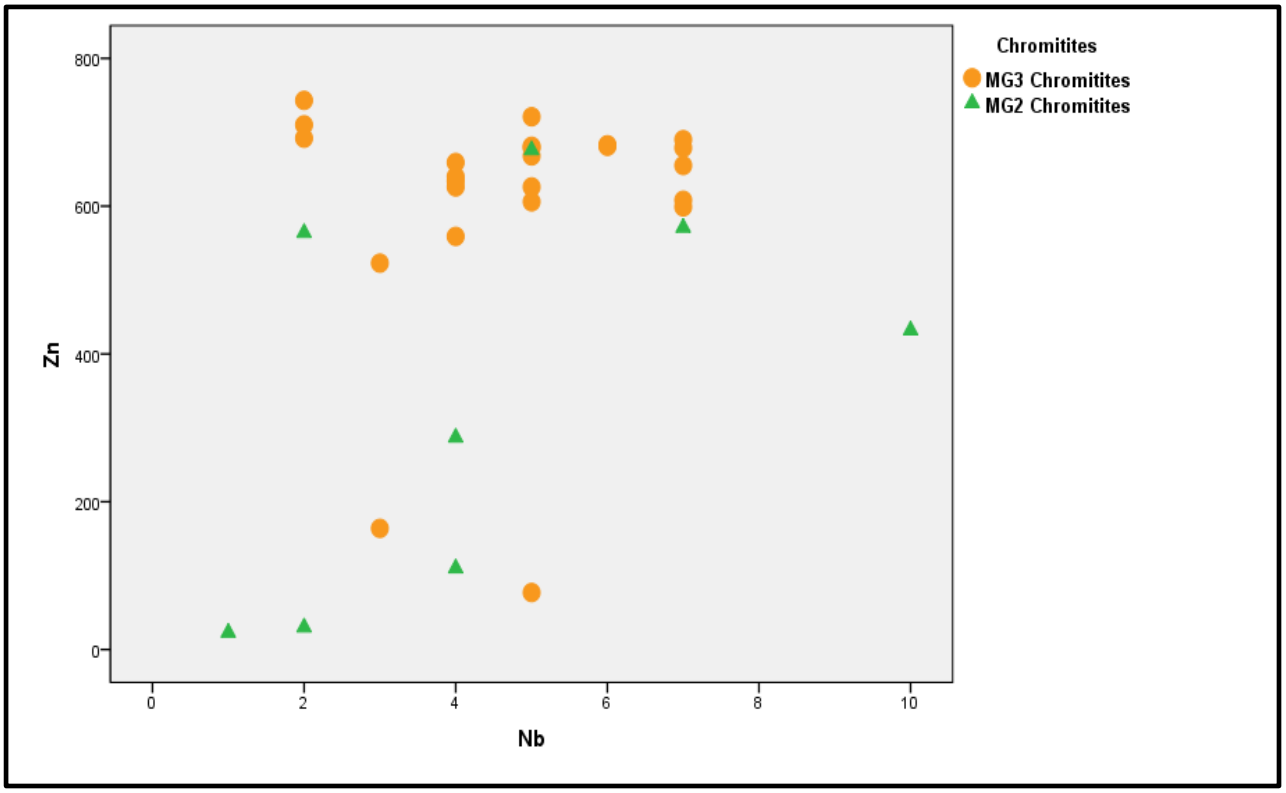

Figure 5.14: Scatter plot of Zn versus Nb within the MG chromitites.

5.1.2.3.3 Anorthosites

The anorthosite samples were sub-divided into two groups, after a combination of cluster and discriminant analysis was used to distinguish these samples. Anorthosites where sampled from above the MG2 package and below the MG3 package.

Table 5.42: One function discriminant structure matrix and function group centroids for the anorthosites above the MG2 package and below the MG3 package.

Structure Matrix

	Function
	1
U[a]	.584
Pb[a]	.505
Cl[a]	.504
P[a]	.467
Zr[a]	.448
La[a]	.396
Ga	.296
Y[a]	.163
Ba[a]	-.094
Ti[a]	.066
Co[a]	.057
S[a]	-.052
Ni	.051
Cu	-.047
Zn[a]	.035
V[a]	-.029
Sr[a]	.022
Nb[a]	.020
Cr[a]	.011
Rb	-.006

Pooled within-groups correlations between discriminating variables and standardized canonical discriminant functions

Variables ordered by absolute size of correlation within function.

a. This variable not used in the analysis.

Functions at Group Centroids

Ward Method	Function
	1
Anorthosites above the MG2 package	53.127
Anorthosites below the MG3 package	-10.625

Unstandardized canonical discriminant functions evaluated at group means

The structure matrix in table 5.42 shows that U, Pb, Cl, P, Zr, La, Y, Ba, Ti, Co, S, Zn, V, Sr, Nb didn't play a significant role in the analysis, thus they were not part of the analysis. Table 5.42 function one is positively loaded with Ni. Nickel can therefore be associated with the anorthosites below the MG3 package, while Cu is negatively loaded and considered to characterise the anorthosites above the MG2 package. Table 5.43 illustrates that the anorthosite samples have been correctly classified by 100%, with the anorthosites above the MG2 consisting of 5 samples and the other sample belong to the anorthosites below the MG3 package.

Table 5.43: Classification results for trace elements within the anorthosites below the MG3 package and anorthosites above the MG2 package.

Classification Results[a]

		Ward Method	Predicted Group Membership		Total
			1	2	
Original	Count	Anorthosites below the MG3 package	1	0	1
		Anorthosites above the MG2 package	0	5	5
	%	Anorthosites below the MG3 package	100.0	.0	100.0
		Anorthosites above the MG2 package	.0	100.0	100.0

a. 100.0% of original grouped cases correctly classified.

Table 5.44: Classification results for trace elements that distinguish the anorthosites below the MG3 package from the anorthosites above the MG2 package using stepwise discriminant analysis.

Variables Entered/Removed[a,b,c,d]

Step	Entered	Wilks' Lambda							
		Statistic	df1	df2	df3	Exact F			
						Statistic	df1	df2	Sig.
1	Ga	.013	1	1	4.000	296.362	1	4.000	.000
2	V	.001	2	1	4.000	1601.747	2	3.000	.000
3	Cl	.000	3	1	4.000	6565.663	3	2.000	.000
4	P	.000	4	1	4.000	17218.143	4	1.000	.006

At each step, the variable that minimizes the overall Wilks' Lambda is entered.

a. Maximum number of steps is 46.

b. Minimum partial F to enter is 3.84.

c. Maximum partial F to remove is 2.71.

d. F level, tolerance, or VIN insufficient for further computation.

Table 5.44 above show Ga, V, Cl and P are the trace elements that can be used to distinguish the anorthosites above the MG2 package and the anorthosites below the MG3 package. Table 5.45 above is stepwise discriminant classification results for the four trace elements used together can correctly be used to distinguish the two types of anorthosites by 100%.

Table 5.45: Classification results for trace elements within the anorthosites below the MG3 package and anorthosites above the MG2 package using stepwise discriminant analysis.

Classification Results[a]

		Ward Method	Predicted Group Membership		Total
			1	2	
Original	Count	Anorthosites above the MG2 package	1	0	1
		Anorthosites below the MG3 package	0	5	5
	%	Anorthosites above the MG2 package	100.0	.0	100.0
		Anorthosites below the MG3 package	.0	100.0	100.0

a. 100.0% of original grouped cases correctly classified.

Teigler (1999) suggested that the pyroxene tend to display high V values as a response to the presences of accessory chromite and pyroxene. Petrographic study of the anorthosite below the MG3 package revealed higher concentration of accessory chromite. This resulted in high content of V relative to the little or absences of accessory chromite within the anorthosites above the MG2 package, which is illustrated by the low content of Ga and V.

5.1.2.3.4 Chromitite pyroxenites

Table 5.46: One function discriminant matrix and function group centroids for chromitite pyroxenites.

Structure Matrix

	Function
	1
Co	1.000
Cr[a]	.951
Ga[a]	.939
Zn[a]	.934
Ti[a]	.934
V[a]	.906
Ni[a]	.870
La[a]	.609
Nb[a]	.574
U[a]	-.524
Y[a]	-.424
Cu[a]	-.373
S[a]	.292
P[a]	.229
Pb[a]	-.197
Zr[a]	.192
Sr[a]	-.136
Rb[a]	.107
Cl[a]	.072
Ba[a]	-.043

Pooled within-groups correlations between discriminating variables and standardized canonical discriminant functions

Variables ordered by absolute size of correlation within function.

a. This variable not used in the analysis.

Functions at Group Centroids

Average Linkage (Between Groups)	Function
	1
Upper chromitite pyroxenites	-1.013
Lower chromitite pyroxenites	2.701

Unstandardized canonical discriminant functions evaluated at group means

The chromitite pyroxenites within the MG2 package can be sub-divided into two, the lower chromitite pyroxenites and upper chromitite pyroxenites based on their relative contents. Certain trace elements which didn't play a role in the characterisation such as Cr, Ga, Zn, Ti, V, Ni, La, Nb, U, Y, Cu, S, P, Pb, Zr, Sr, Rb, Cl and Ba were not part of the analysis (table 5.46).

The first group of chromitite pyroxenites which are found within the upper parts of the MG2 package doesn't show any trace and minor elements that can be used to characterise them. The second group of chromitite pyroxenites can be characterised by Co. In table 5.47 there are 8 chromitite pyroxenites samples within the upper chromitite pyroxenites and lower chromitite pyroxenites consist of 3 chromitite pyroxenites samples. A summary of the results in table 5.47 shows that the samples have been correctly classified by 90.9%. Thus these results can be used with high level of confidence.

Table 5.47: Classification results for trace elements within the upper and lower chromitite pyroxenites.

Classification Results[a]

		Average Linkage (Between Groups)	Predicted Group Membership		Total
			1	2	
Original	Count	Upper chromitite pyroxenites	7	1	8
		Lower chromitite pyroxenites	0	3	3
	%	Upper chromitite pyroxenites	87.5	12.5	100.0
		Lower chromitite pyroxenites	.0	100.0	100.0

a. 90.9% of original grouped cases correctly classified.

Table 5.48: Classification results for trace elements that distinguish the upper and lower chromitite pyroxenites, using stepwise discriminant analysis.

Variables Entered/Removed[a,b,c,d]

Step	Entered	Wilks' Lambda							
		Statistic	df1	df2	df3	Exact F			
						Statistic	df1	df2	Sig.
1	Zn	.237	1	1	9.000	28.946	1	9.000	.000
2	V	.098	2	1	9.000	36.911	2	8.000	.000
3	Y	.044	3	1	9.000	50.731	3	7.000	.000

At each step, the variable that minimizes the overall Wilks' Lambda is entered.

a. Maximum number of steps is 44.

b. Minimum partial F to enter is 3.84.

c. Maximum partial F to remove is 2.71.

d. F level, tolerance, or VIN insufficient for further computation.

Stepwise discriminant analysis was used to assess the trace elements that can be used to distinguish the two types of chromitite pyroxenites within the MG2 package. These elements are Zn, V, and Y. Table 5.49 below shows that the chromitite pyroxenites have been correctly classified by 100%.

Table 5.49: Classification results for trace elements within the upper and lower chromitite pyroxenites, using stepwise discriminant analysis.

Classification Results[a]

		Average Linkage (Between Groups)	Predicted Group Membership		Total
			1	2	
Original	Count	1	8	0	8
		2	0	3	3
	%	1	100.0	.0	100.0
		2	.0	100.0	100.0

a. 100.0% of original grouped cases correctly classified.

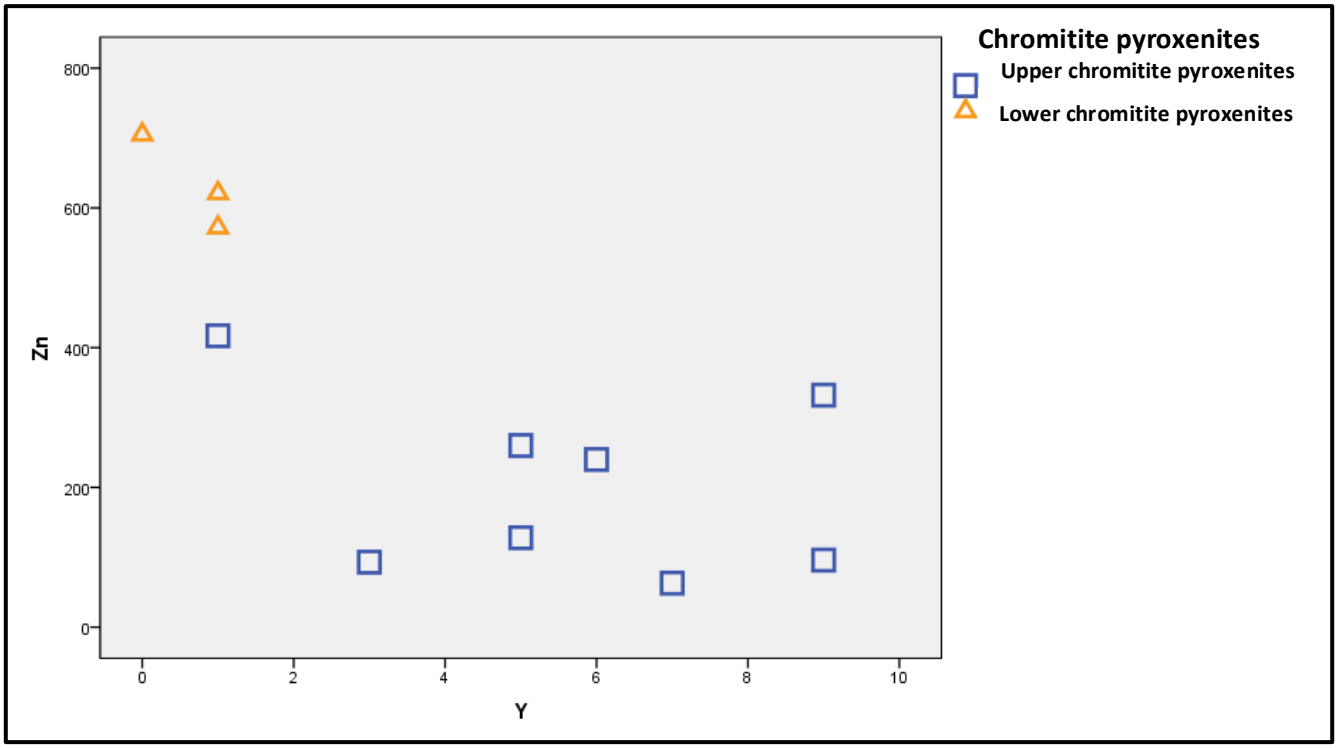

Figure 5.15: Scatter plot of Zn versus Y within the chromitite pyroxenites.

Figure 5.15 show a scatter plot of Zn versus Y for the chromitite pyroxenites. The upper chromitite pyroxenites show high concentration of Y. The yttrium partitions into clinopyroxene this corresponds to the high content of clinopyroxenes within the upper chromitite pyroxenite petrographic sample. The lower chromitite pyroxenites consist of high zinc content. The high zinc content shows that the lower chromitite pyroxenites are more iron rich as compared to the calcium rich upper chromitite pyroxenites. Paktunc and Cabi (1995) noted that the chromite grains of the Eastern Bushveld complex are characterised by the high abundance of Ni and Zn.

5.1.3 Validation of rock types by comparing major elements patterns in the rocks with field based classification.

This section will be comparing the two methods that were used to characterise the different lithologies from the study, based on the presences of oxides. The two different methods used was combination of cluster and discriminant analysis in section 5.1.2 and combination of field identification (core logging) and discriminant analysis in section 5.1.3 to see which is the most reliable for the characterisation of the rock types in the study area.

The difference between the two methods is that the combination of cluster and discriminant analysis was determined in the following way. The geochemical data of the samples of the four rock types were each put through cluster analysis, where each lithology was grouped into two groups, either the MG2 package or MG3 package. Discriminant analysis was applied on the cluster results to determine the oxides that distinguish the two types of each rock lithologies. A summary of the results are presented in table 5.50 within the cluster analysis column.

As for the combination of field identification and discriminant analysis the grouping of the different lithologies into either the MG2 package or MG3 package were based on the classification of the rock types in the Eastern Bushveld complex developed by authors such as Cousins and Feringina (1964), Hatton and Von Gruenewalt, (1987), Schurmann et al., (1998) and Cawthorn et al., (2006). Discriminant analysis was applied on the geochemical data of the field identification classification and the summary of the results are illustrated in table 5.50 in the Field ID results column. The full results (tables) of the geochemical classification for each of the two types of feldspathic pyroxenites, chromitites, anorthosites and chromitite pyroxenites using the two different methods can be found in appendix C.

Table 5.50: Classification results of all the major elements that classify the various lithologies within the MG2 and MG3 package.

Rock type	MG Group	Cluster Analysis results	Field ID(core logging) results
Feldspathic pyroxenites	3	Cr_2O_3, NiO, TiO_2, Fe_2O_3, Al_2O_3	Cr_2O_3, NiO, TiO_2, Fe_2O_3, Al_2O_3, K_2O, CaO, P_2O_5 and Na_2O
	2	K_2O , MgO, CaO, P_2O_5, MnO and Na_2O	MgO and MnO
Chromitites (without Cr_2O_3 and Fe_2O_3)	3	NiO, TiO_2, MnO and K_2O	Na_2O , Al_2O_3, CaO and TiO_2
	2	Na_2O , Al_2O_3, CaO and MgO	MgO, MnO, K_2O , NiO and P_2O_5
Anorthosites	Below MG3	None	None
	Above MG2	Cr_2O_3, Al_2O_3, $Fe_2O_3$and CaO	Cr2O3, Al_2O_3, Fe_2O_3 and CaO
Chromitite Pyroxenites	Lower	MgO, K_2O , CaO and P_2O_5	CaO, K_2O , MgO and Al_2O_3
	Upper	Cr_2O_3, Fe_2O_3 and Al_2O_3	TiO2, Fe_2O_3 and Cr_2O_3

Based on the combination of cluster and discriminant analysis the feldspathic pyroxenites within the MG3 package are associated with oxides such as Cr_2O_3, NiO, TiO_2, Fe_2O_3 and Al_2O_3, while within the MG2 feldspathic pyroxenites it is K_2O, MgO, CaO, P_2O_5, MnO and Na_2O. The combination of the field identification and discriminant analysis shows that major elements such as Cr_2O_3, NiO, TiO_2, Fe_2O_3, Al_2O_3, K_2O, CaO, P_2O_5 and Na_2O are associated with the MG3 feldspathic pyroxenites, MgO and MnO are associated with the MG2 feldspathic pyroxenites.

When comparing the combination of field identification and discriminant analysis with the combination of cluster and discriminant analysis, there are a few similarities in oxides association within the MG2 package and MG3 package of the various rock lithologies.

The combination of cluster and discriminant analysis corresponds to the classification in petrography for all the rocks in the MG3 package and MG2 package. The chromitites and feldspathic pyroxenites in the MG3 package, the lower chromitite pyroxenites and anorthosites petrographic samples revealed higher content of chromite as compared to the samples in the MG2 package. The lithologies in the MG3 package based on the geochemical characterisation can be associated with elements such as Fe_2O_3, Cr_2O_3, NiO and TiO_2, while MgO, CaO and MnO are associated with lithologies in the MG2 package.

To determine which of these two methods is the most reliable; we took the petrography samples of the various lithologies and firstly grouped together into the MG2 package and MG3 package in accordance to the classification results of combination of cluster and discriminant analysis and then for combination of field identification and discriminant analysis. The MG3 feldspathic pyroxenites petrographic samples that were grouped based on the combination of cluster and discriminant analysis, contain higher chromite content than the samples within the MG2 package. This agrees with the classification result of the combination of cluster and discriminant analysis.

The feldspathic pyroxenite samples from the petrographic study were then grouped based on the combination field identification and discriminant analysis method. This revealed that there were certain feldspathic pyroxenite samples from the MG2 package that have higher content of chromite than those in the MG3 package. This contradicts the results obtained from the discriminant analysis on the field samples.

In terms of the chromitites, the discriminant analysis of field classified samples in the MG3 package consists of lower content of chromite as compared to the MG2 package. This classification doesn't agree with the petrographic samples for the chromitites, which suggest that there are certain samples within the MG2 package that have higher chromite content than the MG3 package.

For the anorthosites, both methods show the similar results in terms of the oxides that characterise the anorthosites above the MG2 package as illustrate in table 5.50 above. The chromitite pyroxenites show similar results. There are no chromitite pyroxenites within the MG3 package, but only in the MG2 package.

The combination of the cluster and discrimination results of the chromitites and feldspathic pyroxenites, it is the most reliable method for classification as the geochemical classification results are more compatible with the petrography samples as compared to the combination of field identification and discriminant analysis method.

In summary the important features to note from the combination of cluster and discriminant analysis trace elements are:

- Barium, Y, Pb, Cu, U, Zr, Nb, Sr and Rb are associated with the MG2 feldspathic pyroxenites, while the MG3 feldspathic pyroxenites are Ti, Ni, Ga, Co, Zn, Cr and La. Gallium and uranium differentiate the MG2 feldspathic pyroxenites from the MG3 package feldspathic pyroxenites.

- Elements Co, Cr, Zn, Ni, V, Ti, Ga, La, Zr, Cu, P and S are associated with the MG3 chromitites, while MG2 chromitites are Sr, Ba, Cl, Ce, Y, Nd, Pb, Nb, U and Rb. The MG3 chromitites and MG2 chromitites are distinguished by zinc and niobium.

- Nickel is associated to the anorthosites below the MG3 package, while anorthosites above the MG2 package are copper. The anorthosites below the MG3 package can be differentiate from the anorthosites above the MG2 package with elements such as Ga, V, Cl and P.

- The upper chromitite pyroxenites within the MG2 package don't show any trace elements that can be associated to them but lower chromitite pyroxenites are associated with cobalt while zinc, vanadium and yttrium can be used to differentiate the upper chromitite pyroxenites from the lower chromitite pyroxenites.

5.1.4 Spider diagrams

Spider diagrams are an extension of familiar REE- normalized abundance diagram. There are arrays of trace elements that are plotted on the x-axis in order of increasing compatibility against element abundance on the y-axis (Ridely, 2012). Each version of the spider diagram has slightly different array of elements with a slightly different order (Rollinson, 1993).

The reason for normalizing the trace elements concentration to a common reference standard (eg primoridial or primitive mantle, chrondite and MORB) is because the reservoir which normalization is done are thought to be relatively unfractionated samples (Rollinson,1993).

The primitive mantle is the composition of the mantle before the continental crust is formed. The most frequently used estimates of its composition is that of Wood et al (1979a), who used it as a means of comparing compositional variation between basic lavas.

Thompson (1982) proposed that the normalization to chrondritic values preferable to the primordial mantle composition values which are directly measured rather than estimated. The order of elements slightly differs to that of Wood et al (1979a) and was chosen to give the smoothest overall fit to the data for Icelandic lava and the North Altantic ocean basalt floor.

MORB normalized spider diagrams are the most appropriate for evolved basalt, andesites and crustal rocks. This form of spider diagram was proposed by Pearce (1983) and is based on two parameters. The first being ionic potential, which measures the mobility of an element in aqueous fluids. Elements with low (<3) and high (>12) ionic potential are mobile and those with intermediate values are generally immobile. Secondly the bulk distribution coefficient for the elements between garnet Ihertzolite and the melt used to measure the incompatibility of element in small degree partial melts (Rollinson, 1993).

The elements are ordered so that the most mobile element (Sr, K, Rb and Ba) are placed at the left of the diagram and in order of increasing incompatibility. The immobile elements are arranged from the right to left in order of increasing compatibility (Rollinson 1993).

A slightly different version of the diagram is used by Saunders and Tamey (1984) who arranged the elements into large ion lithophile group (Rb,Ba, K, Th, Sr, La, Ce) followed by an high field strength group (Nb, Ta, Nd, P, Hf, Zr, Eu, Ti, Tb, Y, Yb), followed by the transition metals Ni and Cr.

Sun and McDonough (1989) or McDonough et al (1992), normalization to primitive mantle is the most favoured amongst most authors.

The order of the plotting also variable with the standard of increasing compatibility from the left to the right, but the order of Sun and McDonough is the most favoured as its includes the largest number of trace elements and is ordered systematic and easily understandable way.

The order of the elements abscissa may vary slightly with various authors (Wood et al, 1979; Thompson, 1982). The order is usually based on the author's estimate of increasing incompatibility of elements from right to left in a typical mantle undergoing partial melting.

The spider diagrams were used to compare the behavior of the LILE (Large Ion Lithophile Elements) such as Sr, Rb and Ba and the High field strength elements (HFSE) such as Th, U, Ce, Zr, Nb, Ti and Y in MG2 feldspathic pyroxenites and MG3 feldspathic pyroxenites, MG2 chromitites and MG3 chromitites, anorthosites above the MG2 package and anorthosites below the MG3 package and lastly the chromitite pyroxenites within the upper and lower part of the MG2 package.

5.1.4.1 Feldspathic pyroxenites

The MG3 feldspathic pyroxenites and MG2 feldspathic pyroxenites in figure 5.16 show similar trends in terms of the LILE and HFSE. The variation of trace elements in the MG2 feldspathic pyroxenites shows higher degree of fractionation compared to the MG3 feldspathic pyroxenites. The MG2 feldspathic pyroxenites show enrichment of Ba, which indicate high content of orthoclase in the magma, but this was not seen in the petrography. The MG3 feldspathic pyroxenites show high content of Ce, Pb and Ti. The petrographic study showed that the MG3 feldspathic pyroxenite consists of high content of chromite and low content of clinopyroxene. This shown by the enrichment of titanium that is associated with the enrichment of chromite and depletion of yttrium content within the feldspathic pyroxenite spider diagram. The higher Sr content within the MG2 feldspathic pyroxenites relative to the MG3 feldspathic pyroxenites suggests high content of plagioclase. The MG2 feldspathic pyroxenite has a higher Zr content as compared to the MG3 feldspathic pyroxenites. This suggests higher degree of fractionation and more felsic in composition. The enrichment of Zr and U illustrates that the MG2 feldspathic pyroxenite is more felsic in composition as compared to the more ironic in composition MG3 feldspathic pyroxenites. This is supported by the high content of Na_2O and CaO within the feldspathic pyroxenites relative to the MG3 feldspathic pyroxenites.

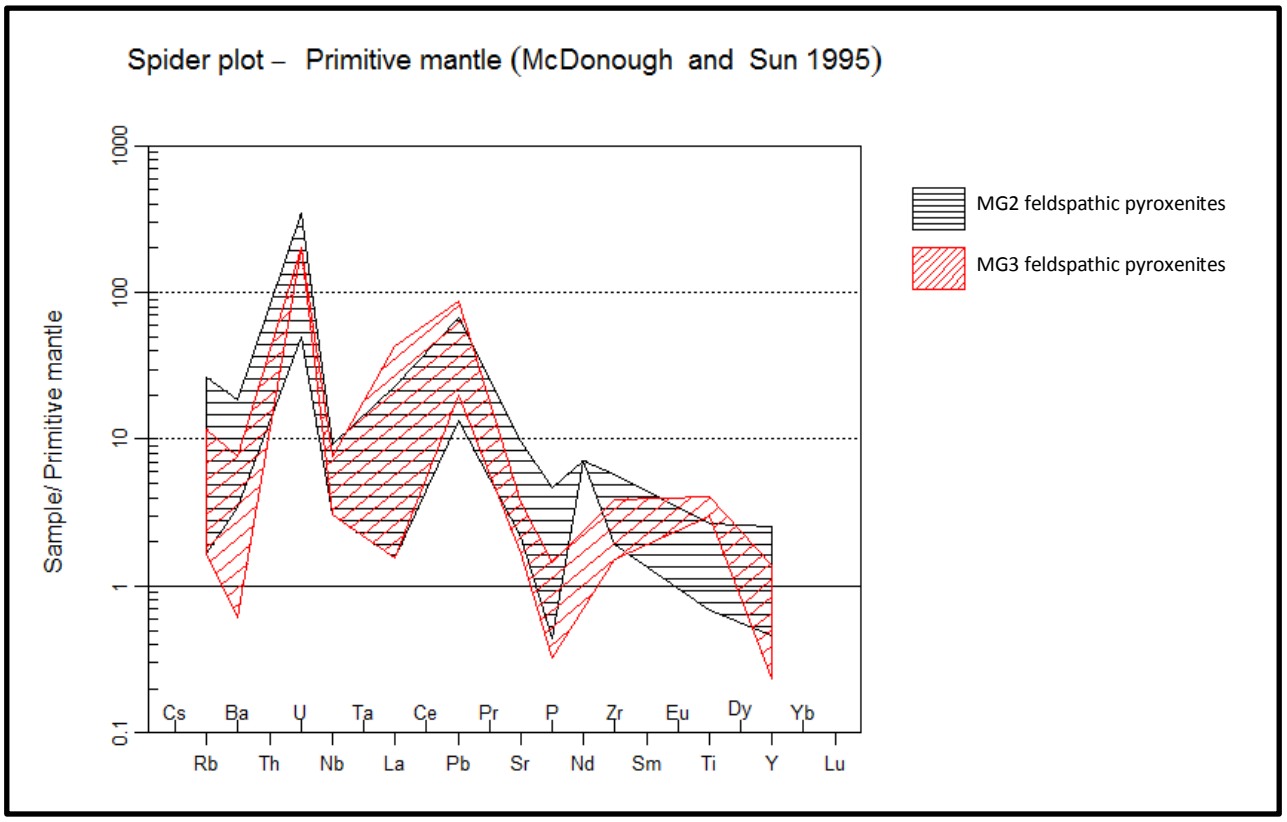

Figure 5.16: Trace element composition of the feldspathic pyroxenites from the MG2 package and MG3 package.

5.1.4.2 Chromitites

The chromitite in figure 5.17 shows enrichment in the large ion lithophile elements relative to high field strength elements. The MG3 chromitites and MG2 chromitites show similar trends in terms of the HFSE and LFSE, but the MG2 chromitites trace elements have a higher degree of fractionation relative to the MG3 chromitites. There was also high content of Zr in the MG2 chromitites relative to the MG3 chromitites, which indicates that the MG2 chromitites are more felsic in composition, as compared to the MG3 chromitites.

The MG3 chromitites show a slightly higher Ti content relative the MG2 chromitites, due to the high chromite content. In the petrography MG2 chromitites shows high plagioclase content relative to the MG3 chromitites. This is confirmed by spider diagram with the MG2 chromitites showing higher Sr content relative to the MG3 chromitites. The MG3 chromitites showed low clinopyroxene and high chromite content. The low clinopyroxene and high chromite is illustrated by the enrichment Ti and depletion of Y.

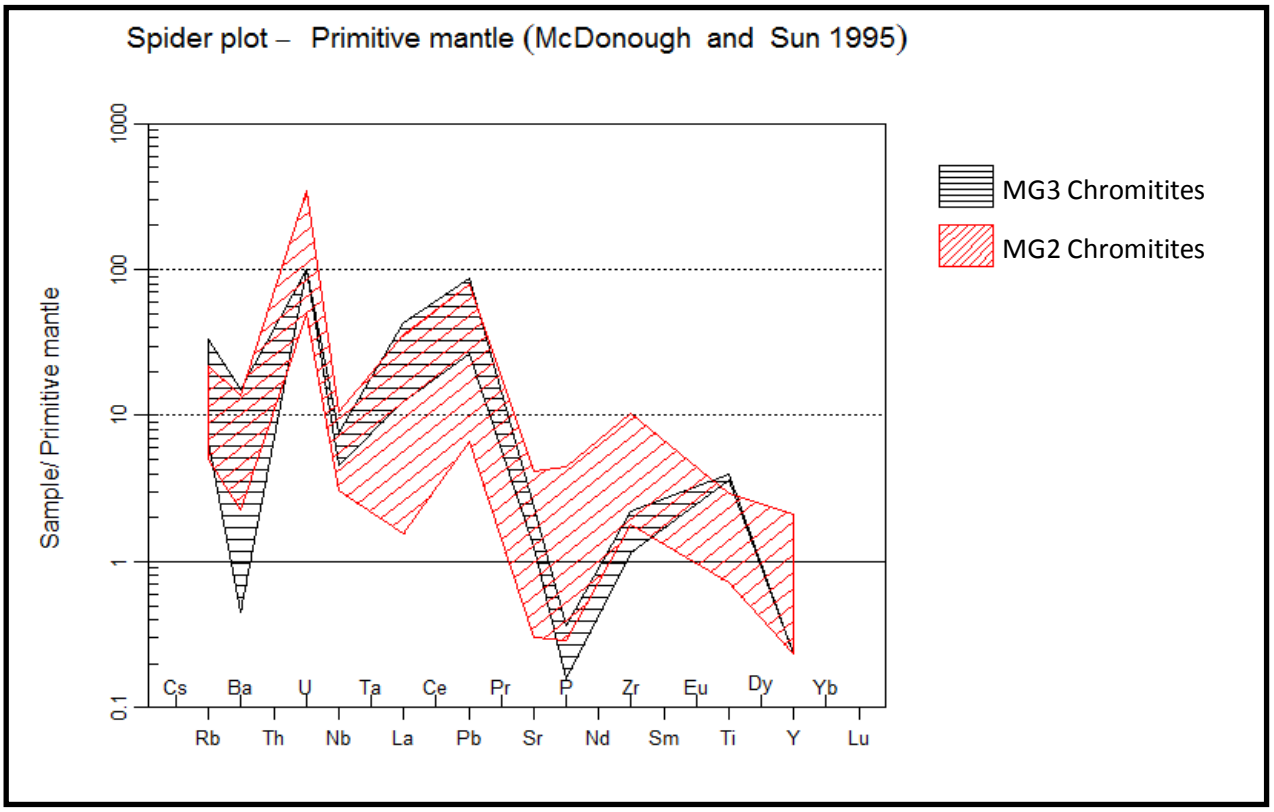

Figure 5.17: Spider diagram illustrating the difference in abundance of trace elements between the MG2 chromitite and MG3 chromitites

5.1.4.3 Anorthosites

The anorthosites show enrichment of large ion lithophile elements relative to the high field strength elements in figure 5.18. The anorthosites below the MG3 package show enrichment Y and depletion in Ti content. This indicates the high content of clinopyroxene and low content of chromite. The petrography of the anorthosites above the MG2 package showed high content of chromite. This is also shown by the enrichment Ti and clinopyroxene occurring as an intercumulus mineral. This can be explained by the yttrium content being below detection level as compared to the enrichment of the anorthosites below MG3 package.

The petrography also revealed that the anorthosites below the MG3 package have lower plagioclase content, which is shown by the Sr content compared to the anorthosites above the MG2 package. In borehole DWR 172, the anorthosites below the MG3 package show higher degree of fractionation as compared to the anorthosites above the MG2 package. This is due to the higher Zr content.

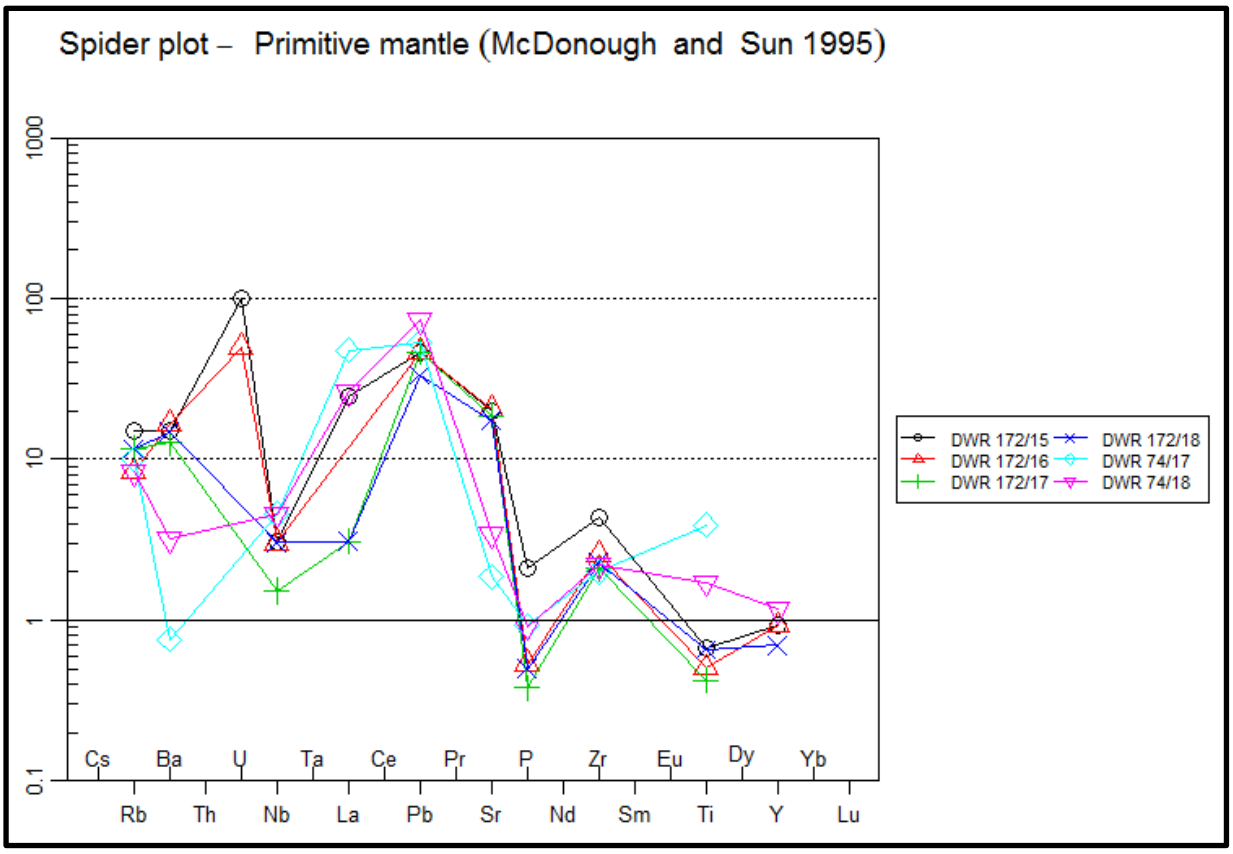

Figure 5.18: Spider diagram illustrating the difference in abundance of trace elements between the anorthosites above the MG2 package and anorthosites below the MG3 package.

5.1.4.4 Chromitites pyroxenites

The chromitite pyroxenites illustrate enrichment of LILE relative to the high field strength elements as illustrated in figure 5.19. The trace elements of the lower chromitite pyroxenites are more fractionated as compared to the upper chromitite pyroxenite. The enrichment of Ti and depletion of Y content within the upper chromitite pyroxenites, which corresponds to the higher chromite and lower clinopyroxene content in the petrographic study as compared to the low chromite and higher clinopyroxene content within the lower chromitite pyroxenite which is illustrated by the depletion in Ti and enrichment of Y content. The lower chromitite pyroxenites shows a higher plagioclase content in petrography relative to the upper chromitite pyroxenites and this is confirmed by the higher Sr content.

The lower chromitite pyroxenite shows a slightly higher Ba content as compared to the highly fractionated upper chromitite pyroxenites. There is enrichment of Ce in the upper chromitite pyroxenites, while the lower chromitite pyroxenites show depletion in Ce concentration. In this case, were the rocks are fresh magmatic rocks that have not been affected by hydrothermal fluids.

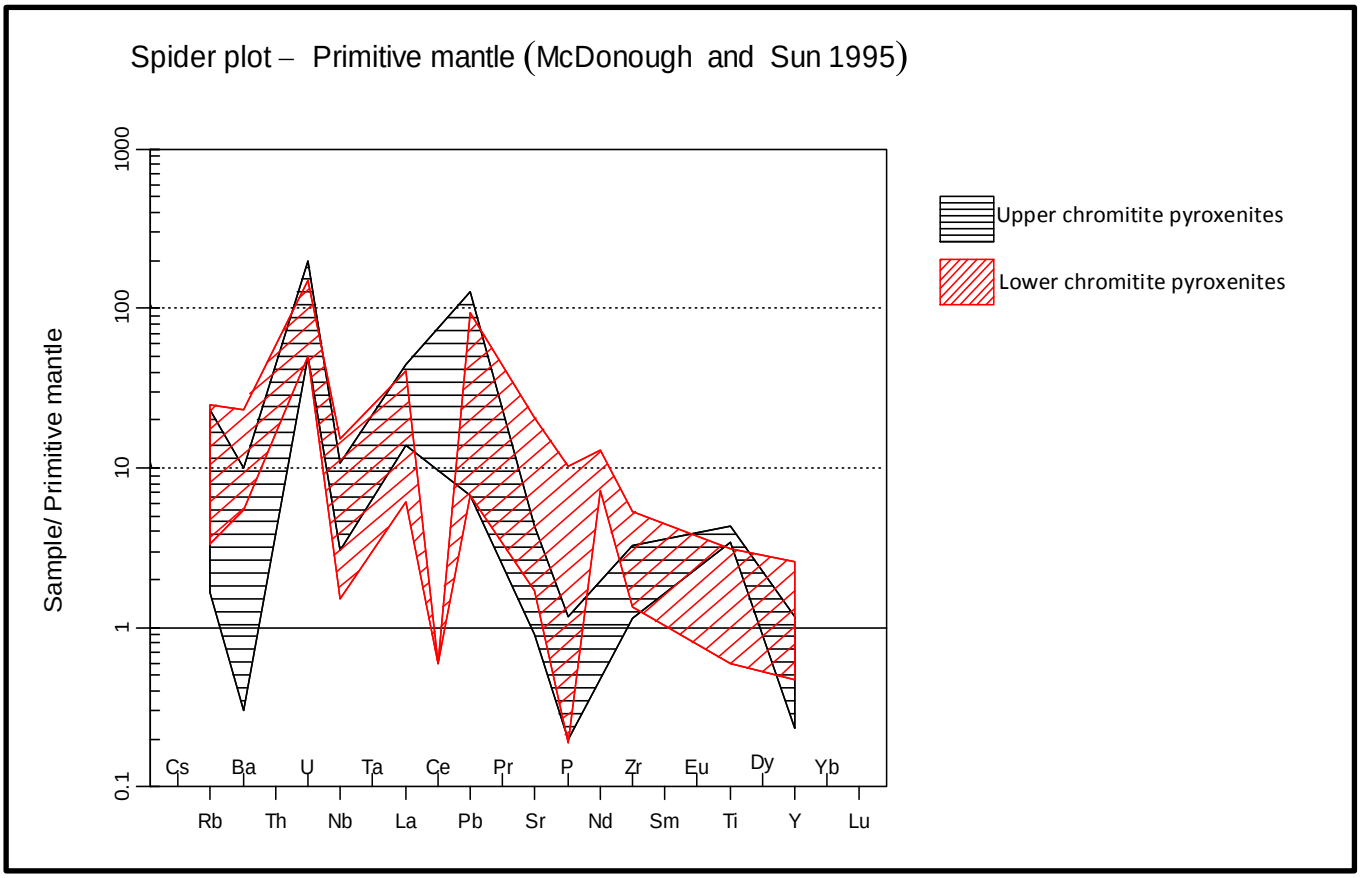

Figure 5.19: Trace element composition between the upper chromitite pyroxenite and lower chromitite pyroxenites within the MG2 package.

5.1.5 Trace element ratios

Over the years various authors have used various ratios in the Bushveld complex to illustrate the influx of magma. Kinnard (2005) suggested that SiO_2/Al_2O_3 ratio could be used as a potential indicator for two different magma sources. If the there were multiple magma pulses and the ratio remained constant, would suggest that it was from a single magma.

Both table 5.51 and 5.52 shows that the MG2 package and MG3 package, the MG2 package has the highest SiO_2/Al_2O_3 ratio.

Eales et al (1986), suggested that the Sr/Ba ratio illustrates fractional crystallization as Sr and Ba are compatible elements in plagioclase, but incompatible elements in all of the major elements in all of the major mafic minerals. Therefore any significant break or change in the geochemistry represents an influx of magma or geochemical hiatus.

There is a break or change in the Sr/Ba ratio from the MG3 package down to the MG2 package as illustrated in table 5.51 and Table 5.52.

The ratio SiO_2/Al_2O_3 and Sr/Ba were not used for the anorthosites rocks as these ratios are sensitive to high content of plagioclase.

Table 5.51: Major and trace elements ratio from DWR74 borehole.

Borehole DWR 74

Layer/ Package	SiO_2/Al_2O_3	Sr/Ba	Co/V	Mg#
MG3 package	2.81	1.77	0.19	0.44
Anorthosite layer	-	-	0.17	0.57
MG2 package	4.45	3.21	0.21	0.48

Eales et al (1986) used the ratio Co/V stating that although a single element will show progressive increase or decrease through cyclic unit as a result of modal control, the ratio would be independent of the modal proportions. Consequently they concluded that the progressive change in element ratios demonstrated fractional crystallization and thus sharp increase indicates a new influx which developed the cyclic units. There is change in Co/V ratio within the Dwarsrivier chrome mine transition zone from the MG3 package to the MG2 package. Table 5.51 above shows a slight increase in the Co/V ratio in borehole DWR74 from the MG2 package to the anorthosite layer, while borehole DWR172 shows a decrease in Co/V ratio as illustrated by table 5.52 below from the MG2 package to the anorthosite layer.

The Mg # (Magnesium number) has been used to measure fractional crystallization in the layered intrusions. The high Mg-Fe ratio of liquidus of the ferromagnesian minerals will result in the change in the Mg# in the early stages of crystallization relative to the host melt (Rollinson, 1993).

Scoon and De Klerk (1985) suggested that an increase in the Mg # is interpreted as a product of mixing of new magma intruding a batch of relatively more primitive magma within fractionated liquid in the chamber. In table 5.51 above shows, a change in the Mg# from the MG2 package to anorthosite layer and again from the anorthosite layer to the MG3 package. While in borehole DWR172 shows a change from MG2 package to the anorthosite layer and remains constant from the anorthosite layer to the MG3 package, illustrated by table 5.52.

Table 5.52: Major and trace elements ratios from borehole DWR 172.

Borehole DWR 172				
Layer/ Package	**SiO_2/Al_2O_3**	**Sr/Ba**	**Co/V**	**Mg#**
MG3 package	3.19	1.33	0.22	0.39
Anorthosite layer	-	-	0.17	0.39
MG2 package	3.82	1.08	0.22	0.44

In summary the important features to take note from the spider diagrams and trace element ratios are:

- The feldspathic pyroxenites, chromitites, anorthosites and chromitite pyroxenites show higher concentration of large ion lithophile elements relative to the high field strength elements. The MG3 feldspathic pyroxenites and MG2 feldspathic pyroxenites show enrichment of the large ion lithophile elements than high field strength elements. The feldspathic pyroxenites show strong enrichment of U and Pb. The MG2 feldspathic pyroxenites illustrate a higher concentration of Rb, U and Nb, while the MG3 feldspathic pyroxenites show higher enrichment of Pb and Ti concentration.

- There is a strong enrichment of U, Pb, Zr and depletion in Ba and P concentration. The MG3 chromitites show enrichment of Rb, Pb and Ti concentration while the MG2 chromitites illustrate higher concentration of U, Sr, Zr and Y.

- The anorthosites show enrichment in U, Pb, Sr and Zr concentration. The anorthosites below the MG3 package (DWR74/17) show a higher concentration in La and Ti, while the anorthosites above the MG2 package are defined by enrichment in U, Pb, Sr, Zr and higher depletion in Nb and P concentration relative to the anorthosites below the MG3 package. There is strong enrichment of U, Pb, Nd and Ti within the chromitite pyroxenites. The lower chromitite pyroxenites show higher concentration of U, Pb, Ti and the highest depletion in Ba and Y concentration.

- The upper chromitite pyroxenites illustrates the highest concentration in Rb, Sr, Nd, Y and the depletion in Nb, Ce and P concentration.

- The SiO_2/Al_2O_3 ratio is the lowest in the anorthosite layer, and then between the MG2 package and MG3 package, the MG2 package has the highest SiO_2/Al_2O_3 ratio. There is a sharp increase in the Cr/V ratio in borehole DWR74 from the MG2 package to the anorthosite layer, while borehole DWR172 shows a decrease in Cr/V ratio as illustrated by table 5.52 from the MG2 package to the anorthosite layer.

- There is a break or change in the Sr/Ba ratio from the MG3 package down to the MG2 package in both boreholes DWR 74 and DWR 172. There is change in the Mg# (magnesium number) from the MG2 package to anorthosite layer and again from the anorthosite layer to the MG3 package in borehole DWR 74. While in borehole DWR172 shows a change in the magnesium number from the MG2 package to the anorthosite layer and remains constant from the anorthosite layer to the MG3 package.

5.2 . Discussion

5.2.1 Introduction

The aim of the project is to use the geochemical and petrographic characteristics to 1.) Distinguish the various rock types within the MG2 and MG3 package of the Eastern Bushveld complex. 2.) Determine whether or not the transition boundary from the MG2 package to the MG3 package was as a result of a single or multiple magma pulses and suggest the most suitable layer for exploitation between the MG2 and MG3 chromitites.

This was done by

1. Determining the petrographical similarities and differences of between the feldspathic pyroxenites and chromitites in the MG3 and MG2 package as well as the underlying and overlying anorthosites.
2. Exploring the differences and similarities between the rock types within the MG3 package and those in the MG2 package, by multivariate statistics analysis and spider diagrams.
3. Using petrographical and geochemical characteristics, to ascertain whether the transition boundary, which is from the MG3 package to the MG2 package is as a result of a single or multiple magma pulses.

To date, only a few publications have focused on the Critical Zone and Main Zone of the Eastern Bushveld Complex. Most of the work in the Eastern Bushveld Complex has focused on the lower, main and upper zones by Cameron (1978, 1982), Sharpe and Snyman (1980), Mondal and Mathez (2007), Nardlett et al (2009), Kottke-Levin (2011) and Jolayeni (2011) in comparison to the well documented Western Bushveld Complex, although the Lower, Main and Upper zones have been better described in the Eastern Bushveld Complex.

Similarities and differences between the feldspathic pyroxenites and chromitites in the MG3 and MG2 Package

5.2.1.1 Feldspathic pyroxenites

The Dwarsrivier feldspathic pyroxenites are composed of 40% clinopyroxene, 30% orthopyroxene, 15% plagioclase and 5% chromitites. An increase in chromitite content occur downhole from MG2 feldspathic pyroxenites to the MG3 feldspathic pyroxenites. Thus Dwarsrivier feldspathic pyroxenites show variable mineralogical composition from the MG2 to the MG3 package.

The feldspathic pyroxenites in the MG3 package contain higher plagioclase and chromitite content, and a lower content of orthopyroxene and clinopyroxene.

According to Levin-Kottke, (2011) the pyroxenites in the Middle Group of the Eastern Bushveld, are compositionally dominated by the orthopyroxene followed by equal proportions of clinopyroxene and plagioclase. In line with the above, Levin-Kottke (2011) observed variation of the chromitite content within the stratigraphic column and corroborates the variation in the contents of orthopyroxene and plagioclase and clinopyroxene from the MG2 to the MG3 pyroxenite packages.

Furthermore, the presence of orthopyroxene, clinopyroxene and plagioclase corroborates high contents of oxides such as CaO, Fe_2O_3, Al_2O_3, SiO_2, K_2O and MgO which can be associated with the feldspathic pyroxenites. Two types of feldspathic pyroxenites were identified namely: 1.) the MG3 feldspathic pyroxenites which contain high content of chromitite and plagioclase are associated with elevated content of Cr_2O_3, Fe_2O_3, TiO_2 and Al_2O_3 and 2.) The MG2 feldspathic pyroxenites contrastingly shows high content of clinopyroxenes and orthopyroxenes and are associated with K_2O, MgO, CaO, P_2O_5, MnO and Na_2O. This subdivision is marked by a change in a cumulus texture in MG3 feldspathic pyroxenites to intercumulus in the MG2 feldspathic pyroxenites.

Noteworthy is also the increase in content of Al_2O_3 and Cr_2O_3 within the Dwarsrivier feldspathic pyroxenites from the MG2 package (7.23 wt. %) towards the MG3 package (10 wt. %) for Al_2O_3 and Cr_2O_3 .The trend is reverse for CaO and MgO content increase from the MG3 package (2.75 wt. %) to the MG2 package (4.09 wt. %).

High content of MgO within the MG2 package implies that the latter to be more orthopyroxene-rich relative to the MG3 package. Feldspathic pyroxenites in the MG2 package contain higher Na_2O content up to 0.63 wt. % compared to MG3 feldspathic pyroxenites with 0.58 wt%, in line with Eales et al (1993a).

The MG3 and MG2 feldspathic pyroxenite spider diagrams display enrichment of U, Sr, Zr, Pb and Y. The MG2 feldspathic pyroxenites show higher content of U, Zr and Y relative to the MG3 feldspathic pyroxenites that show high content of Ti and Pb.

The enrichment of U and Zr coupled with Na_2O and CaO suggest that the MG2 feldspathic pyroxenites are more felsic in composition, relative to the MG3 feldspathic pyroxenites that are more iron rich.
The high content of Y will result it partitioning into clinopyroxenes. This is demonstrated by the high content of clinopyroxene within the MG2 feldspathic pyroxenites, relative to the higher concentration of plagioclase within the MG3 feldspathic pyroxenites.
The MG3 feldspathic pyroxenite spider diagrams are characterised by the enrichment of Ti and Pb.

5.2.1.2 Chromitites

The Dwarsrivier chromitites are composed of 70% chromitites, 15% orthopyroxenes, 10% clinopyroxenes and 5% plagioclase. The MG2 chromitites contain higher content of clinopyroxenes with subdued contents of plagioclase, while the MG3 chromitites consist of are characterised by a lower content of clinopyroxenes, low orthopyroxenes and higher chromite content.

Doig (2000) suggested that there were no petrographic features that distinguish the individual LG and MG chromitite seams. It is only the MG4 chromitite seam that consist of finer-grained than the remaining seams and with fewer triple points and annealed grains. The plagioclase within the chromitites from the MG1 to MG3 occurs as intercumulus mineral and only makes up a small percentage of the rock (Boorman et al, 2003). Levin-Kottke (2011) reported that the chromitites in the Upper Critical Zone are poikilitically enclosed chromite grains within the orthopyroxene and can be observed within all the middle group chromitite layers. According to Levin-Kottke (2011), the amount of chromite and silicate differs within the various chromitite layers and the transition from the LCZ to the UCZ, the amount of cumulus chromite decreases from 79.3% in the MG2C to 50.4% in the MG4B chromitite in favor of the silicate phases.

The petrographic study between the MG3 chromitite and MG chromitites within the transition boundary at Dwarsrivier Chrome mine revealed that MG2 chromitites consist of higher orthopyroxene and plagioclase content, while the MG3 chromitites consist of higher chromite and orthopyroxene content. Orthopyroxene is absent within the MG3 package.

The Dwarsrivier chromitites (both the MG3 and MG2 chromitites) are geochemical associated with high content of Fe_2O_3, NiO, TiO_2 and Cr_2O_3. The following elements MgO, CaO, Al_2O_3, Na2O, NiO, TiO_2, MnO and K_2O were used to differentiate the two types of chromitites. The MG2 chromitites showed high content of clinopyroxenes with little or no presences of plagioclase and are associated with MgO, CaO, Al_2O_3 and Na_2O relative to the MG3 chromitites which are associated with NiO, TiO_2, MnO and K_2O. The MG3 chromitites consist of lower content of clinopyroxenes with no presences of orthopyroxenes.

According to Kottkte-Levin (2011), the chromitite layers illustrate a constant decrease in Cr_2O_3 content from the bottom (46 wt. %) to top (35.4 wt. %) of the middle group chromitites. Doig (2000) suggested that the massive chromitites consists of low content of Na_2O which represent higher site preference energy for the Mg and Fe of the Cr-spinel crystal lattice structure. He also reported that the constant increase from the LG1 to the LG3 seams and that there is a decrease in chromitite concentration from the LG3 to the MG3 seam.

The presences Al_2O_3 and CaO with the chromitites are associated with plagioclase. The amount of plagioclase depends on the Al_2O_3 content within the host rock. In this investigation the MG2 chromitites are characterised by higher content of CaO and Al_2O_3 relative to the MG3 chromitites. The higher content of CaO and Al_2O_3 suggests that there is more crystallisation of plagioclase within the MG2 chromitites relative to the MG3 chromitites.

The MG2 chromitites show higher content of MgO (≥11 wt. %) relative to the MG3 chromitites. This high content of MgO suggests a higher content of orthopyroxene minerals within the MG2 chromitites relative to the MG3 chromitite. The minor concentration of MgO (≤ 10 wt. %) within the MG3 chromitites illustrates the occurrences of orthopyroxene as an intercumulus mineral within the chromitites.

There is higher content of TiO_2 within the MG3 chromitites (0.66 wt. % - 0.85 wt. %) relative to the MG2 chromitites (0.62 wt. % - 0.80 wt. %). This corresponds to the findings of Doig (2000) who suggested that there is a constant increase of TiO_2 content from the LG1 to the MG3 seams. The constant increase in the TiO_2 is related to the fractionation of orthopyroxene and plagioclase from the magma, which Ti is relatively incompatible in the plagioclase and orthopyroxene and increase in the proportion in the melt. Ti has a high partition coefficient in the Cr- spinel and the amount of TiO_2 in the magma increases, thus the TiO_2 content will show an increase in the chromite content.

The MG3 chromitite spider diagrams show enrichment of Ti, Pb and Rb while the MG2 chromitites, spider diagrams illustrate enrichment of Sr, U, Zr and Y.

Kottke-Levin (2011) noted that the chromitite grains within the chromitite layers of the MG sequence consist of high content of Ni (1400ppm), Zn (1100ppm) and Co (400ppm). Doig (2000) suggested that the Ti content within the chromitites is elevated in comparison to the host silicate cumulates. This is due to the higher compatibility in Cr-spinel than in orthopyroxene and plagioclase.

Strontium is an incompatible element, but it's strongly compatible with plagioclase, but the amount of plagioclase in the host rock depends on the Sr content, which in this instance is lower within the MG3 chromitites relative to the MG2 chromitites.
The presences of U, Zr, Nb and Rb indicate that the MG2 chromitites are more felsic in composition, which is supported by the presences of CaO, Na_2O and Al_2O_3 which can be associated with the MG2 chromitites.

The high Ti content reflects high Cr_2O_3 content (≥ 30 wt. %) within the MG3 chromitites relative to the lower Cr_2O_3 content within the MG2 chromitites. The presences of plagioclase within the MG2 chromitites reduces the compatibility of Ti within the Cr-spinel of the MG2 chromitites, as compared to the MG3 chromitites which illustrates the absences of plagioclase, resulting in higher compatibility of Ti within the Cr-spinel.

5.2.1.3 Anorthosites

The anorthosites from the Dwarsrivier chrome mine are composed of 90% plagioclase, 3% chromitite, 3% orthopyroxene and 4% clinopyroxene. The anorthosites can be subdivided into two (anorthosites above the MG2 package and anorthosites below the MG3 package) based on their modal composition. The anorthosites above the MG2 package consist of clinopyroxene that occurs as an intercumulus mineral with high content of chromitites and orthopyroxenes, while the anorthosites below the MG3 package illustrate high content of clinopyroxenes and depletion in the chromitite content.

Levin-Kottke (2011) described the anorthosites from the middle group as consisting of 69.5% - 87.4% plagioclase content with the remainder being pyroxenes. The chromite grains comprise approximately 3% of the modal proportion of this rock. The intercumulus orthopyroxene and clinopyroxene result in the mottled appearance of the rock (Doig, 2000).
Boorman et al (2003) described the sub-division of the critical zone into the upper critical zone (MG3 package) and lower critical zone (MG2 package), the plagioclase changes from the intercumulus mineral to intercumulate mineral. This is the boundary that separates the two chromitite layers,

The anorthosites show increase in SiO_2 (48.7 wt. % - 51.8 wt. %) content, but the opposite is seen with MgO content (2.07 wt. % - 1.20 wt. %) as it decreases from the anorthosites above the MG2 package to the anorthosites below the MG3 package. The increase in the MgO is associated with the formation of the orthopyroxene minerals while the increasing SiO_2 content is due to the crystallisation of plagioclase in large quantities, resulting in high SiO_2 content within the magma.

The anorthosite layers show the high CaO content due to the high content of plagioclase within the anorthosites. The decrease in the CaO content from the anorthosites above the MG3 package suggested that there is a decrease in the plagioclase crystallisation. The increase in Al_2O_3 content, from anorthosites above the MG2 package to anorthosites below the MG3 package suggests the increase in the crystallisation of plagioclase from the anorthosites above the MG2 package to anorthosites below the MG3 package. This was due to the increase in the Na_2O and CaO but depletion in the MgO which suggest the formation of clinopyroxene and indicate a decrease in the orthopyroxene content. The presences of CaO also suggest that the plagioclase is more anorthitic in composition.

Kottke-Levin (2011) noted that the content of CaO is relates to plagioclase but to a certain extend by the crystallisation of clinopyroxene. Doig (2000) suggested that the highest values of the Al_2O_3 are usually associated with the more evolved rocks such as norites and anorthosites.

The anorthosites below the MG3 package are associated with Ni, this can be due to the presences of accessory chromitites, and while the anorthosites below the MG2 package are associated with Cu. Paktunc and Cabri (1995) noted that the high Ni content from the chromitite grains is characteristic feature of the Eastern Bushveld complex.

The spider diagrams of the anorthosites above the MG2 package show enrichment in Ti and La while anorthosites below the MG3 package spider diagrams show enrichment of elements such as U, Pb, Sr and Zr. The anorthosites below the MG3 package are more felsic in composition relative to the anorthosites above the MG2 package due to the enrichment of U and Zr.

5.2.1.4 Chromitite pyroxenites

The chromitite pyroxenites are made up of 35% fine to coarse-grained orthopyroxenes, 30% fine to coarse-grained clinopyroxenes, 25% of fine to coarse-grained chromitite and 10% of the plagioclase that occurs as an intercumulus mineral between the pyroxene grains. The chromitite pyroxenites where subdivided into lower chromitite pyroxenites and upper chromitite pyroxenite. The chromitite pyroxenites found within the upper part of the MG2 package show a low chromitite content, but an enrichment in the plagioclase and clinopyroxene content, while the lower chromitite pyroxenites demonstrates enrichment in the chromitite content.

The chromitite pyroxenites which Dube (2010) named as chromitite rich feldspathic pyroxenites and described as a feldspathic pyroxenite that host the disseminated chromite. They consist of euhedral grains of chromite that are embedded within the intercumulus plagioclase and orthopyroxene crystals. The orthopyroxene crystals exhibits small scale fractures.

Magnesium oxide, CaO, K_2O, MnO and P_2O_5 are associated with the lower chromitite pyroxenites due to the high content of plagioclase and clinopyroxene, while the upper chromitite pyroxenites consist of high content of chromite are associated with Cr_2O_3, Fe_2O_3, Al_2O_3 and TiO_2.

The high content of CaO show a high content of plagioclase, but to a certain extend also suggests presences of clinopyroxenes. The high content of MgO show higher enrichment of orthopyroxene within the upper chromitite pyroxenites relative to the lower chromitite pyroxenites. Phosphorus pentoxide is one of the oxides which characterise the upper chromitite pyroxenites. Phosphorus pentoxide is associated with the formation of apatite, which is one of the minerals that distinguish the upper chromitite pyroxenites from the lower chromitite pyroxenites.

The lower and upper chromitite pyroxenites spider diagrams show the enrichment of Rb, U and Pb. The lower chromitite pyroxenites show high content of U, Ce and Ti while the upper chromitite pyroxenites show enrichment of Sr, U, Ta, P and Y.

The enrichment of Ce in the upper chromitite pyroxenites relative to the depletion of the same element within the lower chromitite pyroxenites, suggest that the upper chromitite pyroxenites are more alkalic in composition relative to the lower chromitite pyroxenites.
The high content of Ti (0.35 wt. % - 0.43 wt. %) and Co (184 ppm – 248 ppm) relative to the lower chromitite pyroxenites is due to the higher content of accessory chromitite within the upper chromitite pyroxenites.

Kottkte-Levin (2011) noted that Co, Zn and Ni are some of the elements show high content within the chromitite grains. Parktunc and Cabri (1995) suggested that the high Ni and Zn are characteristic of the chromitites within the Eastern and Western Bushveld complex.

The presence of elevated values of Rb shows that the upper chromitite pyroxenites are felsic in composition. The high content of Y partitions into clinopyroxene. This is seen by the higher content of clinopyroxene within the lower chromitite pyroxenites relative to the upper chromitite pyroxenites. Strontium strongly partitions into plagioclase and the elevated values within the upper chromitite pyroxenites corresponds to the higher content of plagioclase relative to those from the lower parts.

5.2.2 Summary of the Dwarsrivier chrome mine stratigraphy

The four rock types within the Dwarsrivier Chrome mine transition boundary from the MG2 package to the MG3 package were differentiate based on the petrological and geochemical results. Figure 5.20 is a simplified stratigraphic column of the Dwarsrivier transition boundary.

The feldspathic pyroxenites and chromitites from the MG3 package are associated with high content of Cr_2O_3 and Fe_2O_3 relative to the feldspathic pyroxenites and chromitites within the MG2 package that are associated with high content of CaO, MgO and Na_2O.

The anorthosites below the MG3 package consist of high content of accessory chromitite relative to the anorthosites above the MG2 package due to the high content of MgO, Na_2O and SiO_2.

The chromitite pyroxenites within the upper parts of MG2 package are associated with Cr_2O_3, Fe_2O_3, Al_2O_3 and Co, suggesting they are more iron-rich relative to the chromitite pyroxenites in the lower parts which are associated with CaO, MgO and K_2O(felsic in composition).

In general the MG3 package contains of high content of plagioclase relative to the high orthopyroxene content within the MG2 package.

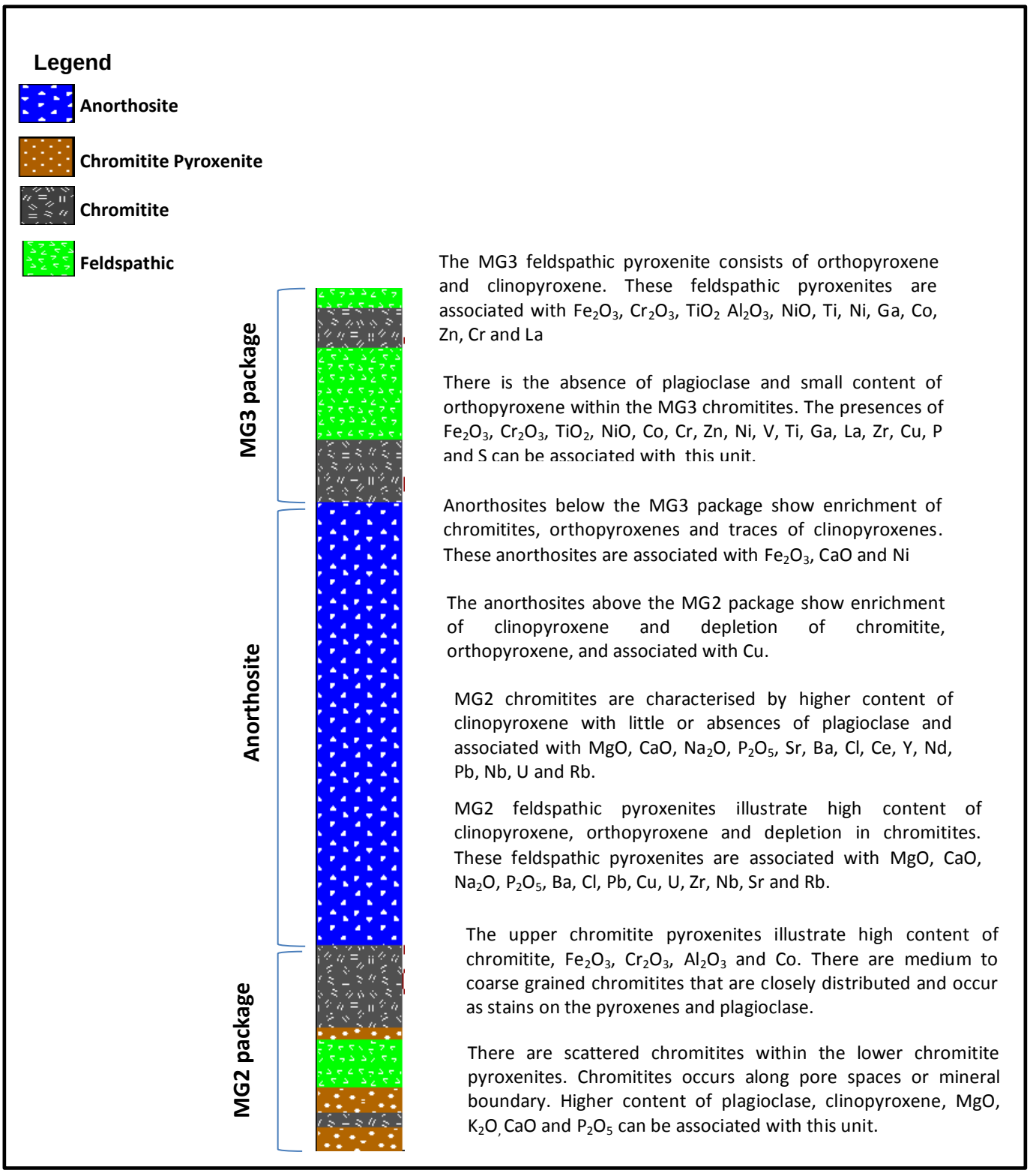

Figure 5.20: Simplified stratigraphic column of Dwarsrivier Chrome mine transition boundary.

5.2.3 Refractory chromite

The Dwarsrivier MG3 chromitites show a higher content of Cr_2O_3 and Fe_2O_3, but lower content of MgO, CaO and SiO_2 as compared to MG2 chromitites. The Cr_2O_3 and MgO contents of the Dwarsrivier MG2 chromitites are below refractory requirements. The Fe_2O_3, CaO and SiO_2 content within the MG2 and MG3 chromitites are not suitable for refractory purposes due to the high MgO and CaO content and a SiO_2 content that is way below the refractory requirements. The two important oxides that determine whether the chromitites are suitable refractory products are Al_2O_3 and MgO. These elements determine the reducibility of the chromite spinel. Table 6.1 below shows higher content of MgO and lower content of Fe_2O_3 suggest that there was more magnesium replacing iron, reducing the spinel as compared to the spinel of the MG3 chromitites which has lower MgO and Fe_2O_3 content. The reducibility of the spinel increases as a result of the iron being replaced by the aluminum, so in the case of the MG2 chromitites, there is higher aluminum and lower iron content relative to the MG3 chromitites. This means that the MG2 chromitites reducibility is lower relative to the higher reducibility of the MG3 chromitites.

Table 5.53: A typical chromitite suitable for refractory purposes compared to the MG2 and MG3 chromitites of Dwarsrivier Chrome mine.

		Dwarsrivier chromitites	
Major elements	Suitable for Refractory	MG3 chromitites	MG2 chromitites
Cr_2O_3	30% -50%	33.91%	26.38%
Al_2O_3	13% - 30%	13.87%	14.01%
Fe_2O_3	12% - 16%	23.15%	20.38%
MgO	14% -20%	10.07%	12.39%
SiO_2	3% - 6%	14.71%	22.35%
CaO	Up to 1%	1.89%	2.69%

Early producers exploited reserves with Cr:Fe ratio of greater than 3. The South Africa Bushveld complex chromite seams are relatively low grade with Cr: Fe ratios of 1.7 or less (Sylavania resource limited, 2010).

There is a large variation in the total and relative amounts of Cr and Fe in the lattice within the various deposits. This affects the ore grade not only in terms of Cr_2O_3 content, but also in the Cr: Fe ratio which determines the chromium content of the ferrochromium produced. The variations in the Cr:Fe ratio affects the reducibility of the ore, for example increasing amounts of magnesium compared with iron in the divalent site will make the spinel more difficult to reduce.

Therefore the increasing amounts of iron in trivalent site, which results in the replacement of aluminum, will increase the reducibility of the spinel. The greater the refractory index, the more refractory or less reducible the ore is.

In Ruighoek section (Western Bushveld Complex) the chromitite stratigraphy from the LG1 to MG4a chromitite seam is well exposed. Doig (2000) showed that the Cr_2O_3 content and Cr: Fe ratio increases from the LG1 chromitite seams to the LG3 – LG4 chromitites. The Cr: Fe ratio within the Dwarsrivier LG6 chromitite layer is 1.5 due to the high Cr_2O_3 content relative to the MG3 and MG2 chromitites (Arm report, 2005).

Table 5.54: MG2 and MG3 chromitites Cr:Fe ratios.

Package	Cr :Fe ratio
MG3 chromitites	1.47
MG2 chromitites	1.29

The chromitite content and Cr: Fe ratio decreases up to the MG3 seam. The LG1 – LG4 chromitites have a higher Cr: Fe ratio (about 2.0) than the LG5 to the MG3 chromitites, which average less than 1.70. The Cr:Fe ratio for the Dwarsrivier chromitites show an increase from MG2 chromitites to the MG3 chromitites as illustrated by table 6.2 above. With the increasing Al_2O_3 and CaO content and decreasing Cr_2O_3 and Fe_2O_3 content within the MG2 chromitites. This suggests that there is an increase in the crystallisation of plagioclase and decrease in the chromitite crystallization from the MG3 chromitites to MG2 chromitites.

5.2.4 Single or multiple magma injections

The transition boundary from the MG3 package to the MG2 package is as a result of a single magma injection. This is illustrated by the whole rock magnesium number, spider diagrams, and element ratios. The spider diagrams suggest that various rocks within the MG3 package and MG2 package are where formed from a single magma.

The MG2 feldspathic pyroxenites, MG2 chromitites and lower chromitite pyroxenites spider diagrams consist of similar trends in terms of the high field strength elements and large ion lithophile elements, but they have a higher degree of fractionation as compared to the MG3 feldspathic pyroxenites, MG3 chromitites and upper chromitite pyroxenites.

Ratios such as SiO_2/Al_2O_3, Ba/Sr, Co/V, Mg#, that were used by various authors to determine whether the transition zone from the MG3 package to MG2 package was as a result of a single or multiple magma pulses in the previous chapter.

The SiO_2/Al_2O_3 ratio was used by Kinnard (2005) as a potential indicator for the different magma sources between the main zone and platreef within the northern limb of the Bushveld complex. A significant change in the ratio will indicate that the formation was as a result of multiple magma pulses as compared to when the ratio remains constant, illustrating that the formation was as a result of a single magma pulse. The same ratio was used by Stevens (2007) in the Sheba Ridge, which the mineralisation is similar to that of the platreef and the satellite Uitkomst complex. Kinnard (2005) described some of her feldspathic pyroxenites be inhomogeneous in texture and believed to have been form a hybrid zone above the footwall of the altered metasedimentary rocks.

The SiO_2/Al_2O_3 ratio for the Dwarsrivier feldspathic pyroxenites illustrated that they are multiple types of magma pulses that lead to the formation of the transition boundary. This contradicts the feldspathic pyroxenite spider diagrams, because they indicate that were formed from a single magma. The feldspathic pyroxenite from the platreef and the main zone differs from those in the eastern Bushveld complex within the critical zone in terms of the different geological settings. Therefore this ratio was not taken into consideration when determining whether a single magma or multiple magma pulses resulted in the formation of the Dwarsrivier transition boundary.

The Dwarsrivier feldspathic pyroxenites exhibits little to no form of alteration that results in the formation of minerals such as serpentine compared to the altered platreef and main zone feldspathic pyroxenites. The silica content (SiO_2) in feldspathic pyroxenites from Stevens (2007) x-ray fluorescence results are greater than 53 wt. % compared to the feldspathic pyroxenites that have consist of samples less than 45 wt.%. This indicates that the feldspathic pyroxenites were formed from different geological settings.

The Ba/Sr ratio illustrated compatibility of elements Sr and Ba within the plagioclase indicates high plagioclase content within MG2 package relative to MG3 package in borehole DWR 172, while in borehole DWR 74, the MG2 package illustrate slightly high content of plagioclase relative to the MG3 package. This demonstrates a change in the composition of the rocks from the MG2 package to the MG3 package. The small change in the Sr/Ba ratio in both borehole DWR74 and DWR 172 suggest that the transition zone was formed from a single magma pulse. The feldspathic pyroxenites from the MG3 package are plagioclase-rich relative to feldspathic pyroxenites within the MG2 package that are orthopyroxene-rich which illustrated in the petrographic study and geochemical data analysis.

Eales et al (1986) used Co/V ratio stating that although a single element will show progressive increase or decrease through cyclic unit as a result of modal control, the ratio would be independent of the modal proportions The Dwarsrivier chrome mine transition boundary from the MG3 package to MG2 package in both DWR 74 and DWR 172 boreholes corresponds to Eales et al conclusions that the slight change in element ratios of Co/V demonstrates fractional crystallization.

The Mg-Fe ratio in borehole DWR 74 illustrates the high content of magnesium rich minerals within the anorthosite layer. The MG2 package illustrates higher magnesium number due to the higher presences of orthopyroxenes relative to the MG3 package. This is due to the Mg crystallization within the MG2 package relative to the MG3 package that shows high Fe crystallization. The Fe-Mg ratio of borehole DWR 172 illustrate that the anorthosite layer and the MG3 package have a magnesium number of 0.39, suggesting that these two layer may have the same content of magnesium rich minerals. The higher magnesium number within the MG2 package is due to the higher content of the orthopyroxenes within the MG2 package relative to the anorthosite layer and MG3 package. The MG3 package can also be due to more Fe crystallising as compared to the Mg. This results in higher chromite content within the various rocks of the MG3 package. Although Levin-Kottke (2000) argued that there was general progressive melt evolution in the Middle Group, with minor influxes of primitive melt at the level of the MG2B and MG4A chromitite layers, this was not seen within the Dwarsrivier chrome mine transition boundary.

Cameron (1977) argued, that the variation of the chromite composition reflects the fractionation of the magma, rather than subsolidus equilibrium. Cameron couldn't find the difference in the MG/Fe ratio of chromite being surrounded by orthopyroxene or plagioclase. This is seen within the Dwarsrivier chromitites, were there is higher chromite content within the MG3 chromitites (38 wt. %) relative to the MG2 chromitites (30 wt. %).

TiO_2 and V concentration within the chromitite lattice are relatively incompatible elements to chromite, which can be considered as indicators for progressive melt evolution. The Dwarsrivier MG3 chromites (Upper critical Zone) illustrates an increase in the TiO_2 (0.78 wt% to 0.82 wt. %) and V concentration, while the MG2 package illustrated a decreasing trend (0.76 wt.% to 0.66 wt.%). According to Kottke-Levin (2011) at the level of the MG2B chromitite layer, there was a slight decrease in the TiO_2 and V concentration, which indicated a period of addition of primitive melt composition. This could be also due to the fractional crystallization of chromitites from the melt which result in the decrease in the TiO_2 and V concentration.

5.3 Summary and Conclusion

This project set out to use geochemical and petrographic characteristics to distinguish the various rock types within the MG2 and MG3 package of the Dwarsrivier transition boundary. In addition used the spider diagrams and various element ratios to determine whether the transition zone was as a result of a single or multiple magma pulses and suggest the most suitable layer for exploitation between the MG2 and MG3 chromitites.

The findings of this investigation demonstrated that the various rock types within the MG2 package and MG3 package of the Dwarsrivier Chrome mine transitions boundary can be differentiated based on their petrographic and geochemical characteristics. The MG3 package is plagioclase-rich as relative to the orthopyroxene-rich MG2 package.

Petrographically the feldspathic pyroxenites are composed of plagioclase, clinopyroxene, orthopyroxene with accessory chromitite. Two types of feldspathic pyroxenite were identified through the petrographic study and were confirmed by the geochemical analysis. The MG3 feldspathic pyroxenites consist of high content of chromitite and plagioclase .These chromitites are associated with elements such as Cr_2O_3, NiO, TiO_2, Fe_2O_3 and Al_2O_3, Ni, Ga, Co, Zn and La.

The second type of feldspathic pyroxenites show the enrichment of orthopyroxenes and clinopyroxenes and are associated with high content of K_2O, MgO, CaO, P_2O_5, MnO, Na_2O, Ba, Cl, Y, Pb, Cu, U, Zr, Nb, Sr and Rb. This characterise the MG2 feldspathic pyroxenites.

Apart from the petrography, there are certain oxides that distinguish the MG3 feldspathic pyroxenites from MG2 feldspathic pyroxenites, namely the NiO, MnO, Ga and U. The presences of NiO and Ga correspond to the high content of accessory chromitite within the MG3 feldspathic pyroxenites.

The high content of orthopyroxene within the MG2 feldspathic pyroxenites is due to the high content of MnO and MgO relative to the plagioclase-rich (Al_2O_3) MG3 feldspathic pyroxenites. Uranium is usually associated with rocks that are more felsic in composition like the MG2 feldspathic pyroxenites as compared to the iron-rich MG3 feldspathic pyroxenites.

Iron (III) oxide, NiO, TiO_2 and Cr_2O_3 and Al_2O_3 characterise the Dwarsrivier chromitites. Microscopically the Dwarsrivier chromitites are composed of chromitites, clinopyroxenes with little to no presences of plagioclase and orthopyroxenes. The chromitites can be subdivided into two groups based on their modal composition. The MG3 chromitites consists of low content of

clinopyroxenes with the absences of orthopyroxenes, while the MG2 chromitites consist of high clinopyroxene content with little or absences of plagioclase.

The MG3 chromitites are associated with elements such as Cr_2O_3 , Fe_2O_3 , NiO, MnO, TiO_2 , Co, Cr, Zn, Ni, Ga, V, Cu and S while high content of CaO, MgO, P_2O_5, Na_2O, Al_2O_3, Sr, Ba, Cl, Ce, Y, Nd, Pb, Nb, U and Rb can be associated with the chromitites from the MG2 package.

Nickel (II) oxide, Magnesium oxide, Calcium oxide, Zinc and niobium are the elements which distinguish the MG3 chromitites from the MG2 chromitites. Calcium oxide and magnesium oxide suggest the presences of orthopyroxene and clinopyroxene within the MG2 chromitites, while NiO and Zn associated with the iron rich MG3 chromitites, relative to the MG2 chromitites which are more felsic in composition due to the higher content of Niobium.

The Dwarsrivier anorthosites within the Critical Zone are composed of plagioclase, clinopyroxenes, orthopyroxenes and the occasional presences of chromitite in trace amounts. The anorthosites below the MG3 package demonstrates the enrichment of chromitite and orthopyroxene, with traces of clinopyroxenes, while the anorthosites above the MG2 package illustrate higher content of clinopyroxene and depleted chromitites and orthopyroxenes content. The high content of SiO_2, Na_2O, P_2O_5 and Ni can be associated with the anorthosites above the MG2 package. The anorthosites below the MG3 package illustrate high content of Fe_2O_3, CaO and Cu.

The anorthosite above the MG2 package and those below the MG3 package can be differentiated based on their association with the following elements; NiO, K_2O, TiO_2, Ga, V, Cl and P. The high content of NiO, TiO_2, Ga and V can be associated with the presences of accessory chromitite within the anorthosites below the MG3 package, while the anorthosites above the MG2 package can suggest the presences of apatite due to the high content of P_2O_5.

The chromitite pyroxenites are composed of mainly clinopyroxene, orthopyroxenes and chromitites, with traces of plagioclase. The lower chromitite pyroxenites consist of high content of chromitite, while the upper chromitite pyroxenites illustrated enrichment in plagioclase, clinopyroxene and depletion in the chromitite content.

Although the chromitite pyroxenites are only found within the MG2 package, factor analysis illustrated that there may be possible occurrences of chromitite pyroxenites within the MG3 package, even though they were not seen during core logging. The chromitite pyroxenites can be sub-divided into two groups. The lower chromitite pyroxenites are associated with high content of Cr_2O_3, Al_2O_3, Fe_2O_3 and TiO_2 and Co while the presences of MgO, CaO, K_2O, P_2O_5, MnO, Sr, Rb, and Y can be associated with the upper chromitite pyroxenites. Magnesium oxide

and K_2O can be used to separate the upper chromitite pyroxenites from the lower chromitite pyroxenites.

The two types of chromitite pyroxenites within the MG2 package can be differentiate based on their association with elements such as MgO, K_2O, Zn, V, and Y. The presences of orthopyroxene and clinopyroxene within the upper chromitite pyroxenite is due to the high content of MgO and Y (partition into clinopyroxene), while the Zn and V are seen in large content within chromitite, indicating the high content of chromitite relative to the upper chromitite pyroxenites.

Spider diagrams of feldspathic pyroxenites and chromitites within the MG3 and MG2 package, anorthosite above the MG2, anorthosites below the MG3 package and the lower and upper chromitite pyroxenites in the MG2 package all illustrated the enrichment of large ion lithophile elements relative to the high field strength elements. The feldspathic pyroxenites, chromitites and anorthosites within the MG3 package demonstrated similar enrichment trends in terms of incompatible and compatible elements of the feldspathic pyroxenites, chromitites and anorthosites within the MG2 package. This was also seen within the lower and upper chromitite pyroxenites. This illustrates that the various rock types from the MG3 package and MG2 package within the Dwarsrivier transition boundary are formed from a single magma pulse.

Although spider diagrams of feldspathic pyroxenites, chromitites, anorthosites within the MG3 package and lower chromitite pyroxenites illustrated enrichment of Ti content while the feldspathic pyroxenites, chromitites, anorthosites within the MG2 package and upper chromitite pyroxenites show depletion in Ti concentration. This associated with ilmenite due to the presences of high content of Fe_2O_3 and TiO_2 content within these various rock types. There was cerium enrichment in the lower chromitite pyroxenites and depletion within the upper chromitite pyroxenites. Cerium is also associated with the rocks that are more alkali in composition. Therefore the enrichment of Ce within the lower chromitite pyroxenites illustrates the higher content of Na_2O and K_2O within these rocks.

Ratios such as Al_2O_3/SiO_2, Ba/Sr, Co/V, Mg#, that were used to show that the transition boundary from the MG3 package to MG2 package was as a result of a single or multiple magma pulses. The significant change in the Al_2O_3/SiO_2 ratio from the MG2 package to the MG3 package demonstrates that the transition zone was formed from multiple magma pulses. This contradicted the spider diagrams as they illustrated that a single magma formed the transition boundary. This ratio was not taken into consideration as the ratio was used for pyroxenites and feldspathic pyroxenites which are from the main zone and platreef. These pyroxenites and feldspathic pyroxenites showed some form of alteration as compared to the Dwarsrivier feldspathic pyroxenites which exhibit little to no presences of alteration.

The Sr/Ba ratio illustrated compatibility of elements Sr and Ba within the plagioclase indicates high plagioclase content within MG2 package relative to MG3 package in borehole DWR 172, while in borehole DWR 74, the MG2 package illustrate slightly high content of plagioclase relative to the MG3 package. This demonstrates a change in the composition of the rocks from the MG2 package to the MG3 package. The small change in the Sr/Ba ratio in both borehole DWR74 and DWR 172 suggest illustrate that the transition zone was formed from a single magma pulse. The Co/V ratio demonstrated a slight changes rather than a sharp change from the MG3 package to MG2 package in both DWR 74 and DWR 172. The slight change in the ratio demonstrated fractional crystallisation.

The high Mg-Fe ratio in borehole DWR 74 demonstrates the high content of magnesium rich minerals within the anorthosite layer. The MG2 package illustrate higher magnesium number due to the higher presences of orthopyroxenes relative to the MG3 package which consist of higher content of iron rich minerals, will demonstrate a low magnesium number. Fe-Mg ratio of borehole DWR 172 illustrate that the anorthosite layer and the MG3 package show a magnesium number of 0.39, suggesting that these two layer may have the same content of magnesium rich minerals. The higher magnesium number within the MG2 package is due to the higher content of the orthopyroxenes within the MG2 package relative to those within the anorthosite layer and MG3 package.

5.4 Recommendations

The entire anorthosite layer between the MG2 and MG3 package wasn't studied in this investigation. It was only a few samples directly above the MG2 package and below the MG3 package. Isotope geochemistry and microprobe analysis was not used due to financial constraints in determining whether the transition boundary was due to a single or multiple magma pulse. The preliminary findings indicate that Dwarsrivier transition boundary was as a result of a single magma pulse, if there was isotope and microprobe data that could be used to substantiate these preliminary findings

The naming of the various chromitite layers by Cousins and Feginga (1964) was based on the location of occurrence within the Bushveld complex stratigraphy. The geochemical classification of the various rock types within the MG2 and MG3 package of the Dwarsrivier transition boundary doesn't correspond to the naming of certain samples. Majority of the samples which were classified as either from the MG3 package or MG2 package according to Cousins and Feginga (1964) through the petrographic study do not correspond to the geochemical classification, only a few were correctly classified.
It is of paramount importance that core logging is combined with geochemical analysis through the use of a handheld XRF machine and the simplified stratigraphic column of Dwarsrivier chrome mine transition boundary developed during this investigation during exploration projects to be able to correctly identify and classify the various rock types.

The MG3 chromitites are the most suitable package for future exploitation, due to the high content of Cr_2O_3 content and Cr: Fe ratio. Although both MG2 and MG3 chromitites can be used to make refractory products, but due to the low Cr_2O_3 and high Al_2O_3 and MgO within the MG2 chromitites, the MG3 chromitites would be the most suitable product. Many other factors need to be taken into consideration when deciding which layer to mine, such as thickness of layer, dilution factor, mining method and etc. The exploitation of the MG3 chromitites was merely based on the high Cr_2O_3 and its suitability as a refractory product. So with further investigation and depending on the client's demands or requirements, the MG2 chromitites maybe the most suitable chromitite layer.

There is a need to do geochemical characterisation of the various rocks within the Bushveld stratigraphy in order to be able to identify and classify these rock types as either being from the MG2 package or MG3 package.

5. References

African Rainbow Minerals Annual Report. (2005). P 68

Artioli, G., Baumgarten, B.,Marelli,M., Giussani, B., Recchia, S., Nimis, P., Giunti, I., Angelini, I., Omenetto, P., (2008): Chemical and isotopes tracers in alpine copper deposits: geochemical links between mines and metal. Geo. Alp. 5. P139–148.

Barker & Associates, (2004): Platinum map of Southern Africa. 2nd Edition. *Bruma 2026*,South Africa.

Boorman, S., Boudreau, A., & Kruger F.J (2003): The Lower zone – Critical zone transition of the Bushveld complex: A quantitative textural study, Journal of petrology, volume 45, issue 6, P 1209 – 1235.

Cameron, E.N. (1963): Structure and rock sequence of the Critical Zone of the Eastern Bushveld Complex, Department of geology, University of Madison, Wisconsin, Mineralogical society of American, Special paper , International mineralogical association. P1-15

Cameron, E.N. (1977): Chromite in the central sector of the eastern Bushveld complex, South Africa. American Mineralogist., volume, 62, P 1082-1096.

Cameron E.N. (1978): The Lower Zone of the Eastern Bushveld Complex in the Olifants river Trough Journal of petrology, Volume 19, issue 3, P 437-462.

Cameron, E.N. (1980): Evolution of the Lower Critical Zone, central sector, eastern Bushveld Complex, Economic Geology volume 75, P 845-871.

Cameron, E.N. (1982): The Upper Critical Zone of the eastern Bushveld Complex…. Precursor of the Merensky Reef, Economic Geology volume 77, P 1307 – 1327.

Cawthorn, R.G., Eales, H.V., Walraven, F., Uken, R. and Watkeys, M.K. (2006): The Bushveld Complex. In: Johnson, M.R, Anhaeusser, C.R. and Thomas, R.J. (Eds.), the Geology of South Africa, Johannesburg/Council for Geoscience, Pretoria, P 261-281.

Christopher Letsoele (2010): North shaft geology Presenatation

Cloutier, V., Lefebvre, R., Therrien, R., Savard, M.M., (2008): Multivariate statistical analysis of geochemical data as indicative of the hydrogeochemical evolution of groundwater in a sedimentary rock aquifer system, hydrology journal, volume 353, P 294–313.

Cousins, C.A. and Feringa, G. (1964): The Chromite Deposits of the Western Belt of the Bushveld Complex, 183 - 202. In Haughton, S.H., Ed., The geology of some ore deposits in Southern Africa, volume 11, Geological Society of South Africa, Johannesburg, P 739.

Davies, J.C., (1986): Statistics and Data Analysis in Geology, 3RD edition, John Wiley & Sons Inc., New York.P1-638

Dawson, K.M., Sinclair, A.J., (1974): Factor analysis of minor element data for pyrites, Endako molybdenum mine, British Columbia, Canada, Economic Geology journal volume 69, P 404–411.

Doig H.L. (2000): Strike comparison of the compositional variation of the lower group and middle group chromitite seams of the critical zone, western Bushveld complex (M.Sc), Rhodes University.

Dube, Z.A (2010). The Merensky Reef and UG2 layers at De Wildt, Western limb of the Bushveld complex, Masters dissertation, University of the Witwatersrand.

Eales, H.V. and Cawthorn, R.G. (1996): The Bushveld Complex. In: Cawthorn RG (ed) Layered Intrusions, Developments in Petrology. Elsevier, Amsterdam, volume 15, P 181–229.

Eales, H.V. De Klerk, W.I and Teigler, B. (1990): Evidence for magma mixing processes within the Critical and Lower Zones of the northwestern Bushveld Complex, South Africa. Chemical Geology journal volume 88,P 261 – 278.

Eales H.V, Marsh J.S, Mitchell A.A, Klerk de W.J, Kruger F.J, Field M. (1986): Some geochemical constraint upon model for the crystallization of the upper critical zone - main zone interval, northwestern Bushveld complex, Mineralogical magazine, volume 50, P 567 – 582.

Eales, H.V. Teigler, B. and Maier, W.D. (1993 a): Cryptic variations of minor elements Al, Cr,Ti and Mn in Lower and Critical Zone orthopyroxenes of the Western Bushveld Complex, mineralogy magazine, volume 57, P257 – 264.

Fourie, G.P. (1959). The chromite deposits in the Rustenburg area. *Geological Survey of* South Africa*,* Bulletin. 27, P 45.

Gakuto Takahashi (2015): Sample preparation for X-ray fluorescence analysis, pressed and loose powder methods, Rigaku Journal, 31(1). P26- 30

Godel, B., Barnes, S.J., Barnes, S.-J. and Maier, W.D. (2011): Platinum ore in three dimensions – Insights from high-resolution X-ray computed tomography. Geology volume 38, P1127-1130.

Hatton, CJ (1988): Formation of the Bushveld Complex at a plate margin (abs). Congress Geology society of South Africa, volume 22 P 251- 254

Hatton, C.J. and Von Gruenewaldt, G. (1985): The geological setting and petrogenesis of the Bushveld chromitite layers. Inst. Geol. Res. Bushveld Complex. University of Pretoria, Report 57,P 48.

Hatton, C.J. and Von Gruenewaldt, G. (1987): The geological setting and petrogenesis of the Bushveld chromitite layers. In: Stowe, C.W. (Ed.), Evolution of Chromium Ore Fields. Van Nostrand Reinhold Co., New York, P109-143.

Harmer, R.E. (2000): New precise dates on the acid phase of the Bushveld and their implications, Workshop on the Bushveld Complex, Burgersfort, University of the Witwatersrand, Johannesburg.

Hubert, P., (1986): Textures et inclusions fluides des quartz aurifères: application au gite de Cros-Gallet (Haute-Vienne, France) et au prospect de Sanoukou (district de Kenieba, Mali). Unpublished PhD Thesis, BRGM. Orleans, France, P 350.

Irvine, T. N. (1975): Crystallisation sequences in the Muskox intrusion and other layered intrusion-II, Origin of chromitite layers and similar deposits of other magmatic ores, Geochimica et Cosmochimica Acta, 39: P 991-1020.

Irvine, T.N, Keith D.W, and Todd S.G. (1983): The J-M platinum and palladium reef of the Stillwater complex, Montana: II Origin by double diffusive convective magma mixing and implication for Bushveld complex, Economic Geology volume 78, P1287 – 1334.

Jolayeni,O. (2012): The silicate mineralogy of the MG4 chromitite package in the eastern part of the Bushveld complex, South Africa, M.Sc. Dissertation, University of Pretoria, South Africa.

Kaiser, H.F., 1958: The varimax criterion for analytical rotation in factor analysis Psychometrika volume 23, P187–200.

Kinnard J.A. (2005): Bushveld Igneous Province, school of Geosciences, University of Witwatersrand, P 3-39.

Kinnard J.A, Kruger F.J. and Cawthorn R.G. (2004): Rb –Sr and Sm-Nd isotopes in fluorite related to granites of the Bushveld Complex, South African Journal of Geology, 107, P 413-430.

Kottke-Levin J. (2011): A geochemical study of the Middle Group Chromitite, Helena mine, Bushveld complex, South Africa, Doctor of Philosophy Dissertation, University of the Free State.

Kruger FJ (1990): The Stratigraphy of the Bushveld Complex: a reappraisal and the relocation of the Main Zone boundaries. South Africa Journal of Geology volume 93, P376–381

Kruger FJ (1992): The origin of the Merensky cyclic unit: isotopic and mineralogical evidence for an alternative orthomagmatic model, Australia Journal of Earth Science, volume 39 :P255–261

Kruger FJ (1994): The Sr-isotopic stratigraphy of the Western Bushveld Complex,South Africa Journal of Geology volume 97, P 393–398

Lee, C.A. and Parry, S.J. (1988): Platinum-group element geochemistry of the Lower and Middle Group chromitites of the Eastern Bushveld Complex, Economic Geology, volume 83, P 1127-1139.

Letsoele C (2013): Dwarsriver mine challenages associated with the mining the LG6 chromitite layer.

Lomberg, K.G., Chunnett, G.K., Lionnet, M.A., Martin, E.S., Nel, J.J., Ruygrok, M. and Steenkamp, F.M. (2004): The Geology of Bafokeng Rasimone Platinum Mine (BRPM), P104-106.

Maier W.D, Barnes S.J (2008). The Platinum group elements in UG1 and UG2 chromitites and Bastard Reef at Impala Platinum mine, Western Bushveld Complex, South Africa: Evidence for late magmatic cumulate instability and reef constitution, South Africa Journal Geology 111: P159- 176

Maier, W.D. and Eales, HY. (1997): Correlation within the UG2-Merensky Reefinterval of the Western Bushveld Complex, based on geochemical, mineralogical and petrological data. Geological of Society of South Africa, Bulletin, volume 120, P 56.

Majdi, H.S; Mohamed, Y; Jumau, Y.T (2014): Uranium content measurement in drinking water for some region in Sudan using Laser Flourometry Technique, Life science Journal volume 11, issue 1. P1-8.

Marques,C de Sa, Noronha, F, E Ferrerira, E da Silva (2014). Factor analysis characterisation of minor element content in sulfides from Pb- Zn- Cu- Ag hydrothermal vein deposits in Portugal. Ore geology reviews volume 62 P 54- 71.

McDonough, W., Sun, S., Ringwood, A., Jagoutz, E. & Hofmann, A. 1992, "Potassium, rubidium, and cesium in the Earth and Moon and the evolution of the mantle of the Earth", Geochimica et Cosmochimica Acta, vol. 56, no. 3, pp. 1001-1012.

McDonough, W.F. and Sun, S.S. (1995): The composition of the Earth *Chemical Geology*, volume 120, P 223-253.

Moh'd, B.K., Powell, J.H., (2010): Uranium distribution in the Upper Cretaceous-Tertiary BelqaGroup, YarmoukValley, northwest Jordan, Earth Environmental Science, volume 3,issue 1, P49–62.

Molyneux, T.G. (1974): A geological investigation of the Bushveld Complex in Sekhukhuneland and part of the Steelport Valley, Transactions of the Geological Society of South Africa, 77, P 329-338.

Mondal S.K, Mathez E.A. (2007): Origin of the UG2 chromitite layers of the Bushveld Complex, Jounral of Petrology Volume 48, p 495- 510

Naldrett, A.J., Kinnaird, J., Wilson, A., Yudovskaya, M., McQuade, S., Chunnett, G. and Stanley, C.(2009): Chromite composition and the PGE content of Bushveld chromitites: Part 1 – the Lower and Middle Groups, Transactions of the Institution of Mining and Metallurgy (Section B: Applied Earth Sciences), volume 118, P131-161.

Nesse, W.D. (2000): Introduction to Mineralogy, New York, Oxford University Press. P1- 512

Paktunc, A.D. and Cabri, L.J. (1995): A proton- and electron-microprobe study of gallium, nickel and zinc distribution in chromian spinel. Lithos, volume 35, P261-282.

Pearce, J.A. (1983): Role of the sub-continental lithosphere in magma genesis at active continental margins.

Patinha, C.A.F., (2002): Impacto de elementos vestigiais na envolvente de antigas explorações mineiras utilizando meios amostrais diferenciados. Unpublished PhD Thesis. Departamento de Geociências, Universidade de Aveiro.

.

Reimann, C., Filzmoser, P., & Garrett, R.G., (2002): Factor analysis applied to regional geochemical data: problems and possibilities, Applied, Geochemistry journal, volume 17, P185–206.

Ridley, W.I. (2012): Petrology of associated igneous rocks in volcanogenic massive sulfide occurrence model, U.S. Geological Survey Scientific Investigations Report 2010 - 5070 - C, chapter 15, P 32.

Rollinson, H. (1993): Using geochemical data: evaluation, presentation, interpretation. Pearson Education Ltd., Essex, England.

Rose, A.W., Hawkes, H.E., & Webb, J.S., (1979): Geochemistry in mineral exploration, 2nd edition, Academic Press, London P657.

Schuurman, L.W. (1991). The geochemistry & petrology of the upper Critical Zone in the Boshoek section, of the Western Bushveld Complex. M.Sc. thesis (unpubl.), University of. Pretoria, P120.

Schuurman, L.W., Grabe, P.J.,. & Steenkamp, C.J. (1998). Chromium: In Wilson, M.G.C. and Anhaeusser, C.R. The Mineral Resources of South Africa 6th edition, Handbook, Council for Geosciences volume 16, P90- 105.

Schweitzer, J.K., Hatton, C.J. & De Waal, S.A. (1995). Regional lithochemical stratigraphy of the Rooiberg Group Upper Transvaal Supergroup: A proposed new subdivision. South African Journal of Geology, volume 98, P 245-255.

Scoon R.N., & De Klerk, W.J. (1985): The relationship of olivine cumulates and mineralisation to cyclic units in part of the Upper Critica1 Zone of the Western Bushveld Complex, Canadian, Mineralogist., P51 -77.

Scoon, R.N & Teigler, B. (1994): Platinum-Group Element Mineralization in the Critical Zone of the Western Bushveld Complex: Sulfide Poor-Chromitites below the UG2, Economic Geology, volume 89, P1094 – 1121.

Sharpe, M.R & Snyman, JA (1980): A model for the emplacement of the Eastern compartment of the Bushveld Complex. Tectonophysics, volume 65,P85 - 110.

Saunders, A.D. & Tarney, J. (1984): Geochemical characteristics of basaltic volcanism within back-arc basins, Geological Society, London, Special Publications, volume 16, no. 1, P 59-76.

Siad, A.M., Matheis, G., Utke, A., & Burger, H., (1994). Discriminant analysis as a geochemical mapping technique for lateritic covered area of South Western and Central Nigeria. ITC Journal, volume 1,P 7-12.

South African Committee for Stratigraphy.(SACS) (1980): Stratigraphy of South Africa, Part I (Compiler L.E. Kent), Geological Survey of South Africa Handbook 8, P690.

Sun, S. & McDonough, W. (1989): Chemical and isotopic systematics of oceanic basalts: implications for mantle composition and processes, *Geological Society, London, Special Publications,* volume 42, no. 1, P 313-345.

Sylania resource limited annual report 2010 P 1-25

Tatsuoka, M M. (1988): Multivariate Analysis: Techniques for Educational and Psychological Research. Macmillan, New York, P 479.

Teigler, B. Eales, H.V. & Scoon, R.N. (1992): The cumulate succession in the Critical Zone of the Rustenburg Layered Suite at Brits, western Bushveld complex. South African Journal of Geology, 95; 1-2, P 17-28.

Teigler B & Eales H.V. (1993): Correlation between chromite composition and PGE mineralization in the Western Bushveld complex, Rhodes University Mineral Deposita, volume 28, P 291-302.

Thompson, R. 1982, "Magmatism of the British Tertiary volcanic province", Scottish Journal of Geology, volume 18, issue 1, P 49-107.

Van der Walt C.F.J (1941). Chrome ores of the Western Bushveld Complex, South African Journal of Geology, Volume 44. P 79-120

Viljoen M.J & Schuurman L.W. (1998): Platinum Group Metals, In Wilson M.G.C and Anshaeussor C.R, The mineral resources of South Africa handbook, Council of Geosciences, P 23-58.

Von Gruenewaldt, G. (1973): The main and upper zones of the Bushveld Complex in the Roossenkaal area, Eastern Transvaal. Geological society of South Africa, volume 76, P 207-227

Walraven F. (1981): The textural geochemical and genetic aspects of the granophyric rocks of the Bushveld complex, Memoir 72, Geological Survey South Africa, P145.

Walraven F. (1987). Textural, geochemical and genetic aspects of the granophyric of the Bushveld complex, Geological Survey of South Africa, volume 72. P145

Winderbaum, L., Ciobanu, C.L., Cook, N.J., Paul,M., Metcalfe, A., & Gilbert, S., (2012): Multivariate analysis of an LA-ICP-MS trace element dataset for pyrite, Mathematical Geoscience, Volume 44, P 823–842.

Wager, L.R. & Brown, G.M., (1968): Layered igneous rocks, 0liver and Boyd, Edinburgh and London, 1st Edition, P 1-588.

Wood, D.A., Joron, J. & Treuil, M. (1979): A re-appraisal of the use of trace elements to classify and discriminate between magma series erupted in different tectonic settings", Earth and Planetary Science Letters, volume 45, issue. 2, P 326-336.

Zdenek K, Serencisova, J., Kozusnikova A.,Kolomaznik I., Studentova S., & Vontorva, J., (2014). Multivariate statistical assessment of coal properties, fuel processing technology (28), P119 –127.

6 Appendix

6.1 DWR74 Geological log

ASSMANG CHROME

DWARSRIVIER MINE

Assmang Dwarsrivier Chrome Mine
Borehole 74
Geological log sheet

From	To	Zone Id	Chromitite Group	Width (cm)
26.07	26.27	Feldspathic Pyroxenite		20
26.27	26.33	Chromitite	MG3C	6
26.33	26.39	Feldspathic Pyroxenite		6
26.39	26.79	Chromitite	MG3C	40
26.79	27.05	Feldspathic Pyroxenite		26
27.05	27.13	Chromitite	MG3B	8
27.13	27.22	Feldspathic Pyroxenite		9
27.22	27.29	Chromitite	MG3A	7
27.29	27.31	Feldspathic Pyroxenite		2
27.31	27.79	Chromitite	MG3A	48
27.79	27.82	Feldspathic Pyroxenite		3
27.82	27.88	Chromitite	MG3A	6
27.88	31.79	Anorthosite		391
31.79	32.23	Chromitite	MG2B	44
32.23	32.26	Feldspathic Pyroxenite		3
32.26	32.56	Chromitite	MG2A	30
32.56	32.91	Chromitite Pyroxenite		35
32.91	33	Chromitite	MG2A	9
33	33.05	Feldspathic Pyroxenite		5
33.05	33.18	Chromitite	MG2A	13
33.18	33.38	Chromitite Pyroxenite		20
33.38	34.28	Feldspathic Pyroxenite		90
34.28	34.76	Chromitite Pyroxenite		48
34.76	34.78	Feldspathic Pyroxenite		2
34.78	35.33	Chromitite	MG1	55
35.33	36.03	Feldspathic Pyroxenite		70
36.03	36.47	Chromitite	MG1	44
36.47	36.695	Chromitite Pyroxenite		22.5
E.O.H- End Of Hole				

6.2 DWR74 XRF major elements results

Sample name	RockType	CaO	Cr2O3	Fe2O3	K2O	MgO	MnO	Na2O	P2O5	SiO2	TiO2	NiO	S
DWR 74/04	Feldspathic Pyroxenite	8.800	0.495	8.543	0.103	13.314	0.165	1.082	0.021	50.381	0.144	0.052	38
DWR 74/05	Chromitite	2.062	32.460	25.456	0.062	10.070	0.218	0.559	0.021	13.210	0.850	0.114	46
DWR 74/06	Feldspathic Pyroxenite	2.853	11.754	16.107	0.117	19.914	0.224	0.682	0.068	39.400	0.438	0.088	65
DWR 74/07	Chromitite	2.427	30.404	23.143	0.094	10.734	0.220	0.659	0.031	16.384	0.837	0.105	20
DWR74/08	Chromitite	1.991	28.838	22.428	0.068	13.563	0.222	0.551	0.039	18.532	0.822	0.106	18
DWR 74/09	Feldspathic Pyroxenite	4.493	2.179	12.477	0.145	21.752	0.227	0.620	0.052	50.176	0.279	0.072	48
DWR 74/10	Chromitite	2.132	32.012	24.410	0.072	10.238	0.216	0.628	0.031	14.090	0.803	0.113	38
DWR 74/11	Feldspathic Pyroxenite	4.547	1.184	11.683	0.161	22.845	0.221	0.482	0.110	52.173	0.221	0.070	314
DWR 74/12	Chromitite	2.028	32.290	25.147	0.051	10.129	0.216	0.597	0.031	13.217	0.762	0.113	2
DWR 74/ 13	Feldspathic Pyroxenite	3.002	13.873	15.208	0.047	19.678	0.189	0.350	0.028	38.087	0.436	0.085	15
DWR 74/14	Chromitite	2.604	28.013	21.309	0.070	11.971	0.200	0.678	0.030	19.543	0.738	0.100	38
DWR 74/15	Chromitite	2.853	27.389	20.636	0.059	11.671	0.197	0.671	0.030	20.448	0.711	0.099	25
DWR 74/16	Chromitite	3.193	22.918	18.114	0.057	13.301	0.188	0.763	0.028	26.140	0.631	0.094	66
DWR 74/17	Anorthosite	14.068	0.744	2.361	0.223	4.083	0.053	1.850	0.032	50.457	0.128	0.000	8
DWR 74/18	Anorthosite	15.238	1.820	2.302	0.449	2.390	0.044	1.765	0.033	48.202	0.164	0.011	24
DWR74/19	Chromitite	1.672	31.387	22.979	0.081	12.959	0.201	0.514	0.030	15.890	0.765	0.111	33
DWR 74/21	Feldspathic Pyroxenite	3.911	9.380	12.957	0.096	19.574	0.191	0.660	0.029	43.134	0.316	0.076	68
DWR 74/22	Chromitite	2.347	26.222	20.395	0.111	14.011	0.202	0.617	0.040	22.792	0.708	0.101	64
DWR 74/23	Chromitite	1.827	32.752	22.816	0.091	11.499	0.282	0.673	0.027	15.371	0.673	0.109	52
DWR 74/24	Chromitite Pyroxenite	4.156	4.555	12.887	0.189	21.251	0.220	0.724	0.105	47.256	0.325	0.073	150
DWR 74/25	Chromitite Pyroxenite	3.605	3.692	12.338	0.166	21.950	0.225	0.801	0.020	49.243	0.264	0.068	185
DWR 74/26	Chromitite	2.024	26.872	22.226	0.080	14.368	0.209	0.389	0.020	20.341	0.778	0.110	109
DWR 74/27	Feldspathic Pyroxenite	3.130	13.512	15.333	0.089	18.984	0.197	0.590	0.030	36.847	0.453	0.089	67
DWR 74/28	Chromitite	1.347	32.251	24.444	0.071	13.258	0.214	0.398	0.020	14.054	0.796	0.122	39
DWR 74/29	Chromitite Pyroxenite	3.009	14.691	16.267	0.132	18.137	0.214	0.722	0.031	35.482	0.529	0.081	99
DWR 74/30	Chromitite Pyroxenite	3.534	10.446	15.508	0.166	18.293	0.260	0.800	0.052	40.058	0.540	0.083	162
DWR 74/31	Chromitite	0.912	32.048	23.694	0.297	13.844	0.208	0.357	0.020	15.093	0.832	0.109	25
DWR 74/32	Chromitite	0.757	33.832	24.641	0.444	12.402	0.222	0.283	0.020	12.917	0.747	0.111	2
DWR 74/33	Feldspathic Pyroxenite	1.934	1.078	13.617	0.111	28.331	0.272	0.030	0.020	52.523	0.181	0.081	44
DWR 74/34	Feldspathic Pyroxenite	3.006	5.646	14.704	0.119	24.256	0.247	0.079	0.020	45.743	0.316	0.079	126
DWR 74/35	Chromitite	0.612	30.125	23.237	0.038	16.474	0.239	0.507	0.019	16.311	0.689	0.105	0
DWR 74/36	Chromitite	1.416	31.303	23.232	0.089	13.597	0.218	0.545	0.020	16.072	0.703	0.109	8
DWR 74/37	Chromitite Pyroxenite	2.641	12.230	15.718	0.068	20.776	0.234	0.633	0.029	38.569	0.429	0.078	79

6.3 DWR74 XRF trace elements results

Sample name	RockType	Ni	Cu	Zn	Ga	Rb	Sr	Y	Zr	Nb	Pb	Th	U	Ti	V	Cr	Co	Ba	La	Ce	Nd	S	Cl	P
DWR 74/04	Feldspathic Pyroxenite	352	19	57	9	1	191	5	20	2	2	0	2	828	97	3,897	56	83	2	0	9	20	87	40
DWR 74/05	Chromitite	1,059	0	710	53	2	55	0	18	2	4	0	0	5,040	1,978	**285,316**	270	-3	18	0	0	33	71	45
DWR 74/06	Feldspathic Pyroxenite	767	5	290	23	8	60	5	26	4	6	0	1	2,797	794	**103,155**	138	40	15	0	0	61	219	269
DWR 74/07	Chromitite	1,048	0	640	51	4	56	0	20	4	11	0	0	4,968	1,832	**262,702**	216	-5	15	0	0	2	72	67
DWR 74/08	Chromitite	1,058	0	676	54	0	48	2	21	5	6	0	0	5,261	1,845	**271,845**	226	0	23	0	0	0	103	100
DWR 74/09	Feldspathic Pyroxenite	531	12	96	6	6	66	9	32	3	12	0	3	1,708	206	16,980	88	15	11	0	0	0	125	189
DWR 74/10	Chromitite	1,021	0	680	46	1	55	1	23	3	13	0	0	4,788	1,915	**283,421**	248	18	28	0	0	21	67	88
DWR 74/11	Feldspathic Pyroxenite	514	23	77	6	8	55	11	26	5	5	0	3	1,349	162	9,555	80	59	9	0	9	371	172	456
DWR 74/12	Chromitite	967	0	681	53	2	59	3	25	6	0	0	0	4,772	2,021	**277,278**	238	-10	25	0	0	0	74	50
DWR 74/13	Feldspathic Pyroxenite	820	21	317	26	2	51	5	27	4	8	0	3	2,838	929	**126,382**	150	23	12	0	0	0	61	63
DWR 74/14	Chromitite	968	4,595	626	52	-2	65	1	20	4	5	0	0	4,575	1,864	**252,225**	223	13	25	0	0	104	110	94
DWR 74/15	Chromitite	922	0	639	53	2	73	2	17	2	3	0	4	4,476	1,739	**249,543**	210	4	17	0	0	5	93	60
DWR 74/16	Chromitite	894	15	564	45	6	86	2	16	2	0	0	4	4,163	1,608	**216,498**	205	7	13	0	0	65	108	52
DWR 74/17	Anorthosite	53	11	23	17	6	400	3	21	1	14	0	0	711	73	5,802	9	93	13	1	16	0	106	87
DWR 74/18	Anorthosite	61	18	30	19	12	410	2	19	2	7	0	0	919	127	13,499	15	154	8	0	0	8	121	74
DWR 74/19	Chromitite	1,049	0	620	48	6	37	0	21	3	8	0	0	4,719	1,638	**284,342**	255	-10	31	0	0	18	63	83
DWR 74/21	Feldspathic Pyroxenite	647	7	210	17	5	68	5	23	3	11	0	0	2,065	622	**83,051**	119	21	17	0	0	57	81	82
DWR 74/22	Chromitite	965	6	559	35	4	49	2	24	4	6	0	2	4,332	1,712	**232,722**	203	18	21	0	0	54	87	106
DWR 74/23	Chromitite	979	0	606	53	10	50	0	33	5	12	0	0	4,825	1,773	**266,738**	211	2	13	0	0	0	88	72
DWR 74/24	Chromitite Pyroxenite	603	2,278	113	8	4	59	7	25	4	7	0	0	1,864	295	**35,927**	93	70	7	0	0	257	171	416
DWR 74/25	Chromitite Pyroxenite	610	41	110	8	8	63	6	30	4	10	0	1	1,638	273	**31,201**	92	81	11	0	0	199	141	52
DWR 74/26	Chromitite	1,027	6	523	46	6	47	0	18	3	0	0	0	4,809	1,401	**242,841**	203	4	27	0	0	108	71	31
DWR 74/27	Feldspathic Pyroxenite	796	7	260	26	5	57	5	19	4	1	0	0	2,825	712	**117,702**	138	29	23	0	0	61	64	64
DWR 74/28	Chromitite	1,123	0	621	49	4	29	1	17	3	4	0	2	4,805	1,571	**289,039**	237	3	20	0	0	23	52	33
DWR 74/29	Chromitite Pyroxenite	817	0	287	21	6	63	2	19	4	4	0	1	3,246	774	**124,543**	134	36	9	0	0	97	90	52
DWR 74/30	Chromitite Pyroxenite	731	28	223	17	7	63	5	27	3	8	0	0	3,147	606	**84,680**	115	70	6	0	0	134	114	159

DWR 74/31	Chromitite	1,038	13	692	47	14	23	0	13	2	19	0	3	5,232	1,742	**297,647**	247	66	18	0	0	6	106	19
DWR 74/32	Chromitite	1,091	0	705	52	20	25	0	12	5	13	0	0	4,586	1,850	**309,224**	244	100	8	0	0	0	88	14
DWR 74/33	Feldspathic Pyroxenite	632	0	93	3	3	6	3	20	2	9	0	7	1,079	139	8,702	91	50	-2	0	0	27	203	26
DWR 74/34	Feldspathic Pyroxenite	639	63	164	7	2	34	4	14	3	8	0	1	1,953	433	**47,495**	114	61	4	0	0	130	71	17
DWR 74/35	Chromitite	1,033	0	743	55	6	23	0	12	2	0	0	0	4,503	1,992	**290,147**	239	-14	14	0	0	0	81	18
DWR 74/36	Chromitite	999	0	719	49	5	33	0	16	3	7	0	4	4,482	2,145	**290,367**	232	25	25	0	0	0	108	29
DWR 74/37	Chromitite Pyroxenite	752	0	285	22	2	47	2	20	3	0	0	7	2,717	857	**107,491**	132	35	12	0	0	76	264	80

6.4 DWR 172 Geological log

Assmang Dwarsrivier Chrome Mine
Borehole 74
Geological log sheet

From	To	Zone Id	Chromitite Group	Width (cm)	Remarks
205.23	205.42	Feldspathic pyroxenite		19	Peg intrusion (5cm) from 205.32
205.42	205.77	Chromitite	MG3	35	
205.77	206.2	Feldspathic pyroxenite		43	
206.2	206.34	Chromitite	MG3	14	Peg intrusion 206.28m - 206.31m
206.34	206.46	Feldspathic pyroxenite		12	
206.46	207.01	Chromitite	MG3	55	
207.01	207.21	Anorthosite		20	Anorthosite below MG3 package
210.76	210.96	Anorthosite		20	Anorthosite above MG2 package
210.96	211.06	Chromitite	MG2	10	1cm pyroxenite stringer at 211.01m
211.06	211.67	Chromitite	MG2	61	From 211.13m - 211.16m peg intrusion
211.67	211.77	Chromitite pyroxenite		10	
211.77	212.31	Feldspathic pyroxenite		54	
212.31	212.41	Peg with disseminated chromitite		10	
212.41	212.54	Chromitite	MG2	13	
212.54	212.74	Chromitite pyroxenite		20	
E.O.H - End of hole					

6.5 DWR172 XRF major elements result

Sample name	**Zone id**	Al2O3	CaO	Cr2O3	Fe2O3	K2O	MgO	MnO	Na2O	P2O5	SiO2	TiO2	NiO	S
DWR172/01	Feldspathic Pyroxenite	10.32	2.82	17.43	17.19	0.17	14.68	0.20	0.61	0.03	35.95	0.51	0.09	128
DWR172/02	Feldspathic Pyroxenite	11.02	2.14	26.11	20.86	0.11	12.52	0.21	0.62	0.02	25.48	0.79	0.11	167
DWR172/03	Chromitite	14.87	2.13	35.08	22.63	0.07	8.20	0.20	0.84	0.02	15.06	0.77	0.11	97
DWR172/04	Chromitite	13.99	1.69	35.52	23.01	0.12	8.96	0.20	0.83	0.03	14.73	0.80	0.11	103
DWR172/05	Chromitite	13.86	1.78	35.42	23.22	0.09	8.91	0.21	0.77	0.03	14.80	0.79	0.11	99
DWR172/06	Feldspathic Pyroxenite	6.37	3.73	2.10	12.75	0.35	19.06	0.22	0.74	0.08	54.27	0.27	0.06	125
DWR172/07	Feldspathic Pyroxenite	7.00	3.91	2.90	13.38	0.22	18.65	0.23	0.83	0.06	52.46	0.29	0.07	124
DWR172/08	Feldspathic Pyroxenite	10.56	2.57	23.47	18.76	0.16	13.44	0.21	0.65	0.04	29.48	0.57	0.09	112
DWR172/09	Feldspathic Pyroxenite	5.64	4.13	0.65	11.96	0.20	20.46	0.23	0.53	0.05	55.91	0.18	0.06	91
DWR172/10	Chromitite	15.17	2.77	31.62	21.24	0.10	8.48	0.20	0.79	0.02	18.75	0.76	0.10	99
DWR172/11	Chromitite	13.72	3.29	22.04	17.73	0.09	11.68	0.19	0.82	0.03	29.76	0.60	0.08	86
DWR172/12	Chromitite	15.97	3.25	28.76	20.22	0.08	8.59	0.19	0.81	0.02	21.27	0.73	0.10	82
DWR172/13	Chromitite	15.78	2.69	32.59	22.20	0.11	8.14	0.20	0.70	0.03	16.62	0.84	0.10	98
DWR172/14	Chromitite	15.75	2.95	31.47	21.76	0.06	8.15	0.19	0.67	0.02	18.06	0.82	0.10	110
DWR172/15	Anorthosites	26.99	15.11	0.47	1.97	0.25	1.20	0.03	1.97	0.05	51.82	0.15	0.00	90
DWR172/16	Anorthosites	27.61	15.47	0.45	1.72	0.21	1.12	0.03	2.01	0.02	51.25	0.10	0.00	67
DWR172/17	Anorthosites	30.21	15.09	1.10	1.67	0.10	0.85	0.02	1.55	0.02	49.28	0.09	0.01	0
DWR172/18	Anorthosites	28.49	14.39	1.84	2.67	0.13	2.07	0.04	1.47	0.02	48.75	0.13	0.01	0
DWR172/19	Chromitite	13.88	3.77	31.91	21.12	0.04	9.25	0.21	0.47	0.02	18.51	0.73	0.09	75
DWR172/20	Chromitite	8.11	3.84	16.49	15.89	0.44	15.74	0.20	0.49	0.20	38.06	0.47	0.08	124
DWR172/21	Chromitite	13.33	2.83	36.41	22.47	0.04	9.21	0.21	0.42	0.03	14.20	0.73	0.11	106
DWR172/22	Chromitite	13.37	2.22	37.41	22.31	0.05	9.86	0.21	0.40	0.02	13.34	0.71	0.11	94
DWR172/23	Chromitite	13.17	1.03	42.24	24.50	0.11	9.93	0.23	0.26	0.03	7.61	0.76	0.12	104
DWR172/24	Chromitite	12.72	1.46	38.87	22.78	0.12	10.68	0.21	0.34	0.03	11.95	0.72	0.11	111
DWR172/25	Chromitite	11.96	1.53	34.99	21.31	0.07	12.54	0.20	0.45	0.03	16.16	0.66	0.10	141
DWR172/26	Chromitite pyroxenite	8.18	4.89	5.32	12.24	0.07	17.99	0.20	0.76	0.02	50.01	0.26	0.06	127
DWR172/27	Feldspathic Pyroxenite	6.97	2.91	6.22	13.65	0.25	18.75	0.22	0.89	0.07	49.66	0.35	0.07	208
DWR172/28	Feldspathic Pyroxenite	5.93	3.97	3.84	12.42	0.38	19.22	0.21	0.69	0.06	52.93	0.28	0.06	130

DWR172/29	Feldspathic Pyroxenite	7.46	4.08	9.65	14.40	0.20	17.18	0.21	0.78	0.04	45.51	0.43	0.07	174
DWR172/30	Feldspathic Pyroxenite	6.63	3.72	5.28	12.98	0.25	19.00	0.21	0.72	0.08	50.78	0.30	0.06	144
DWR172/32	Chromitite Pyroxenite	8.80	5.24	1.20	9.94	0.32	17.76	0.19	0.92	0.04	55.40	0.14	0.05	105
DWR172/33	Chromitite	13.58	1.34	39.55	23.94	0.06	9.33	0.21	0.53	0.02	10.53	0.79	0.11	63
DWR172/34	Chromitite pyroxenite	11.54	2.62	24.21	18.30	0.06	13.43	0.20	0.64	0.02	28.32	0.56	0.09	86
DWR172/35	Chromitite pyroxenite	6.06	2.49	12.51	14.76	0.25	18.73	0.20	0.62	0.09	43.70	0.52	0.08	135

6.6 DWR172 XRF trace elements results

Sample name	Zone id	Ni	Cu	Zn	Ga	Rb	Sr	Y	Zr	Nb	Pb	Th	U	Ti	V	Cr	Co	Ba	La	Ce	Nd	S	Cl	P
DWR 172/01	Feldspathic Pyroxenite	841	2	367	33	11	62	4	35	6	2	0	0	3,177	1,037	**134,301**	166	48	14	0	0	80	129	120
DWR 172/02	Feldspathic Pyroxenite	990	7	528	40	7	47	0	41	5	3	0	0	4,865	1,570	**201,693**	219	30	-2	0	0	120	79	79
DWR 172/03	Chromitite	1,032	0	681	57	7	58	0	23	5	5	0	0	4,711	1,984	**271,648**	249	41	16	0	0	41	52	49
DWR 172/04	Chromitite	1,063	0	690	51	7	48	3	31	7	1	0	0	4,872	1,969	**274,372**	248	37	15	0	0	49	89	96
DWR 172/05	Chromitite	1,044	0	679	50	7	50	3	29	5	9	0	4	4,827	2,058	**270,747**	249	33	17	0	0	51	70	77
DWR 172/06	Feldspathic Pyroxenite	547	18	105	7	10	61	8	46	5	5	0	1	1,598	233	15,363	95	124	5	0	0	71	239	365
DWR 172/07	Feldspathic Pyroxenite	570	16	112	9	9	59	5	37	4	5	0	0	1,679	265	20,713	91	66	1	0	0	67	143	229
DWR 172/08	Feldspathic Pyroxenite	876	0	463	34	3	46	6	28	5	4	0	0	3,587	1,331	**182,285**	192	50	12	0	0	57	92	132
DWR 172/09	Feldspathic Pyroxenite	529	10	70	5	8	49	11	44	5	0	0	1	1,028	122	4,784	86	68	0	0	0	31	157	193
DWR 172/10	Chromitite	928	0	608	48	5	73	1	27	7	5	0	0	4,690	1,669	**243,975**	220	47	13	0	0	22	43	56
DWR 172/11	Chromitite	818	0	432	39	8	77	4	31	10	6	0	0	3,727	1,310	**171,863**	173	46	26	0	0	32	71	100
DWR 172/12	Chromitite	884	0	571	53	1	84	4	25	7	5	0	1	4,577	1,854	**225,129**	231	36	18	0	0	24	47	44
DWR 172/13	Chromitite	981	10	655	60	9	72	2	30	7	6	0	1	5,152	2,007	**252,045**	228	25	20	0	0	41	83	88
DWR 172/14	Chromitite	923	3	626	53	6	77	2	26	5	0	0	0	5,072	1,995	**244,360**	254	0	20	0	0	56	47	44
DWR 172/15	Anorthosites	39	20	21	21	9	399	4	46	2	7	0	2	804	49	3,274	8	99	16	0	0	35	98	190
DWR 172/16	Anorthosites	30	13	19	20	5	409	4	27	2	7	0	1	611	54	3,280	14	110	0	0	0	12	31	48
DWR 172/17	Anorthosites	36	15	26	20	7	374	0	22	1	7	0	0	510	75	8,123	10	84	2	0	0	4	33	34
DWR 172/18	Anorthosites	87	16	40	19	7	347	3	24	2	5	0	0	789	148	13,769	19	98	2	0	0	30	30	45
DWR 172/19	Chromitite	887	0	634	57	8	54	2	27	4	1	0	0	4,559	1,967	**251,232**	223	25	14	0	0	19	51	33
DWR 172/20	Chromitite	742	14	332	27	15	38	9	56	6	1	0	0	2,925	1,054	**127,858**	141	118	15	0	0	69	359	932
DWR 172/21	Chromitite	993	0	679	48	2	37	5	30	7	4	0	0	4,501	2,248	**281,726**	253	33	29	0	0	55	60	77
DWR 172/22	Chromitite	1,009	0	683	42	1	35	3	27	6	3	0	2	4,354	2,291	**292,433**	240	27	24	0	0	40	57	67
DWR 172/23	Chromitite	1,070	0	721	48	9	18	1	33	5	7	0	0	4,528	2,107	**324,320**	273	27	22	0	0	54	75	81
DWR 172/24	Chromitite	976	0	659	45	6	27	1	34	4	4	0	0	4,335	1,750	**300,661**	260	30	26	0	0	58	74	101
DWR 172/25	Chromitite	926	0	599	47	6	33	1	30	7	3	0	0	4,101	1,522	**273,980**	244	19	9	0	0	31	70	88
DWR 172/26	Chromitite Pyroxenite	513	17	128	9	3	72	5	27	5	6	0	2	1,537	312	**39,310**	98	58	0	0	0	70	86	40
DWR 172/27	Feldspathic Pyroxenite	585	30	153	9	5	50	7	31	6	4	0	0	2,127	368	**46,380**	95	66	8	0	0	162	226	297
DWR 172/28	Feldspathic Pyroxenite	528	17	108	10	16	43	7	38	6	6	0	0	1,702	254	**28,199**	95	98	4	0	0	76	251	236

DWR 172/29	Feldspathic Pyroxenite	621	23	210	14	8	53	5	29	5	8	0	0	2,626	527	**72,356**	119	60	8	0	0	128	111	129
DWR 172/30	Feldspathic Pyroxenite	553	21	131	9	12	50	7	60	6	10	0	0	1,808	319	**39,134**	101	72	13	0	0	92	222	339
DWR 172/31	Chromitite Pyroxenite	965	0	572	44	6	47	1	23	5	6	0	2	4,343	1,439	**257,819**	248	34	28	0	0	54	48	27
DWR 172/32	Chromitite Pyroxenite	447	35	63	4	10	82	7	43	5	2	0	1	858	113	8,907	72	90	0	0	0	48	170	146
DWR 172/33	Chromitite	1,060	7	668	49	8	38	0	22	5	3	0	0	4,822	1,681	**306,277**	256	35	28	0	0	7	64	60
DWR 172/34	Chromitite pyroxenite	851	2	417	35	4	59	1	26	6	6	0	0	3,512	1,120	**188,561**	184	27	16	0	0	35	70	44
DWR 172/35	Chromitite pyroxenite	718	28	240	19	13	41	6	110	7	7	0	2	3,242	652	**97,681**	141	78	7	0	0	84	375	397

The grouping of borehole DWR172 and DWR 74 samples after cluster and discriminant analysis being applied

Feldspathic pyroxenites

Group 1- K_2O, MgO, CaO, P_2O_5, MnO and Na_2O Al_2O_3 (MG3)

DWR 74/04
DWR 74/09
DWR 74/11
DWR 74/21
DWR 74/33
DWR 74/34
DWR 172/06
DWR 172/07
DWR 172/09
DWR 172/27
DWR 172/28
DWR 172/29
DWR 172/30

Group 2- Cr_2O_3, NiO, TiO_2, Fe_2O_3, and

DWR 74/06
DWR74/13
DWR74/27
DWR 172/01
DWR 172/02
DWR 172/08

Chromitites

Group 1- Cr_2O_3, NiO, TiO_2, Fe_2O_3, MnO and K_2O (MG3)

DWR 74/05
DWR 74/07
DWR 74/10
DWR 74/12
DWR 74/19
DWR 74/23
DWR 74/28
DWR 74/31
DWR 74/32
DWR 74/35
DWR 74/36
DWR 172/03
DWR 172/04
DWR 172/05
DWR 172/10
DWR 172/13
DWR 172/14
DWR 172/19
DWR 172/21
DWR 172/22
DWR 172/23
DWR 172/24
DWR 172/25
DWR 172/33

Group 2- K_2O, MgO, CaO, P_2O_5, MnO and Na_2O

DWR 74/08
DWR 74/14
DWR74/15
DWR 74/16
DWR 74/22
DWR74/26
DWR 172/11
DWR 172/12

Anorthosites

Group 1 (above MG2 package) - Fe_2O_3, CaO

DWR 74/18
DWR 172//17
DWR 172/18

Group 2 (below MG3 package) - None

DWR 74/17
DWR 172/15
DWR 172/ 18

Chromitite pyroxenites

Group 1- Cr_2O_3, TiO_2, Fe_2O_3 and Al_2O_3 (Lower)

DWR 74/24
DWR 74/25
DWR 74/29
DWR 74/30
DWR 74/37
DWR 172/20
DWR 172/26
DWR 172/ 31
DWR 172/32
DWR 172/35

Group 2- MgO, CaO, P_2O_5, MnO and K_2O (Upper)

DWR 172/31
DWR 172/34